

# The effects of differing drought-heat signatures on terrestrial carbon dynamics and vegetation composition using dynamic vegetation modelling

Inauguraldissertation

der Philosophisch–naturwissenschaftlichen Fakultät  
der Universität Bern

vorgelegt von

**Elisabeth Andrea Tschumi**

aus Liestal, BL

Leiter der Arbeit:

Dr. Jakob Zscheischler

Abteilung für Klima– und Umweltphysik  
Physikalisches Institut der Universität Bern



Dieses Werk ist unter einem Creative Commons Namensnennung-Keine kommerzielle Nutzung-Keine Bearbeitung 2.5 Schweiz Lizenzvertrag lizenziert. Diese Lizenz gilt nicht für Kapitel 2 und 3. Um die Lizenz anzusehen, gehen Sie bitte zu <http://creativecommons.org/licenses/by-nc-nd/2.5/ch/> oder schicken Sie einen Brief an Creative Commons, 171 Second Strees, Suite 300, San Francisco, California 94105, USA.



# The effects of differing drought-heat signatures on terrestrial carbon dynamics and vegetation composition using dynamic vegetation modelling

Inauguraldissertation

der Philosophisch–naturwissenschaftlichen Fakultät  
der Universität Bern

vorgelegt von

**Elisabeth Andrea Tschumi**

aus Liestal, BL

Leiter der Arbeit:

Dr. Jakob Zscheischler

Abteilung für Klima– und Umweltphysik  
Physikalisches Institut der Universität Bern

Von der Philosophisch–naturwissenschaftlichen Fakultät angenommen.

Bern, 27.10.2022

Der Dekan

Prof. Dr. Marco Herwegh



## Urheberrechtlicher Hinweis

Dieses Dokument steht unter einer Lizenz der Creative Commons Namensnennung-Keine kommerzielle Nutzung-Keine Bearbeitung 2.5 Schweiz. <http://creativecommons.org/licenses/by-nc-nd/2.5/ch/>

**Sie dürfen:**



dieses Werk vervielfältigen, verbreiten und öffentlich zugänglich machen

**Zu den folgenden Bedingungen:**



**Namensnennung.** Sie müssen den Namen des Autors/Rechteinhabers in der von ihm festgelegten Weise nennen (wodurch aber nicht der Eindruck entstehen darf, Sie oder die Nutzung des Werkes durch Sie würden entlohnt).



**Keine kommerzielle Nutzung.** Dieses Werk darf nicht für kommerzielle Zwecke verwendet werden.



**Keine Bearbeitung.** Dieses Werk darf nicht bearbeitet oder in anderer Weise verändert werden.

Im Falle einer Verbreitung müssen Sie anderen die Lizenzbedingungen, unter welche dieses Werk fällt, mitteilen.

Jede der vorgenannten Bedingungen kann aufgehoben werden, sofern Sie die Einwilligung des Rechteinhabers dazu erhalten.

Diese Lizenz lässt die Urheberpersönlichkeitsrechte nach Schweizer Recht unberührt.

Eine ausführliche Fassung des Lizenzvertrags befindet sich unter <http://creativecommons.org/licenses/by-nc-nd/2.5/ch/legalcode.de>



# Thesis overview and summary

The global carbon cycle is essential for many aspects of the climate system and life in general. Within this carbon cycle, the natural terrestrial carbon sink plays an important role removing CO<sub>2</sub> from the atmosphere. Many factors influence this terrestrial cycle, particularly climate variability, both natural and human-made. Especially in the face of global warming, the evolution of the natural carbon sink is quite uncertain. In particular, the effects of extreme weather and climate events, which are expected to become more frequent and more severe in the future, on the carbon cycle are hard to quantify, since the extremes themselves are also associated with uncertainties. To contribute to the ever-growing scientific field of carbon cycle and extreme event research, this thesis is concerned with analysing the effects of differing drought-heat signatures on terrestrial carbon dynamics using dynamic vegetation modelling.

We built six hypothetical 100-year long climate scenarios which differ in their occurrence frequency of hot and dry extremes. They are based on a large ensemble simulation generated by the climate model EC-Earth. This data has several advantages. Firstly, it represents present-day climate without any trends. Secondly, it is available on a global grid, and thirdly, it offers a very long time series, which is needed to study extreme events in order to have a large enough sample size. The scenarios only differ in their extreme occurrence, but are similar in their global means. However, the data does present some regional biases which have a potentially large impact on modelled impacts. The scenarios are described and characterized in Chapter 2.

The six hypothetical scenarios were used to run the dynamic global vegetation model LPX-Bern v1.4, as well as five additional dynamic global vegetation models. The models were run using constant CO<sub>2</sub> concentrations and not allowing any land-atmosphere feedbacks which might change our initially sampled scenarios. They also only consider natural vegetation, meaning no crops or other land uses. The LPX-Bern results, described in detail in Chapter 3, show clear differences between scenarios as well as between climate zones. While trees thrive under climate scenarios with few extremes or only hot extremes, especially in higher latitudes, they show a clear reduction in coverage for dry extremes and especially compound hot and dry extremes. The relatively large increase in tree coverage in high latitudes under more hot extremes is associated with an increased growing season length in these regions which are generally energy-limited. Grasses tend to compensate the changes in tree coverage to some extent. Changes in tree coverage are also associated with changes in plant productivity and carbon stored in vegetation. Most of these results are shown as global means with regional differences being potentially large.

Chapter 4 discusses the comparison of different vegetation models all run with the same input scenarios. The carbon variables are comparable between the models in the global mean, but we see quite large differences in vegetation coverage, most likely due to biases in the input data. Regionally, these differences may be even larger. There is still overall agreement between the models that a compound hot and dry climate leads to a reduction in tree coverage with an associated reduction in carbon stored in vegetation. The scenario with frequent dry extremes suggests similar results, with slightly less agreement between the models. The effects of a climate with hot extremes and those of a climate with no compound extremes are generally small. Large differences can be seen in a climate with no extreme events at all, where some models simulate

an increase in vegetation and others a decrease. However, it is clear that compound hot and dry events are associated with a reduction of carbon stored on land.

Our results suggest a possible reduction in the natural land carbon sink under future climate change. The coupling of temperature and precipitation can vary substantially between models and biases can exist in the input data. Therefore, results can differ when studying compound events. This thesis contributes to the understanding of feedbacks and processes concerning variable interaction, which is crucial to improve models. The field of compound event research is still emerging and ever-growing and there is still a lot to investigate when it comes to the effects of extremes on the terrestrial carbon cycle. Future work could focus on other types of compound events, such as temporally compounding or preconditioning, or different impact models could be used, for example, crop or fire models.





# Contents

<b>Urheberrechtlicher Hinweis</b>	<b>4</b>
<b>Thesis overview and summary</b>	<b>5</b>
<b>1 Introduction</b>	<b>13</b>
1.1 About the carbon cycle . . . . .	13
1.1.1 The global carbon cycle . . . . .	13
1.1.2 The terrestrial carbon cycle . . . . .	14
1.2 About extreme events . . . . .	17
1.2.1 Extreme weather and climate events . . . . .	17
1.2.2 Compound extreme weather and climate events . . . . .	17
1.3 Hot-dry extremes and the carbon cycle . . . . .	19
1.4 The challenges of disentangling compound drivers . . . . .	21
1.5 Dynamic global vegetation modelling using large ensemble simulations . . . . .	22
1.6 Motivation and Goal of this thesis . . . . .	23
<b>2 A climate database with varying drought-heat signatures for climate impact modelling</b>	<b>25</b>
2.1 Introduction . . . . .	26
2.2 Data description . . . . .	27
2.2.1 EC-Earth climate simulations . . . . .	27
2.2.2 Regional biases in annual temperature and precipitation . . . . .	27
2.2.3 LPX-Bern stability . . . . .	28
2.2.4 Scenario sampling . . . . .	28
2.2.5 Available variables . . . . .	29
2.3 Scenario characterization . . . . .	29
2.3.1 Heatwaves . . . . .	30
2.3.2 Droughts . . . . .	31
2.3.3 Compound extremes . . . . .	31
2.4 Discussion and conclusions . . . . .	32
2.5 Supporting information . . . . .	36

<b>3</b>	<b>The effects of varying drought-heat signatures on terrestrial carbon dynamics and vegetation composition</b>	<b>39</b>
3.1	Introduction . . . . .	40
3.2	Data and Methods . . . . .	41
3.2.1	Forcing scenarios . . . . .	41
3.2.2	LPX-Bern . . . . .	42
3.3	Results . . . . .	43
3.3.1	Changes in vegetation coverage and associated NPP changes . . . . .	43
3.3.2	Changes in carbon dynamics . . . . .	44
3.3.3	Path to model equilibrium . . . . .	45
3.4	Discussion . . . . .	46
3.5	Conclusion . . . . .	49
3.6	Supporting information . . . . .	51
<b>4</b>	<b>Large variability in simulated response of vegetation composition and carbon dynamics to variations in drought-heat occurrence</b>	<b>53</b>
4.1	Introduction . . . . .	54
4.2	Data and Setup . . . . .	55
4.2.1	Climate forcing . . . . .	55
4.2.2	Modelling setup . . . . .	56
4.2.3	Model descriptions . . . . .	56
4.3	Results . . . . .	57
4.3.1	Features of the input scenarios stemming from the sampling method . . . . .	57
4.3.2	Vegetation cover, carbon pools and fluxes in the Control . . . . .	58
4.3.3	The effect of varying drought-heat signatures . . . . .	59
4.4	Discussion . . . . .	63
4.5	Conclusion . . . . .	64
4.6	Supporting information . . . . .	65
<b>5</b>	<b>Conclusions and Outlook</b>	<b>71</b>
5.1	Summary of results . . . . .	71
5.1.1	The input data . . . . .	71
5.1.2	The effects of hot and dry extremes . . . . .	71
5.2	Modelling implications . . . . .	72
5.3	Outlook . . . . .	73
	<b>Acknowledgements</b>	<b>97</b>
	<b>Erklärung gemäss Art. 18 PromR Phil.-nat. 2019</b>	<b>99</b>





# Chapter 1

## Introduction

### 1.1 About the carbon cycle

#### 1.1.1 The global carbon cycle

The global carbon cycle refers to the exchange of CO<sub>2</sub> between four major reservoirs, which are important on time scales from seconds to centuries: the atmosphere, oceans, land, and fossil fuels (Houghton, 2007; Archer et al., 2009). The slowest to affect the atmospheric CO<sub>2</sub>, on timescales of millennia, are processes such as weathering, vulcanism, and ocean sedimentation, but since the annual amount of carbon exchanged via these mechanisms is very small, they are generally ignored in budgets of a century (Houghton, 2007). Of the three, relatively fast exchanging, pools the ocean is the largest with about 40000 PgC and a turnover time of about 500 years. The terrestrial biosphere pool is considerably smaller (2000-3000 PgC) but with a much faster turnover time of about 20 years (Ciais et al., 2013). Other land pools include permafrost (1100-1500 PgC, Lindgren et al., 2018) and peat- or wetlands (400-600 PgC, Yu, 2012).

The main processes controlling the uptake of carbon by the oceans are the ocean's carbon chemistry, the air-sea exchange, the mixing between surface and deep waters, and ocean biology (Houghton, 2007). Anthropogenic CO<sub>2</sub> perturbations in the atmosphere lead to an increased uptake of carbon by the ocean due to an increased sea-air gas exchange. To a lesser extent, the marine carbon sink may also be changed through alterations of the natural carbon cycle, for example, by warming, which affects CO<sub>2</sub> solubility, and by changes in the circulation, which changes the marine biological cycles. Between 1991 and 2002, the ocean CO<sub>2</sub> sink has grown, but uncertainties in the estimates are large. Between 2011 and 2020, the ocean was a sink for 26 % of total CO<sub>2</sub> emissions (Friedlingstein et al., 2022).

The exchange between the atmosphere and terrestrial ecosystems is mainly the result of biological processes, namely photosynthesis and respiration (Houghton, 2007). However, the land ecosystems have been changed profoundly by human land use and land-use change, which affects not only vegetation distribution but is also associated with carbon emissions. Some aspects of it, like the increased CO<sub>2</sub> concentration in the atmosphere and additional nitrogen availability through deposition and fertilization as well as climate change, have led to an uptake of carbon by the biosphere. Between 2011 and 2020, the biosphere has taken up about 30 % of anthropogenic CO<sub>2</sub>. The terrestrial carbon cycle is explained in more detail in the following section.

In comparison to the ocean and land pool, the atmosphere contains little carbon with about 600 PgC pre-industrial. However, the redistribution of fossil carbon (in the form of coal, oil, and natural gas which are residuals of organic matter formed millions of years ago by green plants, the reservoir estimated to be 5000-10000 PgC) to the atmosphere dominates the global

carbon budget (Houghton, 2007).  $\text{CO}_2$  in the atmosphere is the largest contributor to the anthropogenically enhanced greenhouse effect.  $\text{CO}_2$  concentrations in the atmosphere have reached 414.7 ppm in 2021, which is 50 % above pre-industrial levels (Friedlingstein et al., 2022). Since the atmosphere couples the land and the ocean, it plays an important role in the global carbon cycle despite its size for carbon storage. Feedbacks between the carbon cycle and the climate system are critical for predicting changes in climate (Houghton, 2007). Warming of the climate system can lead, for example, to increased decay of organic matter in soils or a decrease in oceanic carbon uptake. Both of this would directly affect the atmospheric  $\text{CO}_2$  concentration, which would rise more quickly than without these positive feedbacks, which in turn also increases the rate of warming (Houghton, 2007). On the other hand, higher  $\text{CO}_2$  concentrations in the atmosphere may enhance photosynthesis and the storage of carbon in vegetation and soils, which is a negative feedback that leads to a less rapid rise of atmospheric  $\text{CO}_2$  levels.

### 1.1.2 The terrestrial carbon cycle

The terrestrial biosphere exchanges carbon with the atmosphere via plant activity. Plants transform energy via photosynthesis from short-wave radiation into chemical energy, as water and  $\text{CO}_2$  from the atmosphere are synthesized to form carbohydrates and oxygen, which is released as a byproduct. Environmental conditions such as light and temperature or water and nutrient availability are important factors for photosynthesis. Gross primary production (GPP) is the amount of carbon absorbed by photosynthesis on land. About 50 % of this is released back into the atmosphere via plant respiration (autotrophic respiration). The carbon remaining fixed in the plants is called net primary production (NPP). The assimilation of carbon is opposed by the decomposition of dead organic material, called heterotrophic respiration (HR). The difference between NPP and HR is called net ecosystem production (NEP) and describes how much carbon is stored in an ecosystem without disturbances (Lienert, 2018). Net ecosystem exchange (NEE) describes the term of carbon that is stored long term after disturbances. A schematic of these fluxes is shown in Figure 1.1. An imbalance between photosynthesis and respiration will cause an ecosystem to be either a source or a sink of carbon. If everything is in equilibrium, an increase in productivity also means an increase in carbon storage until the carbon lost from the detritus pool comes into a new equilibrium with the higher input of productivity (Houghton, 2007). Various measurements suggest that respiration is more sensitive to variations in climate than photosynthesis (Valentini et al., 2000; Saleska et al., 2003; Myneni et al., 1995; Hicke et al., 2002).

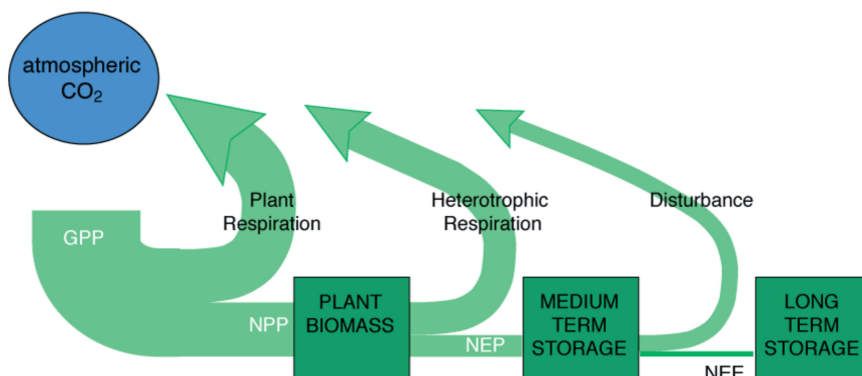


**Figure 1.1:** Schematic of the terrestrial carbon fluxes. GPP = Gross Primary Production; NPP = Net Primary Production; NEP = Net Ecosystem Production; NEE = Net Ecosystem Exchange. Heterotrophic respiration is the release of carbon through the decomposition of dead organic material. Disturbances include, for example, fire or human-made deforestation. Credits to Nicolas Gruber.

Historical patterns suggest that the terrestrial ecosystems were a net source before the 1930s (Joos et al., 1999; Houghton, 2007) and then became a net sink. The current terrestrial carbon sink has kept the airborne fraction of total CO<sub>2</sub> emissions at about 47 % for the period of 2011-2020, having taken up about  $1.9 \pm 0.9$  PgC yr<sup>-1</sup> between 2011 and 2020 or about 30 % of total anthropogenic emissions (Friedlingstein et al., 2022). As a result of anthropogenic activity and changing climate, the carbon balance has begun to shift. There is concern that the present terrestrial carbon sink may not persist (Canadell et al., 2007). A diminished terrestrial sink or even a source would lead to higher concentrations of CO<sub>2</sub> in the atmosphere than predicted. This turns the management of fossil fuel emissions into an even greater challenge (Houghton, 2007). It would clearly help in managing the carbon cycle if the airborne fraction were to remain the same or even get smaller in the future (Houghton, 2007). Observations show that the total northern hemisphere carbon sink has diminished since 1992. Since the uptake by the oceans seems to have increased (Manning & Keeling, 2006), it is suggested that the diminished sink is terrestrial (Houghton, 2007), although Friedlingstein et al. (2022) show a continued increase of the land CO<sub>2</sub> sink between 2011 and 2020, primarily due to increased atmospheric CO<sub>2</sub>. Some studies estimate the net terrestrial carbon uptake to have declined from  $1.2 \pm 0.8$  PgC yr<sup>-1</sup> to  $0.5 \pm 0.7$  PgC yr<sup>-1</sup> between 1990 and 2000 (Manning & Keeling, 2006). During 2002 and 2003, the releases of CO<sub>2</sub> from land was anomalously high (Allison et al., 2005). In 2002, they were from the tropics and in 2003 from Eurasia. The 2003 summer drought and heatwave in Europe is estimated to have reduced primary productivity there by 30 %, resulting in an anomalous net source (Ciais et al., 2005). If climate change is weakening the natural carbon sink, the rate of CO<sub>2</sub> increase in the atmosphere may be expected to accelerate (Jones et al., 2005). Other estimates, however, show an increase of the terrestrial CO<sub>2</sub> sink from  $1.2 \pm 0.5$  PgC yr<sup>-1</sup> in the 1960s to  $3.1 \pm 0.6$  PgC yr<sup>-1</sup> during 2010-2019, indicating only a decreased land sink during El Niño events (Friedlingstein et al., 2022). This general increase of the land sink is believed to occur mainly due to CO<sub>2</sub> fertilization which increases photosynthesis as well as plant water use in water-limited systems (Friedlingstein et al., 2022). Overall, it is unclear how the terrestrial sink will develop in the future (Friedlingstein et al., 2022).

Two aspects are considered to be responsible for the carbon sink on land, human-made factors and natural processes. Human-made changes include actions such as regrowth from past disturbances and changes in land use or management (Houghton, 2007). Land use and land-use change have altered the terrestrial carbon stocks significantly, but cumulative CO<sub>2</sub> estimates for land-use change are uncertain (Friedlingstein et al., 2022). The change depends on the area of land affected, the carbon stocks before and after the change, and the rates of decay and recovery after the change (Houghton, 2007). Over the past 300 years, forests have been replaced by agricultural lands (Houghton, 2003), especially in tropical regions where croplands expanded substantially (Friedlingstein et al., 2022). This leads to a decrease of carbon stored on land, since trees hold much more carbon per unit area than other types of vegetation (Houghton, 2007). Thus, land-use change caused a global emission of CO<sub>2</sub> from land of about  $0.9 \pm 0.7$  PgC yr<sup>-1</sup> for the year 2020, having decreased slightly over the last two decades mostly due to lower emissions from cropland expansions in tropical regions (Friedlingstein et al., 2022). This would indicate a net source of carbon from the land. However, this estimate only considers human-made changes and does not include other sources or sinks, unrelated to land-use change. Of course, there are mechanisms considered responsible for the carbon sink on land without considering anthropogenic change. These natural processes concern the rates of photosynthesis, respiration, growth, and decay. Changes in climate variables, such as warmer temperatures and changes in soil moisture, often favour the growth of trees and, on longer terms, the spread of trees into tundra, savanna, and grasslands. In colder ecosystems (e.g. in high latitudes), warmer temperatures increase productivity and therefore carbon storage. One reason for this are longer growing seasons, especially over boreal zones and temperate Europe (Myneni et al., 1997; Friedlingstein et al., 2022). Experiments have shown that most C3 plants (plants which

fix CO<sub>2</sub> into a compound containing three carbon atoms before entering the Calvin-Benson cycle of photosynthesis as opposed to C4 plants, which fix CO<sub>2</sub> into a molecule containing four carbon atoms), which include all trees and vegetation from cold regions, respond to elevated concentrations of CO<sub>2</sub> with increased rates of photosynthesis, increased productivity, and increased biomass (Norby et al., 2005). Litter and soil carbon pools also increase under elevated CO<sub>2</sub> (Jastrow et al., 2005; Luo et al., 2006). However, these factors often interact non-additively to influence carbon storage (Houghton, 2007). For example, under higher CO<sub>2</sub> concentrations, plants can acquire the same amount of carbon with a smaller loss of water through their stomata, which reduces the effects of droughts. Negative interactions are also possible. Shah & Paulsen (2003) observed increased net primary production in a Californian grassland with separate increased temperature, precipitation, nitrogen deposition, and atmospheric CO<sub>2</sub>. For combined treatments, however, elevated CO<sub>2</sub> decreased the positive effects of the other treatments, most likely because some soil nutrients became limited (Shah & Paulsen, 2003). Climate change and variability can counterbalance CO<sub>2</sub> effects, so that climate change reduced the land sink by 15 % for the period of 2011-2020, mainly in South and Central America, Southwest USA and Central Europe (Friedlingstein et al., 2022). Even though CO<sub>2</sub> fertilization is an important factor in the current terrestrial carbon sink, its persistence in the future is uncertain (Houghton, 2007).

Terrestrial carbon sources and sinks vary depending on the region. The separation of atmosphere-land fluxes between the northern hemisphere land and the tropical land is of importance because each region has its own history of land-use change, climate drivers, and impact of increasing atmospheric CO<sub>2</sub> and nitrogen deposition (Friedlingstein et al., 2022). While the overall (ocean and land) carbon fluxes in the northern extratropics were shown to be a sink (Houghton, 2007; Friedlingstein et al., 2022), there are large uncertainties in quantifying the drivers, especially for the global net land CO<sub>2</sub> flux (Arneth et al., 2017; Huntzinger et al., 2017). The distribution between the tropics and high northern latitudes for the atmosphere-to-land fluxes are also uncertain (Baccini et al., 2017; Ciais et al., 2019; Gaubert et al., 2019).

The discrepancies of the net land-atmosphere exchange are large, especially over the northern extratropics. This highlights the difficulty of quantifying complex processes such as CO<sub>2</sub> fertilization and climate change, to name but a few, that determine the net land CO<sub>2</sub> flux (Friedlingstein et al., 2022). In the southern extratropics, the net land flux (consisting of natural as well as land-use components) is approximately neutral, meaning that all carbon uptake in these regions occurs due to the ocean sink. This ocean dominance also means that interannual variability is low (Friedlingstein et al., 2022).

In northern regions, a net land source during the 1980s changed to a net sink during the 1990s (Houghton, 2003). The regrowth of forests after deforestation for wood production led to an accumulation of carbon (Houghton, 2007). It is possible that non-forest ecosystems in these regions also accumulate carbon, although the extent of this is unclear, since an above-ground increase of carbon stocks through woody encroachments can be offset by losses in below-ground carbon stocks (Jackson et al., 2002; Houghton, 2007). Arctic and boreal lands are of considerable interest because of their large reserves of soil carbon and the greater warming expected for high latitudes (Houghton, 2007). The initial greening of these regions was interpreted as increased productivity, which is plausible due to the warming (Myneni et al., 1997). More recent studies, however, show a trend of reduced productivity in some forests after 1990 (Angert et al., 2005; Goetz et al., 2005; Bunn & Goetz, 2006), probably due to more summer droughts (Barber et al., 2000; Lloyd & Fastie, 2002). The deciding factor is whether higher temperatures or, maybe even more importantly, less soil moisture enhance photosynthesis and growth (carbon sink) or whether they lead to more respiration (carbon source). In addition, higher temperatures (and more droughts) go hand in hand with fires, in boreal regions (Kasischke & Turetsky, 2006) as well as in the tropics (Nepstad et al., 1999; Page et al., 2002).

The net fluxes in the tropics are associated with large uncertainties as well (Friedlingstein

et al., 2022). While most estimates indicate an approximately neutral tropical ocean flux, estimates on the net land flux vary, some indicating a net land sink (mainly estimates from dynamic global vegetation models (DGVMs)) to a possible land source. In the tropics, interannual variability is generally highest out of all regions, especially in terms of the land flux (Houghton, 2007; Friedlingstein et al., 2022). The tropics were calculated to be a net source of carbon between 1992 and 1996 (Gurney et al., 2002). The uncertainties in the tropics are high due to a lack of CO<sub>2</sub> sampling stations and the more complex atmospheric circulation (Houghton, 2007). Land-use changes in the tropics are a clear source of carbon to the atmosphere, but the estimates are vague due to uncertainties in deforestation estimates (Fearnside, 2000; DeFries et al., 2002; Houghton, 2003) as well as biomass estimates (Houghton, 2005, 2007).

## 1.2 About extreme events

### 1.2.1 Extreme weather and climate events

Weather and climate extremes are episodes of rare weather conditions. They are commonly defined as the “occurrence of a value of a weather or climate variable above (or below) a threshold value near the upper (or lower) ends of a range of observed values of the variable” (Seneviratne et al., 2012). The occurrence likelihood and magnitude of climate extremes can alter substantially with climate change. This might happen due to a shift in mean conditions, increased variability, a changed shape of occurrence probability or a combination of the above mentioned factors. The disaster risk that arises from extreme events consists of three factors: the weather and climate event, the vulnerability, and the exposure of the society or ecosystem. Unlike the anthropogenic climate change, the natural variability cannot be influenced by humans. However, vulnerability and exposure can be managed through adaptation and mitigation.

### 1.2.2 Compound extreme weather and climate events

Extreme weather and climate events usually happen due to multiple drivers interacting on different spatial and temporal scales which may overwhelm natural or human systems and thus lead to ecological or societal impacts (Zscheischler et al., 2020). Often, impacts from multiple drivers or hazards are amplified in comparison to the simple addition of single impacts (Zscheischler et al., 2018). The concept of compound events was first introduced by the Intergovernmental Panel on Climate Change (IPCC) Special Report on Climate Extremes (SREX, IPCC, 2012) and research on the matter has evolved from there. Since the SREX report, the definition of compound events has also developed and is now generally defined as “a combination of multiple drivers and/or hazards that contributes to societal or environmental risk” (Zscheischler et al., 2018). The goal of compound-event research is to improve predictability and assessment of environmental and societal risks and impacts arising from weather and climate related hazards as well as to develop methods for detection and attribution (Moftakhari et al., 2017; Hendry et al., 2019). It aims at increasing the understanding of key physical processes that contribute to an event, assess associated risks, quantify projected changes, and explore suitable adaptation strategies (Zscheischler et al., 2020). A compound event is typically constituted by four characteristics: modulators, drivers, hazards, and impacts (Zscheischler et al., 2020). The hazard is the climate-related phenomenon that precedes a potential impact, for example, droughts or heatwaves leading to a loss in vegetation productivity. The hazard does not necessarily need to be extreme in the statistical sense, provided that it triggers an impact. The hazards are triggered by one or several climatic drivers, for example, tropical cyclones or cold fronts. Drivers are affected by modulators, for example, low-frequency modes of climate variability like the El Niño-Southern Oscillation. Climate change has the potential to alter all elements of compound

events (Zscheischler et al., 2020). Once the key variables relevant for a specific impact have been identified, it is important to determine the strength of relationships between different causal components (modulators, preconditions, drivers and hazards) to estimate the likelihood of an event (Hao et al., 2018; Tilloy et al., 2019).

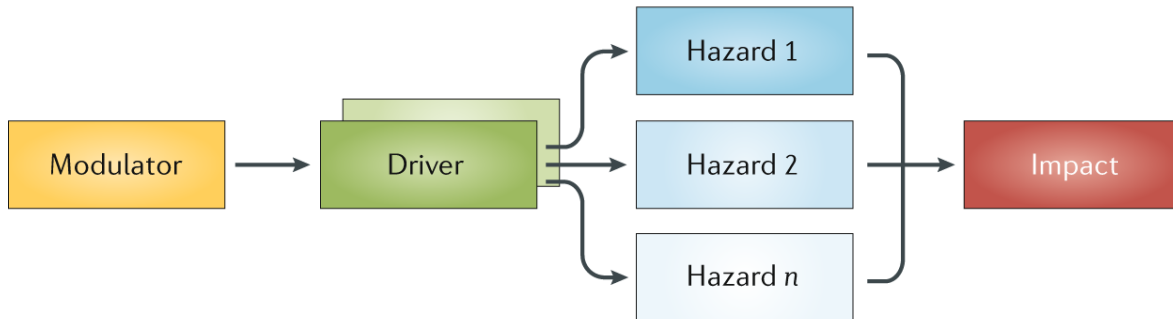


**Figure 1.2:** Schematic for multivariate compound events as classified by Zscheischler et al. (2020). For the events discussed in this thesis, the modulator could be La Niña, the drivers are high temperatures and low precipitation, the hazards are heatwaves and droughts and the impacts are vegetation shifts and changes in carbon uptake. The figure is adapted from Zscheischler et al. (2020), where similar schematics for the other types of compound events can be seen.

In order to provide a coherent framework for compound-event analysis, Zscheischler et al. (2020) presented a typology of compound weather and climate events. The events are grouped into four categories: multivariate (of which a schematic can be seen in Fig. 1.2), preconditioned, temporally compounding, and spatially compounding. A multivariate event refers to the co-occurrence of multiple climate drivers and/or hazards in the same location which lead to an impact. Multiple drivers can cause one or more hazards or a single driver can cause multiple correlated hazards. One example for such an event are co-occurring low precipitation and high temperature extremes, namely concurrent droughts and heatwaves. This is the type of compound event focused on in this thesis. A preconditioned event describes an event where one or more hazards only cause an impact because of a pre-existing condition. An example for a preconditioned event is a false spring, where ecosystems have a high activity due to higher temperatures (the precondition) at the end of winter and thus the impact is larger when it is followed by a frost event (the hazard) in spring (Zscheischler et al., 2020). Temporally compounding events refer to a succession of hazards that affect a given geographical region, leading to, or amplifying, an impact when compared to a single hazard. The hazards are promoted by one or more drivers. A much studied example of a temporally compounding event is the temporal clustering of extratropical and tropical cyclones. Spatially compounding events occur when multiple connected locations are affected by the same or different hazards within a limited time window, thereby causing an impact (Zscheischler et al., 2020). The hazards and hazard drivers are often caused by a modulator (Steptoe et al., 2018), which creates a physical link between the different locations. An example for such an event is the global food system, wherein synchronous crop failure due to spatially co-occurring hazards poses a potential threat to food security (Singh et al., 2018; Mehrabi & Ramankutty, 2019). The impact of multiple simultaneous hazards can also be increased due to societies' inability to respond to them, as can be the case, for example, with many co-occurring wildfires. The above classifications are comprehensive, but of course not all events fit perfectly into one category. Some might fit into multiple categories, like the hot and dry summer in Texas in 2011, which fits into the multivariate event, but also into the preconditioned category, since an earlier precipitation deficit amplified the magnitude of the heatwave and drought via land-atmosphere feedbacks (Berg et al., 2015; Quesada et al., 2012). Determining the boundaries between preconditioning and temporally compounding events is also often challenging.

Anthropogenic climate change is expected to alter the distribution of practically all climate variables as well as some of their dependencies (Zscheischler & Seneviratne, 2017). This can happen in different ways as schematically shown in Figure 1.3. It is therefore expected that trends can be seen in the likelihood of compound events on timescales of multiple decades. Compound event research is necessary to disentangle the effects of climate change on the different elements of a compound event, as well as the spatial and temporal scales of events and their spatio-temporal dependencies. This is a challenging task, especially due to the small sample size, since compound extremes are by definition rare and have a low signal-to-noise ratio (Zscheischler et al., 2020). With rising temperatures due to climate warming, the frequency of compound hot and dry conditions is also expected to increase, even in regions where precipitation trends are negligible (Sarhadi et al., 2018) or even positive (Coffel et al., 2019).

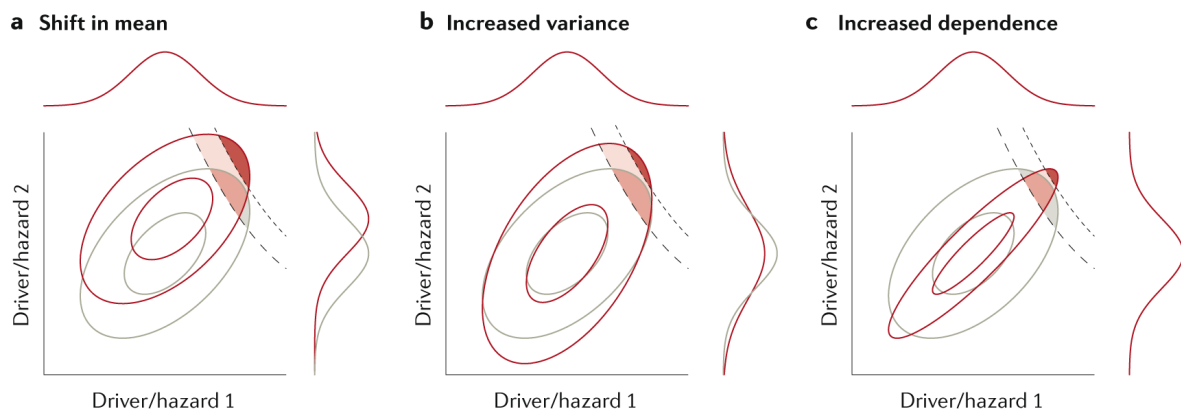


**Figure 1.3:** Potential effects of climate change on drivers of compound events. These changes (shifts in mean, increased variance, and increased dependence) can affect one or multiple drivers. The dashed line indicates a threshold with moderate impact, the dotted line indicates a threshold that is only exceeded under climate change conditions. These patterns can occur in combination and have an effect on both frequency and magnitude of the compound event. Taken from Zscheischler et al. (2020).

### 1.3 Hot-dry extremes and the carbon cycle

Exploring the effects of hot-dry extremes on the carbon cycle is still challenging (Sippel et al., 2018). Firstly, there is the unclear issue of definition. Secondly, the sample size of observed extremes is by definition small. Thirdly, many different approaches are being applied, from local experiments to global remote sensing and modelling. Impacts on the carbon cycle depend not only on the intensity of the extreme but also on the initial ecosystem state when the extreme happens (e.g. soil moisture or snow anomalies before a drought, Buermann et al., 2013; Papagiannopoulou et al., 2017), the timing, and duration (Denton et al., 2017; De Boeck et al., 2011). This includes sequences of events (Jentsch et al., 2011), drought-heat interactions (Seneviratne et al., 2010), and other interactions with climatic trends (Beierkuhnlein et al., 2011), which are all types of compound events. Depending on the initial state, a climatological extreme might not lead to an impact in an ecosystem while vice versa an impact might occur following statistically non-extreme climate conditions (Galvagno et al., 2013; Zscheischler et al., 2016; Sippel et al., 2018; Vogel et al., 2021). Spring water savings due to elevated  $\text{CO}_2$ , for example, might reduce transpiration and thus alleviate summer drought impacts to some extent (Lemordant et al., 2016). The timing of the onset of an extreme is crucial for the severity of the impact. For example, the impacts of droughts and heatwaves on grasslands seem to be largest at very early development stages and in summer (Denton et al., 2017; Darenova et al., 2017). The duration also plays a role. However, these different sensitivities to timing and duration might also lead to antagonistic mechanisms, as shown by von Buttlar et al. (2018). Different types of



important for post-drought recovery. When drought or heat stress exceeds a threshold, mortality can occur. This is especially important for forests (Allen et al., 2010) due to their high carbon storage and long recovery time. Under such conditions, the plants have to choose between carbon starvation and the disruption of their water transport system (McDowell et al., 2011) and it seems that carbon starvation occurs rather rarely (Hartmann et al., 2013). To account for the importance of timing, the focus of this thesis lies on the months when vegetation is most productive for the onset of extremes. However, the importance of antecedent conditions as well as legacy effects are not taken into consideration if they go beyond a calendar year, since the sampling procedure does not consider years which are climatologically consecutive.

Different vegetation types react differently to extremes, having individual growth patterns and thus distinct C allocation responses to extreme conditions (Larcher, 2003). For example, forests do not show a significant change in canopy characteristics during a heatwave, although GPP is reduced, while grasslands respond fast through canopy changes (Zhang et al., 2016; Teuling et al., 2010). Grasses generally react faster to drought conditions, because trees have deeper roots with which they can reach deep soil water for a longer period of time (Zhang et al., 2016). In remote sensing based studies, the question arises whether they simply do not detect the drought stress in forests because forests do not change their canopy characteristics as fast as grasslands (Zhang et al., 2016). Even between different grasses exists a different resilience to extremes. C4 grasses are usually better adapted to higher temperatures and are thus more drought resistant than C3 grasses (Taylor et al., 2014). Differences also exist among different tree species. Since the work presented in this thesis only distinguishes between trees and grasses, the differences between species will not be discussed further.

Extreme impacts on vegetation carbon depend on the interplay between photosynthesis and carbon release processes (Ahlström et al., 2015; Zeng et al., 2005). The largest effects on GPP occur in semi-arid regions (Zscheischler et al., 2014c). Generally, regions can be separated into “energy-limited” and “water-limited” evapotranspiration regimes. The highest vulnerability to extremes and thus GPP loss occur in regions that are transitional between water-limited and energy-limited regimes, mainly semi-arid regions. The main drivers of GPP loss in such regions have been associated with water scarcity, fire, or heat and thus show the importance of drought-heat events in these regions (Seneviratne et al., 2010; Zscheischler et al., 2014a).

Plants may adapt carbon allocation strategies to overcome resource limitations (Bloom et al., 1985; Denton et al., 2017; Sevanto & Dickman, 2015). Higher CO<sub>2</sub> levels, also known as CO<sub>2</sub> fertilization, have a positive effect on plant photosynthesis and leaf area in the absence of extreme conditions (Zhu et al., 2016; Obermeier et al., 2017), but they also have an indirect effect during droughts because they reduce stomatal opening and therefore transpiration, which saves water (Roy et al., 2016). However, it is unclear whether this phenomenon increases or decreases temperatures (Lemordant et al., 2016). It is difficult to completely understand these different effects, in an experimental setup as well as in the modelling world, because each setup has its limitations (experiments ignore the coupling with the boundary layer and models have certain assumptions on stomatal behaviour). Despite these considerations, the benefits of elevated CO<sub>2</sub> might be limited under high temperatures or very dry conditions (Obermeier et al., 2017). Additionally, as mentioned above, the combined effects of two drivers are not simply additive (Dieleman et al., 2012) and thus pose a challenge for model development and evaluation.

## 1.4 The challenges of disentangling compound drivers

The dependence between two variables, for example, temperature and precipitation, as is the case in this study, can be represented statistically using multivariate probability distribution functions, the most common of which is the correlation coefficient (Zscheischler et al., 2020).

However, choosing the appropriate temporal and spatial scales for an event is challenging. A good start to understand the potential impacts of compound events are process-based model experiments with which it is possible to test a wide range of hazard scenarios. Once the drivers are modelled and understood, they need to be mapped to potential impacts (Zscheischler et al., 2020). This is usually done using predefined hazard scenarios, which represent combinations of events that are of interest. Choosing these hazards is somewhat subjective and depends on the event, expert judgement, and available data. In this case, we use the so-called “and” hazard scenario for the compound event which corresponds to concurrent exceedance of two variables above a predefined threshold for the compound scenario (Salvadori et al., 2016; Zscheischler & Seneviratne, 2017; Zscheischler et al., 2014d). For the single event scenarios, we use the “or” approach, where either one or the other variable is exceeding its threshold.

Since compound events are typically rare by design, assessing their occurrence probability is difficult (Zscheischler et al., 2020). A robust analysis requires many samples. Usually, observations do not include enough data points, either in time or in space, for a robust analysis. In addition, field experiments are difficult to set up and it is hard to control all variables, especially in a compound setup. In contrast, the modelling setup allows for an easily controlled environment, where it is possible to change variables independently or combined and rerun the model to get different but comparable time series of sufficient length. The modelling approach also offers different strategies with advantages and disadvantages. Adding artificial extremes to an existing reanalysis time series, for example, leads to physically inconsistent time series. Large ensembles or reanalysis data are often pre-industrial or transient, meaning they change over time, which makes the analysis of the influence of single drivers complicated. A good approach to generate long, physically consistent and temporally stable time series is through large-ensemble model experiments (Posch et al., 2020).

## 1.5 Dynamic global vegetation modelling using large ensemble simulations

First attempts at modelling vegetation have been made in the 1970s (Botkin et al., 1972). Two basic approaches have been developed to model vegetation responses to a changing climate: static (time-independent) and dynamic (time-dependent, Prentice & Leemans, 1990). These are biogeographical and biogeochemical models, because the potential distribution of vegetation depends not only on climatic variables such as temperature, moisture or atmospheric CO<sub>2</sub> and available nutrients, but also on environmental gradients such as topography and geology (Woodward & Woodward, 1987; Stephenson, 1990; Prentice et al., 1992). The dynamic biogeographical model incorporates explicit representation of key ecological processes such as establishment, tree growth, competition, death and nutrient cycling (Peng, 2000). This type of model was designed to capture the transient response of vegetation to a changing environment (Shugart Jr & West, 1980; Shugart, 1984). Over the years, the simple model from the 1970s has been developed and adapted for a range of different biomes (Peng, 2000).

The vegetation models in this thesis were driven by climate data from EC-Earth’s large ensemble simulation. Large ensemble climate model simulations are valuable tools that can be used to quantify and separate the internal variability of the climate system and its response to external forcing (Maher et al., 2021). They typically consist of a set of simulations from a single model, forced with identical external forcings but starting from different initial conditions (Maher et al., 2021). Large ensemble simulations can be used to investigate internal variability and dependencies (Maher et al., 2021), but they can also be used as forcings for impact modelling. They provide the possibility to generate a lot of data, which deals with the problem of data scarcity in observations, providing coherent and standardised data. This allows to identify and

robustly sample by definition rare extreme events, which have potentially large impacts on society and the environment (Haugen et al., 2018; Suarez-Gutierrez et al., 2018). Extremes and also compound extremes are dynamically altered under climate change, which poses a major challenge. Large ensemble simulations can be used to analyse the non-linear response to multiple meteorological drivers and land surface responses (Zscheischler et al., 2018) by means of spatially explicit and process-based models.

## 1.6 Motivation and Goal of this thesis

It is clear that the terrestrial carbon sink plays an important role in the global carbon cycle, but its development in the future is uncertain (Friedlingstein et al., 2022). Especially under extreme events, vegetation which currently acts as a sink may be turned into a reduced sink or even a source of CO<sub>2</sub>. While many studies have investigated the effects of single extreme events, compound event studies are fairly new (they only emerged about ten years ago). Despite the increased complexity when analyzing compound events compared to univariate events, their importance in extreme event research is evident (Zscheischler et al., 2018, 2020).

This study aims at investigating the development of the natural terrestrial carbon cycle as well as vegetation distribution under extreme events. The focus lies on compound hot and dry extremes, which are amongst the most harmful extreme events for ecosystems (Sippel et al., 2018). To reach this goal, dynamic global vegetation models were forced with hypothetical scenarios sampled from a large ensemble climate model simulation.

Chapter 2 focuses on the input data used throughout this thesis, explains the sampling method, and quantifies the sampled scenarios. Chapter 3 details the results obtained by running the dynamic global vegetation model LPX-Bern and focuses on the effects on different biomes. Finally, Chapter 4 presents a comparison between six dynamic vegetation models and focuses on their agreements and differences.



## Chapter 2

# A climate database with varying drought-heat signatures for climate impact modelling

Elisabeth Tschumi, Sebastian Lienert, Karin van der Wiel, Fortunat Joos and Jakob Zscheischler

Published in *Geoscience Data Journal*, 2021;9:154-166.

### Abstract

Extreme climate events such as droughts and heatwaves can have large impacts on the environment. Disentangling their individual and combined effects is a difficult task due to the challenges associated with generating controlled environments to study differences in their impacts. One approach to this problem is creating artificial climate forcings with varying magnitude of univariate and compound extremes, which can be applied to process-based impact models. Here, we propose and describe a set of six 100-year long climate scenarios with varying drought-heat signatures that are derived from climate model simulations whose mean climate is comparable to present-day climate conditions. The changes in extremes are most notable in the three months in which vegetation activity is highest and where arguably hot and dry extremes may have the largest impacts. Besides a control scenario representing natural variability (Control), one scenario has neither heat nor drought extremes (Noextremes), one has univariate extremes but no compound extremes (Nocompound), one has only heat extremes but few droughts (Hot), one has only droughts but few heatwaves (Dry), and one has many compound heat and drought extremes (Hotdry). These scenarios differ only moderately in their global mean climate (about 0.3 °C in temperature and 6 % in precipitation) and do not contain any long-term trends. The data are provided on a daily timescale over land (except Antarctica and parts of Greenland) on a regular 1° × 1° grid. These scenarios were constructed primarily to investigate the impact of varying drought-heat signatures on vegetation and the terrestrial carbon cycle. However, we believe that they may also prove useful to study the differential impacts of droughts and heatwaves in other areas such as the occurrence of wildfires or crop failure. The data described here can be found on zenodo (<https://doi.org/10.5281/zenodo.4385445>, Tschumi et al. (2020)).



This work is distributed under the Creative Commons Attribution 4.0 License.  
Please visit <https://creativecommons.org/licenses/by/4.0/> to see the licence.

## 2.1 Introduction

Climate extremes such as droughts, heatwaves, storms and floods are important stressors to the natural environment. They can lead to large and devastating impacts on ecosystems and society (IPCC, 2012; Reichstein et al., 2013; Frank et al., 2015; Tschumi & Zscheischler, 2020). Extreme impacts in turn may also be caused by meteorological conditions that are not necessarily extreme in a statistical sense (Zscheischler et al., 2016; Vogel et al., 2020; van der Wiel et al., 2020). In many cases, impacts are caused by multiple extremes or a combination of anomalous meteorological drivers (Flach et al., 2017), also referred to as compound events (Zscheischler et al., 2018, 2020). The multiple drivers behind compound events are often correlated (Leonard et al., 2014; Zscheischler & Seneviratne, 2017). Furthermore, the combined impact of compound extremes can be more severe than a simple linear combination of univariate extremes, for instance, the effect of drought and heat on terrestrial carbon uptake (Zscheischler et al., 2014b) or crop yields (Cohen et al., 2020; Ribeiro et al., 2020). Hence, quantifying the differential impact of compound versus univariate extremes and the relevance of driver dependence is important for a better understanding of climate risks.

The land biosphere plays an important role in the global carbon cycle, taking up between a quarter and a third of anthropogenic CO<sub>2</sub> emissions (31% in the last decade according to the most recent estimate of the Global Carbon Project, Friedlingstein et al. 2020). Different factors enhance this land sink such as increased atmospheric CO<sub>2</sub> concentrations and warmer temperatures in the high latitudes, which increase the growing season length in the high latitudes (Zhu et al., 2016). However, at the local scale, vegetation productivity can be limited by factors such as water availability, temperature conditions, light conditions, availability of nutrients, and CO<sub>2</sub> concentrations (Schlesinger & Bernhard, 2013). These factors can vary greatly, especially during extreme climate conditions.

The effect of climate extremes on vegetation and the terrestrial carbon cycle can be studied from different perspectives, for instance based on (i) lab or field experiments (De Boeck et al., 2011; Beier et al., 2012; Song et al., 2019), (ii) observational data such as long-term forest observations (Anderegg et al., 2013a) and local measurements of carbon exchange (Ciais et al., 2005; von Buttlar et al., 2018; Pastorello et al., 2020), (iii) indirect estimates from satellite observations (Ciais et al., 2005; Zhao & Running, 2010; Zscheischler et al., 2013; Stocker et al., 2019) and (iv) dynamical vegetation models (Ciais et al., 2005; Zscheischler et al., 2014a,b,c,d; Rammig et al., 2015; Xu et al., 2019; Bastos et al., 2020a; Pan et al., 2020). Hereby, process-based vegetation models allow for the development and testing of novel hypotheses in a controlled environment and at the global scale. Arguably, drought and heat are among the most damaging hazards to terrestrial vegetation (Allen et al., 2010; Reichstein et al., 2013; Zscheischler et al., 2014b; Frank et al., 2015; Sippel et al., 2018). However, differentiating impacts between drought and heat alone and compound drought and heat remains a challenging task. Despite large model uncertainties, it is widely acknowledged that drought and heat extremes will increase in frequency and severity in many land regions in the future (Seneviratne et al., 2012). Though it is still uncertain exactly how these increases will affect the terrestrial biosphere, there are concerns they might substantially reduce the current terrestrial carbon sink (Reichstein et al., 2013).

Temperature and precipitation are strongly correlated in most land regions in the warm season (Madden & Williams, 1978; Trenberth & Shea, 2005) and this dependence controls the occurrence of compound drought and heatwave events (Zscheischler & Seneviratne, 2017). Similar to regional biases in mean temperature and precipitation, climate models can have biases in the temperature-precipitation dependence, i.e. in the correlation between temperature and precipitation. Given the relevance of drought and heat for carbon dynamics and in particular the disproportional impacts of compound drought and heat (Allen et al., 2010; Zscheischler et al., 2014d; von Buttlar et al., 2018), differences in the dependence between temperature and precipitation in the climate forcing might affect estimates of carbon dynamics and uptake. In particular, Earth system models collected in the coupled model intercomparison projects (e.g. CMIP5 Taylor et al. (2012)) show a substantially stronger dependence than the forcing that is used in the regular carbon budget estimates provided by the Global Carbon Project (Friedlingstein et al., 2020) in the Southern Hemisphere (Zscheischler & Seneviratne, 2017). It is unclear whether these differences originate from an overestimation of the dependence in climate models or a lack of observational constraint in observation-based gridded climate data sets. However, independent of a potential bias with respect to observations, differences in this dependence across climate models may contribute to uncertainties in carbon-cycle climate feedbacks with ongoing climate change (Friedlingstein et al., 2014).

Disentangling the effects of varying temperature-precipitation dependence and the associated occurrence

of compound drought and heat on terrestrial carbon dynamics is challenging, as non-stationarity and the use of different vegetation models in different Earth system models confound the assessment. Here, we present a range of climate scenarios that have been developed specifically to study the differential effects of single or compound drought and heat events and their impacts on vegetation and the terrestrial carbon cycle with dynamical vegetation models. The scenarios span a period of 100 years and all have a similar mean climate but differ in their occurrence frequency and intensity of droughts, heatwaves and compound drought and heatwave events during the peak of the growing season. Although the scenarios are somewhat tailored to study carbon dynamics, they may also be used to explore the effects of drought and heat on other climate impacts, for example, wildfires or crop failure.

## 2.2 Data description

This section describes the climate model simulations from which the scenarios were sampled. We further provide an assessment of biases in precipitation and temperature and show that our climate simulations with approximately constant forcing result in a stationary vegetation composition over time. Finally, we describe how we sampled scenarios with different drought-heat signatures.

### 2.2.1 EC-Earth climate simulations

The data for the drought-heat scenarios were sampled from a large ensemble climate modelling experiment. This experiment consisted of 2000 years of simulated present-day climate data, which were created with the fully-coupled global climate model EC-Earth (v2.3, Hazeleger et al., 2012). The large ensemble was built out of 400 short five-year runs, which were unique in initial condition and/or stochastic physics seed. EC-Earth combines atmospheric, oceanic, land, and sea-ice model components and simulates the global climate including feedbacks between, for example, land and atmosphere. The horizontal resolution in the atmosphere for the simulations was T159 (approximately  $1.1^\circ$ ). For creating the scenarios, the climate model output has been bilinearly interpolated to a regular  $1^\circ \times 1^\circ$  grid. All analysis was based on daily data.

In the large ensemble experiment, we defined the ‘present-day climate’ by means of the observed global mean surface temperature over the years 2011-2015. We selected the five year EC-Earth model period (2035-2039) that minimized the difference between simulations and observation of the global mean surface temperature from sixteen transient climate runs (1861-2100, RCP8.5). Each of these sixteen runs were then used, at the start of the selected period, as an initial condition for an ensemble of 25 members of five years each. By choosing different seeds for the atmospheric stochastic perturbations (Buizza et al., 1999) each of these members developed unique weather. Together this resulted in  $16 \times 25 \times 5 = 2000$  years of simulated present-day climate data. More details on the large ensemble climate model experiment setup are provided in Van der Wiel et al. (2019c). Note that, within the ensemble, the influence of forced climate change is small. We therefore assume that all variability in the data set is due to natural variability in the climate system.

### 2.2.2 Regional biases in annual temperature and precipitation

Despite the annual mean surface temperature being unbiased at the global scale by experimental design (Section 2.2.1), model biases may exist at the regional and seasonal scale. We therefore compare a random 100 year sample from the EC-Earth data to a 30-year climatology of the climate data from the Climate Research Unit (CRU TS3.26) (Harris et al., 2014). We compared against the time period 1988-2017, though using a shorter time period of 2011-2015 (the same time period as represented by EC-Earth) results in very similar biases. Generally, averaged over land (excluding Antarctica and most of Greenland), temperature differs by  $-0.5^\circ\text{C}$  and precipitation by 7 % compared to CRU. However, biases can be relatively large at the regional scale. In the tropics (between  $23.5^\circ\text{S}$  and  $23.5^\circ\text{N}$ ), EC-Earth has a cold bias of  $-1.8^\circ\text{C}$  compared to CRU (Fig. 2.1a). In the extratropics, EC-Earth has a small warm bias of about  $0.2^\circ\text{C}$  on average, with most of this bias being concentrated in the very high latitudes and nearly no bias in the mid-latitudes (Fig. 2.1a). With respect to annual precipitation, many land regions have a wet bias in EC-Earth compared to CRU (Fig. 2.1b). The extratropics have a wet bias of about 43.5 %. In the tropics, some regions are drier (e.g., the Amazon and Indonesia) while others have very little bias in

EC-Earth compared to CRU (tropical Africa). Note, however, that observation-based estimates differ strongly in their absolute precipitation amounts (Sun et al., 2018).

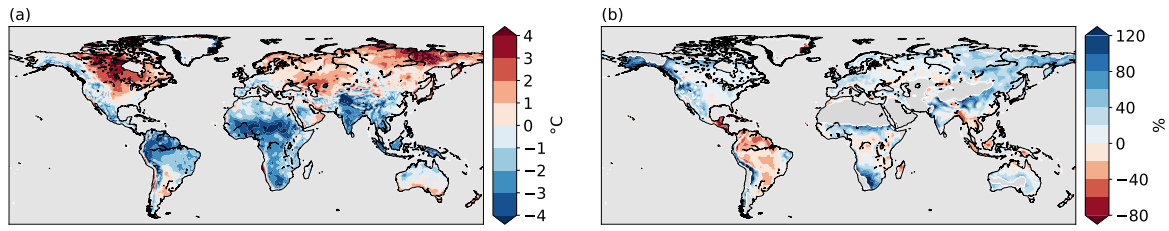


**Figure 2.1:** Biases in EC-Earth simulations with respect to observation-based data from CRU. (a) Difference in annual mean temperature between EC-Earth and CRU in °C. (b) Relative difference in annual precipitation between EC-Earth and CRU in %. The time period 1988-2017 was used for CRU and randomly sampled 100 years (representing 2011-2015) for EC-Earth. The land regions depicted in grey in (b) are desert regions with a mean annual precipitation of less than 250 mm in the CRU data set and were excluded in the maps to avoid dividing by very small numbers.

### 2.2.3 LPX-Bern stability

LPX-Bern v1.4 (Lienert & Joos, 2018) is a Dynamic Global Vegetation Model (DGVM) based on Lund-Potsdam-Jena (LPJ) model (Sitch et al., 2008). The model features coupled water, nitrogen, and carbon cycles and represents different types of vegetation using Plant Functional Types (PFTs). Here, only natural vegetation is considered, which is internally represented by eight tree PFTs and two herbaceous PFTs competing for resources and adhering to bioclimatic limits. In this study, daily temperature, precipitation, and short-wave radiation are provided to the model. Additionally, the model uses information on the soil type (Wieder et al., 2014), CO<sub>2</sub> concentration in the atmosphere at 1901-level (296.8 ppm), and nitrogen deposition (NMIP, Tian et al. (2018)). A spin-up of 1500 years (recycling the first 30 years of the climate forcing) was performed to make sure all carbon pools are in equilibrium.

To make sure that the climate forcing is appropriate for climate impact modelling, we assessed whether LPX-Bern simulations are stable over the course of the entire 2000 years of EC-Earth data. Except for a slight decreasing trend in tropical broadleaved evergreen trees (TrBE), the global fraction of each of the ten PFTs present in LPX-Bern shows no apparent trends over the 2000 years (Fig. 2.8). Hence, despite relatively large biases at the regional scale (Section 2.2.2), LPX-Bern seems to be stable using input from this global climate model. This gives us confidence to use this control simulation as a baseline to estimate the effect of climate scenarios with different drought-heat signatures. We can assume that any trends and non-stationarities in the LPX-Bern output will be due to the scenarios. In addition, this test run was used for the sampling described in Section 4.2.1.

### 2.2.4 Scenario sampling

This section describes the steps taken to create climate scenarios with varying drought-heat signatures. We sampled 100-year long scenarios from the original 2000 years of EC-Earth data. The selection of the different scenarios was based on temperature and precipitation values during the time of the year where the vegetation is most active. Arguably, the vegetation is most vulnerable to climate extremes during the growing season (Orth et al., 2016; Zscheischler et al., 2017). Therefore, for the scenario creation we focused on the three months around the most productive month in the climatology. We first identified the most productive month at each pixel, that is, the month with the highest net primary production (NPP) in the mean seasonal cycle of NPP, as simulated by LPX-Bern (Section 2.2.3). The month of maximum NPP differs from pixel to pixel, depending on the geographical location (Fig. 2.9). For instance, in the northern mid and high latitudes, July is typically the most productive month whereas it is January or February in most of the southern mid and high latitudes. In contrast, in the tropics and subtropics, the most productive month varies quite strongly across locations, depending on the dominant rainy season (Wang & Ding, 2008).

We selected the six different scenarios for each pixel separately based on mean temperature and precipitation over the three months around the month of highest vegetation productivity: Control,

Noextremes, Nocompound, Hot, Dry, and Hotdry. Years contributing to the scenarios were sampled based on quantiles of the three month temperature and precipitation averages as indicated in Figure 2.2, where the quantiles were computed based on the full 2000-year EC-Earth simulation. If more than the required number of years fall into the quantiles in question, a random selection was performed. If less years than necessary were available, some randomly chosen years were selected multiple times.

- For Control, 100 years were sampled randomly out of the 2000 years (Fig. 2.2a).
- For Noextremes, 100 years were sampled for which temperature and precipitation are both within the 40<sup>th</sup> to 60<sup>th</sup> percentile (Fig. 2.2b).
- For Nocompound, 100 years were sampled for which temperature and precipitation do not exceed the 85<sup>th</sup> percentile in any direction at the same time (Fig. 2.2c).
- For Hot, 50 years were sampled for which temperature exceeds the 85<sup>th</sup> percentile and precipitation is within the 40<sup>th</sup> to 60<sup>th</sup> percentile and 50 years were sampled randomly from the rest (Fig. 2.2d).
- For Dry, 50 years were sampled for which precipitation lies below the 15<sup>th</sup> percentile and temperature is within the 40<sup>th</sup> to 60<sup>th</sup> percentile and 50 years were sampled randomly from the rest (Fig. 2.2e).
- For Hotdry, 50 years were sampled for which temperature lies above the 85<sup>th</sup> percentile and precipitation lies below the 15<sup>th</sup> percentile at the same time and 50 years were sampled randomly from the rest (Fig. 2.2f).

The reason for only selecting 50 years from the extreme quantile for the Hot, Dry and Hotdry scenarios is twofold. Firstly, for many pixels, not a huge amount of years fall into the extreme quantiles. Sampling only 50 years from there reduces the numbers of times a year is re-sampled. Secondly, the mean climatology is kept more similar to the other scenarios if only half the years were sampled with extreme conditions and the other half from the rest.

This method of scenario creation, for each pixel separately, destroys any spatial coherence, so that the climate in a pixel is not correlated to the climate in nearby pixels. Furthermore, due to the sampling of individual years, there are always slight discontinuities between 31 December and 1 January in the climate forcing. The same is true for leap years, since all leap days (29 February) were removed.

### 2.2.5 Available variables

To allow for impact modelling for a wide range of sectors we provide temperature variables (mean, minimum, maximum), precipitation, radiation (short- and longwave downward radiation and shortwave net radiation) and wind (zonal (eastward,  $u$ ) and meridional (northward,  $v$ ), see Table 2.1) at daily timescales. For this study, we only analyzed mean temperature and precipitation to quantify differences in the occurrence of droughts and heatwaves between the scenarios. All variables are available at a regular  $1^\circ \times 1^\circ$  grid over land, except Antarctica and large parts of Greenland. Leap days were removed, so there are  $365 \times 100$  time steps for each scenario. Whenever global means are given, they are area-weighted means over all land cells except Antarctica and Greenland. The data can be accessed via zenodo (<https://doi.org/10.5281/zenodo.4385445>, Tschumi et al. (2020)).

## 2.3 Scenario characterization

A key goal of the design of the different scenarios is that they vary in their characteristics of climate extremes, in particular droughts and heatwaves, while differing only little in their mean climate conditions. The scenarios differ moderately in their global land mean temperature and annual precipitation sums and all scatter closely around global CRU averages (Fig. 2.3). Temperature differences are in the order of  $0.3^\circ\text{C}$  and precipitation differences are up to 6 %, which corresponds to about one and two standard deviations of the inter-annual variability in CRU, respectively. The precipitation differences between scenarios and with respect to CRU are thus noticeably smaller than the difference across different precipitation data sets (Sun et al., 2018). Spatially explicit differences illustrate that the difference in annual mean temperature is mostly below  $1^\circ\text{C}$  for the Hot and Hotdry scenario at the regional scale, and much smaller for the other scenarios (Fig. 2.10). Similarly, the difference in annual precipitation at the regional scale is mostly below 20 % for the Hot, Dry and Hotdry scenario and much smaller for the others (Fig. 2.11).

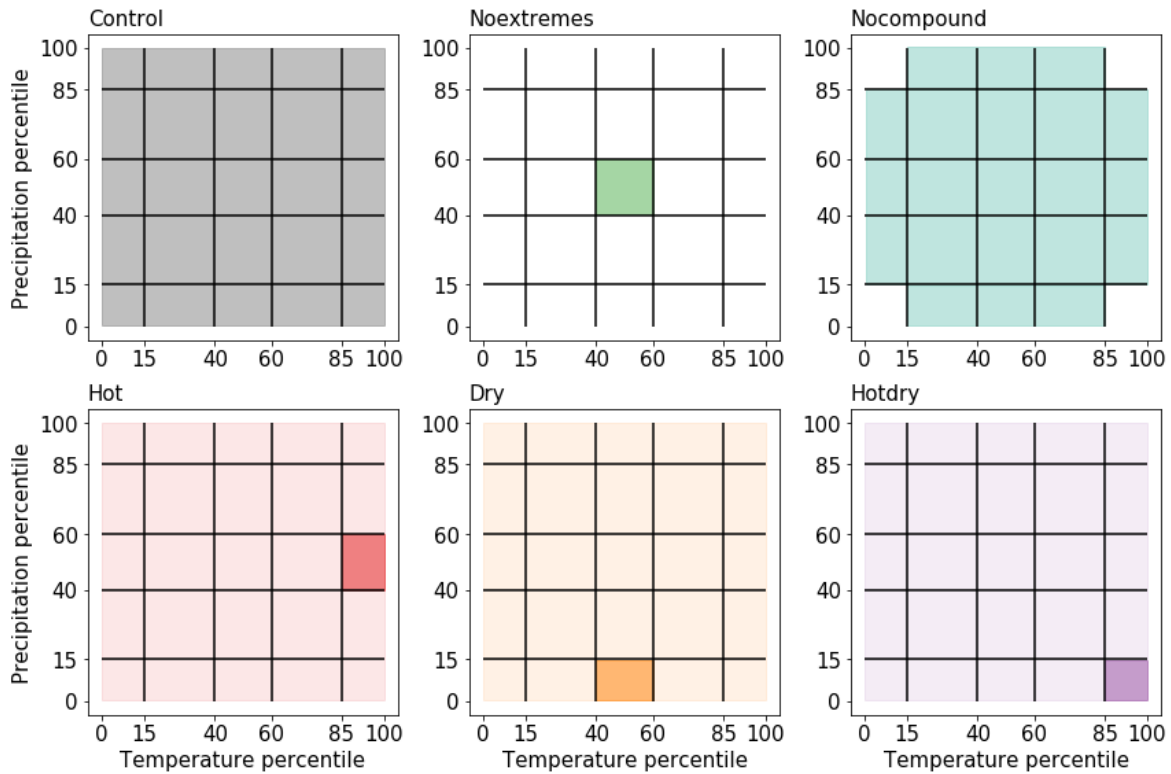


**Figure 2.2:** Sampling of scenarios from their respective quantiles, details provided in the main text. Two colouring shades (for Hot, Dry, and Hotdry) means 50 years were sampled from each shade. The quantiles were calculated based on the full 2000 years EC-Earth data.

### 2.3.1 Heatwaves

Temperature extremes were quantified based on cooling degree days (CDD). Being aware of the multitude of heatwave indices (Perkins, 2015) we chose this index because it is an integrative measure for cumulative magnitude, frequency and duration of the heatwaves (Laufkötter et al., 2020). Choosing another index would result in different numbers but likely not affect the ranking between the different scenarios. Heating and cooling degree days are generally used in the energy sector to determine the energy needed to heat or cool a building, which is directly proportional to the number of heating or cooling degree days. Here, we calculated CDD as the sum of all temperature exceedances over a high threshold, in this case, the 90<sup>th</sup> percentile of the control scenario at each pixel, using daily temperature data:

$$CDD = \sum_{i=1}^N (T_i - T_{90}) I_{T_i > T_{90}} \quad (2.1)$$

Here,  $i$  indicates daily time steps,  $N$  is the total number of time steps ( $100 \times 365 = 36500$  days),  $T_{90}$  denotes the 90<sup>th</sup> percentile of the local temperature time series and  $I$  denotes the indicator function, which is 1 if  $T_i > T_{90}$  and 0 otherwise.

In the Control scenario, CDD varies between close to zero and about 100 °C per year, with higher numbers for regions further away from the equator, which can be explained by the higher temperature variability in extratropical regions compared to the tropics (Fig. 2.4a). The Noextremes (global area-weighted mean relative difference between Noextremes and Control: 0.06 %), Nocomound (global mean difference 6.9 %) and Dry (global mean difference 4.7 %) scenarios are very close to the Control in terms of CDD (Fig. 2.4b, c, e). In contrast, in the Hot (global mean difference 42.7 %) and Hotdry (global mean difference 47.9 %) scenarios the CDDs increase by up to 160 %, with the increases being slightly larger in the Hotdry scenario.

**Table 2.1:** Available variables with a daily time step over land (except Antarctica and large parts of Greenland) on a  $1^\circ \times 1^\circ$  grid.

Variable	Variable name	Unit	Description
Mean temperature	tas	$^\circ\text{C}$	Mean daily near-surface (2 m) temperature
Minimum temperature	tasmin	$^\circ\text{C}$	Minimum daily near-surface (2 m) temperature
Maximum temperature	tasmax	$^\circ\text{C}$	Maximum daily near-surface (2 m) temperature
Precipitation	pr	$\text{mm d}^{-1}$	Daily precipitation
Shortwave net radiation	sw	$\text{J d}^{-1} \text{m}^{-2}$	Shortwave net radiation
Shortwave downward radiation	swd	$\text{J d}^{-1} \text{m}^{-2}$	Shortwave downward radiation
Longwave downward radiation	lwd	$\text{J d}^{-1} \text{m}^{-2}$	Longwave downward radiation
Zonal wind	uas	$\text{m s}^{-1}$	Near-surface (10 m) eastward wind
Meridional wind	vas	$\text{m s}^{-1}$	Near-surface (10 m) northward wind

### 2.3.2 Droughts

For the quantification of droughts we rely on the Standardized Precipitation Index (SPI) (McKee et al., 1993), one of the most widely used drought indicators. We use a three-month timescale based on monthly precipitation values and calculate SPI with the R package SPEI (Vicente-Serrano et al., 2010). The SPI is computed by fitting the three-month running mean monthly precipitation data to a Gamma distribution for each calendar month. The fitted Gamma distribution is then transformed to a standard normal distribution (McKee et al., 1993). We investigate how the scenarios differ in their occurrence likelihood of severe droughts, defined as  $\text{SPI} < -1.5$ . Given that SPI is standard normally distributed, the occurrence probability of severe droughts is about 6.7 %, which is captured well by most locations in the Control, except in the Sahara desert (Fig. 2.5a). There is a slight reduction in number of severe droughts for the Noextremes scenario of -22.5 % in the global mean (Fig. 2.5b), whereas the Nocompound (-4.7 %) and the Hot (3.4 %) scenario are fairly similar to the control (Fig. 2.5c, d). The Dry (54.1 %) and Hotdry (89.2 %) scenario show large and very large increases in severe drought occurrence, up to 200 % with respect to the control (Fig. 2.5e, f). We repeated the drought analysis using the Standardized Precipitation-Evapotranspiration Index (SPEI) (Vicente-Serrano et al., 2010) instead of SPI. The SPEI also takes the effects of evapotranspiration into account and thus requires precipitation as well as temperature for its calculation (calculated here with the Hargreaves function based on monthly minimum/maximum temperature and precipitation (Vicente-Serrano et al., 2010)). The spatial patterns are similar overall, though the changes are larger in particular for the Hotdry scenario (Fig. 2.12).

### 2.3.3 Compound extremes

Temperature and precipitation are negatively correlated during the most productive months in most regions of the world with a global mean Pearson correlation coefficient of -0.47 in the control scenario (Fig. 2.6). This inter-annual correlation was calculated using the vegetation periods most productive three-month mean value per year for temperature and precipitation (the same three months that were used for the sampling). In contrast, in the Noextremes scenario, temperature and precipitation are hardly correlated at all (global mean -0.02). The Nocompound (-0.31), Hot (-0.37), and Dry (-0.34) scenarios all show a negative correlation between temperature and precipitation, but slightly less so compared to the control. The Hotdry scenario is the only scenario that features a strongly increased negative correlation between temperature and precipitation, with a global average of -0.72.

To measure the occurrence of compound hot and dry conditions, we assess the occurrence of compound

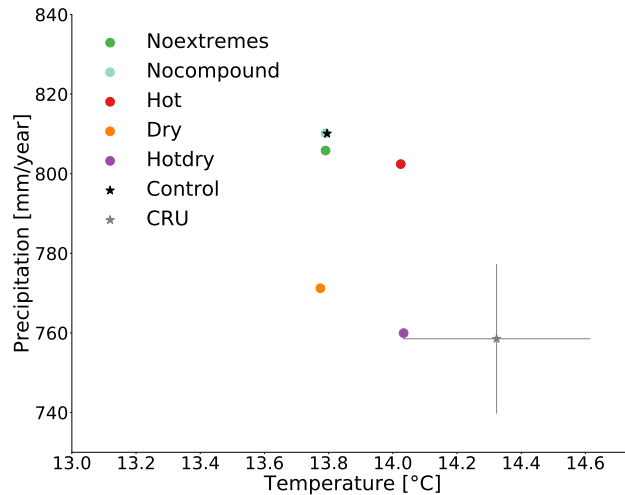


**Figure 2.3:** Global annual average temperature and precipitation over land (excluding Antarctica and much of Greenland) for all scenarios and CRU (1988-2017). The bars on CRU indicate one standard deviation of annual means over the entire time period.

hot and dry years. To this end, we calculate the frequency  $F$  of years for which the three-month temperature lies above the 90<sup>th</sup> percentile and the three-month precipitation lies below the 10<sup>th</sup> percentile of the control scenario.

$$F = \sum_{i=1}^{100} I_{T_i > T_{90}} I_{P_i < P_{10}} / 100. \quad (2.2)$$

In this equation (unlike equation 2.1)  $i$  denotes a yearly time steps, ranging from 1 to the total number of years, i.e., 100. If temperature and precipitation were completely independent, we would expect one out of 100 years to be a compound extreme year ( $F = 10\% \times 10\% = 1$ ). However, since they are strongly correlated over most land regions (Fig. 2.6a) the global mean of compound hot and dry years for the control scenario is 3.6 years (Fig. 2.7a). We further investigate probability ratios of compound extreme occurrence between scenarios and Control. Numbers smaller than one mean fewer years with compound extremes than in the Control and vice versa. The Noextremes scenario contains no years with compound extremes (Fig. 2.7b) and there are very few in the Nocompound scenario (probability ratio of 0.03, Fig. 2.7c). In the global mean, Hot (0.65, Fig. 2.7d) and Dry (0.66, Fig. 2.7e) have a slight reduction of the number of years with compound extremes compared to Control. The Hotdry scenario shows a large increase in the occurrence of compound hot and dry years, with a probability ratio of 11.23 in the global average (Fig. 2.7f). This shows that our scenario selection method, aimed to either remove or increase compound event occurrence, has been successful.

## 2.4 Discussion and conclusions

Disentangling the effects of single and compound drivers of climate impacts is challenging due to the difficulty to create a controlled environment, the representativity of local climate change experiments and many confounding factors related to non-stationarities in the climate system. One approach that allows to overcome most of these challenges is the use of climate models in combination with process-based impact models. Climate models allow for generating climate conditions without long-term trends that are representative of the present-day climate as well as scenarios with varying intensity and frequency of single and compound drivers. Process-based impact models can then be used to estimate the effects of such varying climate conditions on different types of impacts for different regions.

Here we present a data set of daily climate forcing with varying drought-heat signatures for modelling climate impacts. Six 100-year long scenarios cover different conditions, varying from very few extremes overall, over many single drought or heat extremes, to many compound drought and heat events. The scenarios were sampled from a 2000-year climate data set representing present-day climate simulated with a global circulation model at  $1^\circ \times 1^\circ$  spatial resolution. Despite differences in the occurrence of droughts

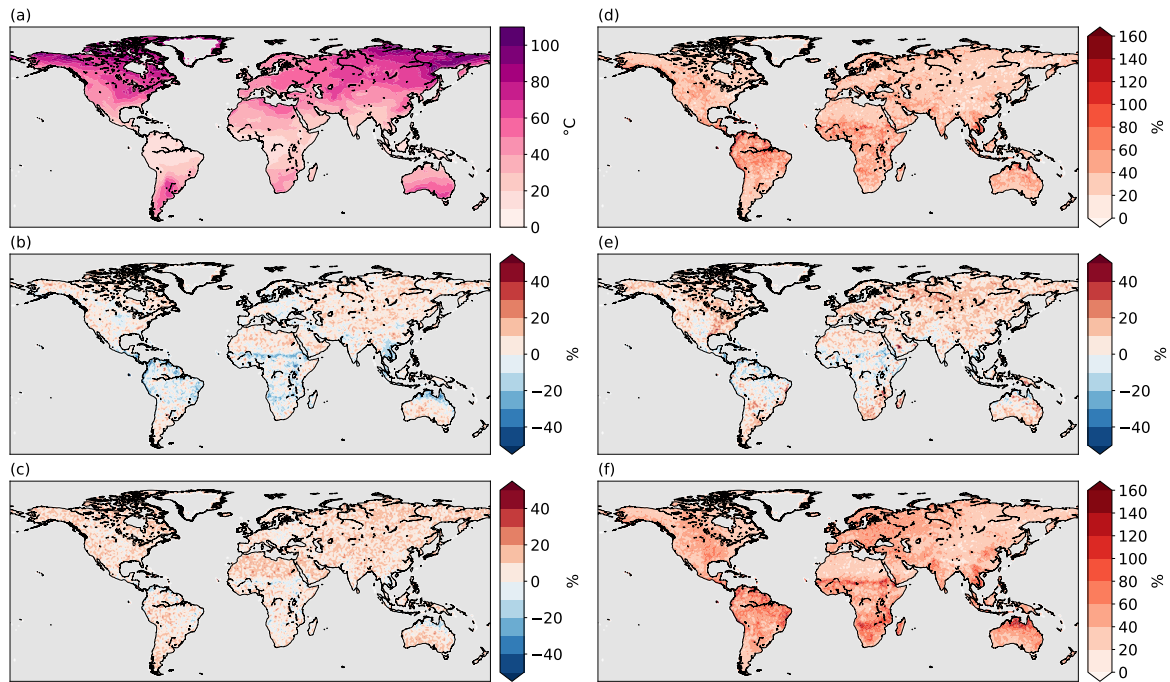


**Figure 2.4:** Cooling Degree Days (CDD, normalized per year) as a metric for temperature extremes. (a) CDD in the Control scenario in  $^{\circ}\text{C}$ . (b) - (f): relative difference in CDD with respect to the Control scenarios in % (Noextremes (b), Nocompound (c), Hot (d), Dry (e) and Hotdry (f)). Note the different colour scales.

and heatwaves between scenarios, their mean climate is comparable and representative of the observed climate of 2011-2015.

The climate forcing was generated with EC-Earth, a fully coupled global climate model (Hazeleger et al., 2012). The 2000-year climate data set and its companions with +2 and +3  $^{\circ}\text{C}$  global climate change has already been used to identify drivers of crop failure (Vogel et al., 2020), study extreme river discharge in a warmer world (Van der Wiel et al., 2019c), evaluate extremes in the renewable energy sector (Van der Wiel et al., 2019b,a), assess changes in heatwaves in India (Nanditha et al., 2020) and detect changes in mountain-specific climate indicators in a warmer world in High Mountain Asia (Bonekamp et al., 2020), highlighting its applicability for assessing climate impacts.

In addition to temperature and precipitation, we provide a range of variables that are common inputs to climate impact models, including radiation and wind speed (Table 2.1). Despite a good alignment of global mean temperatures with present-day conditions, EC-Earth is not free of biases at the local to regional scale (Section 2.2.2). In particular, there is a cold and dry bias in the tropics and a warm and wet bias in the high latitudes (Fig. 2.1). Depending on the application, these biases need to be accounted and potentially be adjusted for when modelling impacts (Vogel et al., 2020). For global vegetation models, a spin-up to equilibrate carbon pools is probably required. Furthermore, given the method presented for the creation of the scenarios, there is no spatial coherence in the data set, and hence no correlation in weather conditions between neighbouring locations or around the world. Again, this needs to be taken into account when modelling impacts and precludes modelling impacts for which spatial interactions matter (e.g. many hydrological applications).

The presented scenarios are primarily designed to study the effect of varying drought and heat conditions on terrestrial carbon dynamics. The scenario design, therefore, focuses on creating different likelihoods of dry and/or hot conditions during the peak of the growing season, when plants are most vulnerable (Section 2.2). In this context, the scenarios could form the basis for model intercomparison projects (MIPs) using a suite of global vegetation models (e.g. Zscheischler et al., 2014b; Friedlingstein et al., 2019; Bastos et al., 2020a; Pan et al., 2020). Despite the focus on the carbon cycle during the design of the scenarios, we believe they also could be well suited for studying the differential effects of droughts and heatwaves on other impact types, for instance with the impact models used in the Inter-Sectoral Impact Model Intercomparison Project (ISIMIP, <https://www.isimip.org>, Warszawski et al., 2014). Two impact types we deem of particular relevance here are wildfire occurrence and agriculture. Outside hot

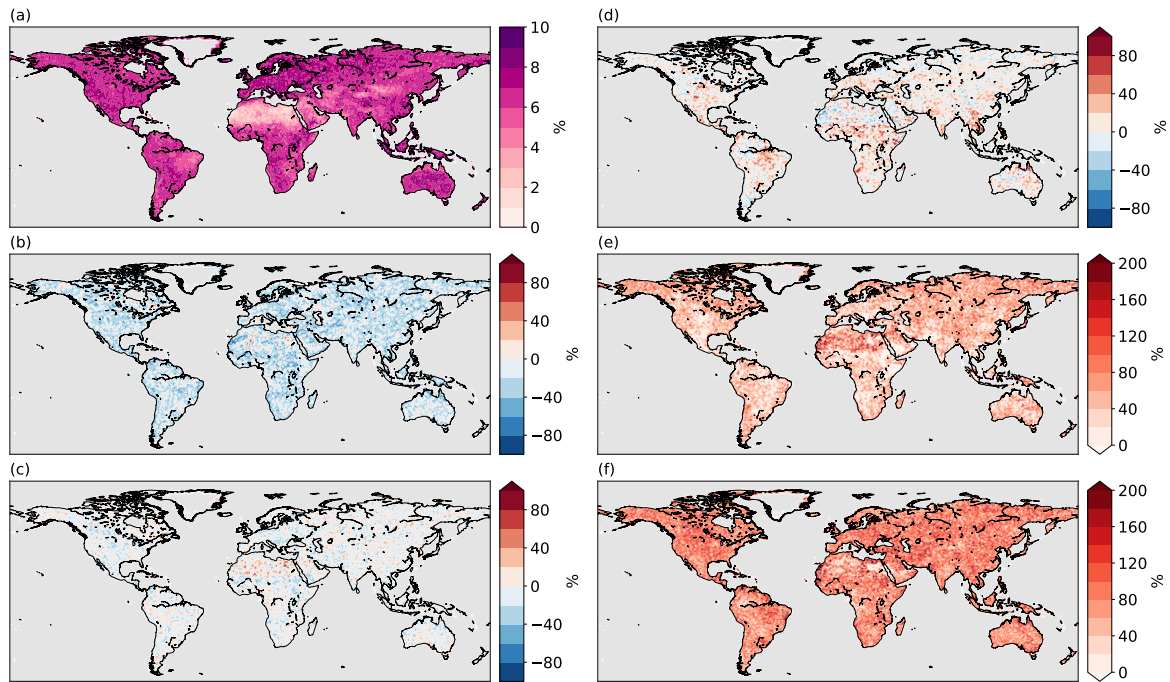


**Figure 2.5:** Severe droughts. (a) Occurrence probability of severe droughts (SPI < -1.5) in the Control scenario. (b) - (f): relative difference in the percentage of severe droughts with respect to the Control scenario in % (Noextremes (b), Nocompound (c), Hot (d), Dry (e) and Hotdry (f)). Note the different colour scales.

and dry conditions, factors such as wind speed, lightning occurrence and land use change govern wildfire risk. Our scenarios could be used to investigate how wildfire regimes change under different drought-heat regimes and may help pin down reasons behind the large differences in modelled fire characteristics across models (Forkel et al., 2019; Teckentrup et al., 2019). Common protocols for modelling wildfire occurrence have already been set up in the FireMIP (Rabin et al., 2017). Note, however, that the effect of spatial interactions cannot be simulated with our scenarios, as there is no spatial coherence. Another possible area of application of the scenarios are crop models, as for instance collected in the Agricultural Model Intercomparison and Improvement Project (AgMIP, <https://agmip.org>, Rosenzweig et al., 2013). AgMIP focuses specifically on agricultural impacts and is designed to study and improve world food security. Crops are highly sensitive to hot and dry conditions (Shah & Paulsen, 2003; Cohen et al., 2020) and crop models differ strongly in their response to climate extremes and climate change (Rosenzweig et al., 2014) though uncertainties have been reduced recently (Toreti et al., 2020). Our scenarios might help to disentangle how different crop models respond to different types of droughts, heatwaves and compound drought and heatwave events.

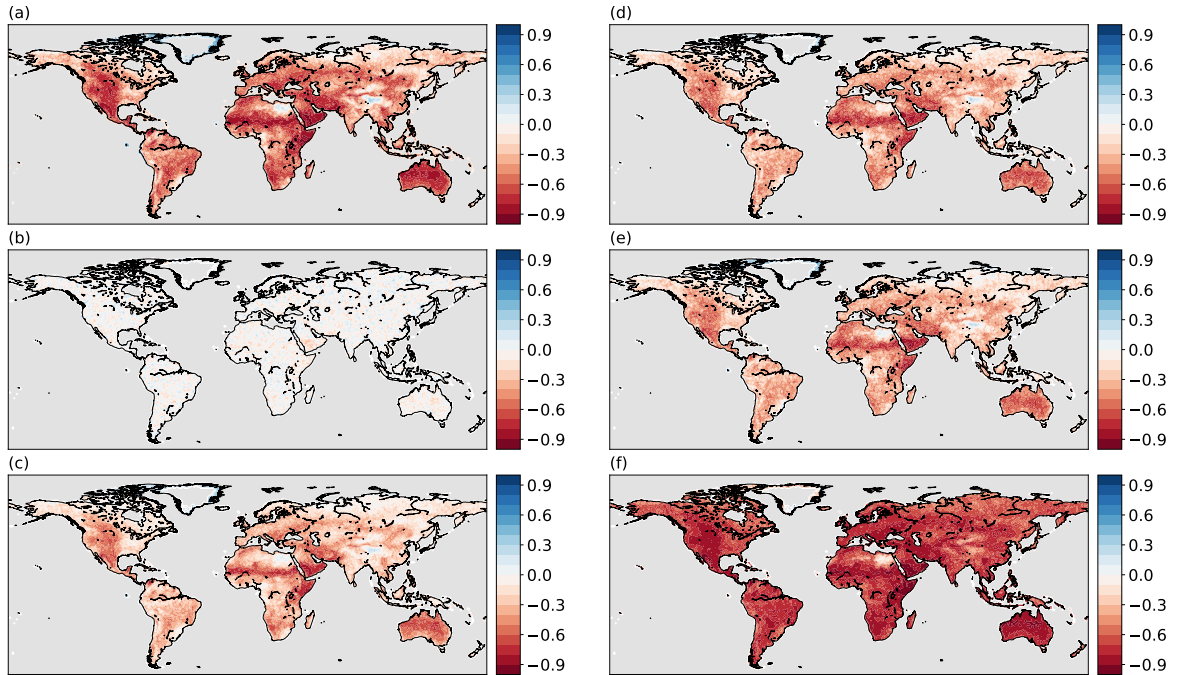


**Figure 2.6:** Inter-annual correlation between temperature and precipitation during the three months when vegetation is most active. (a) - (f) show the correlations between temperature and precipitation for Control (a), Noextremes (b), Nocompound (c), Hot (d), Dry (e) and Hotdry (f).

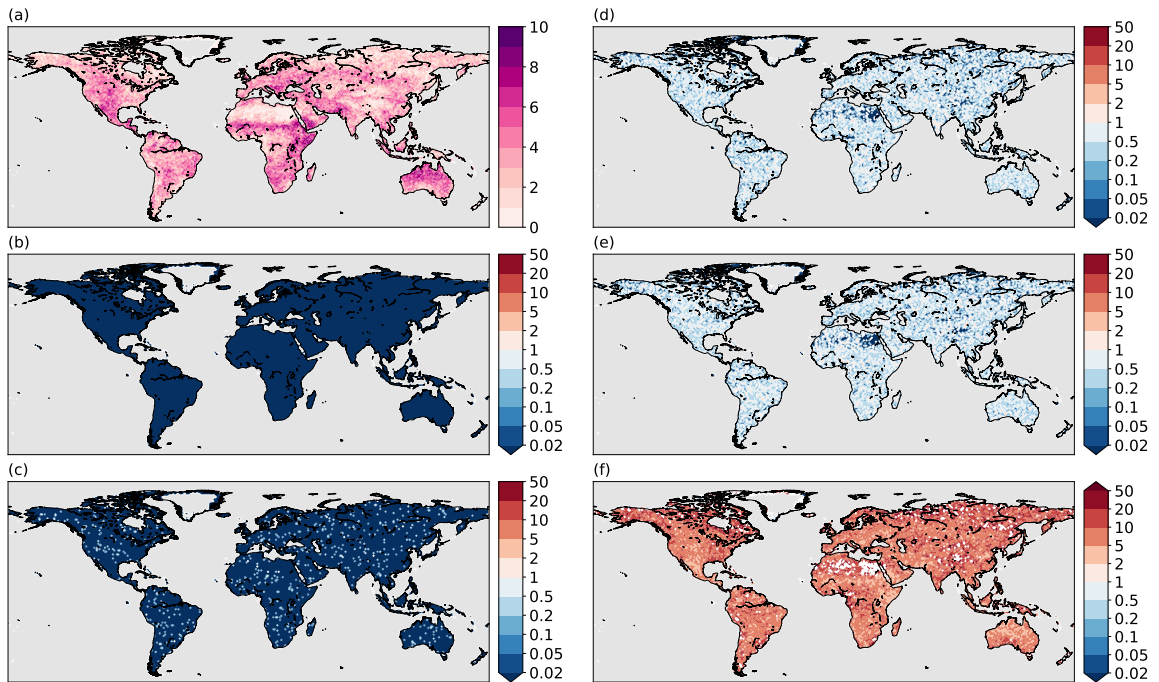


**Figure 2.7:** Occurrence of compound extremes. (a) Number of years where temperature exceeds the 90<sup>th</sup> percentile and precipitation lies below the 10<sup>th</sup> percentile in the Control scenario. Temperature and precipitation are averaged over the three months where vegetation is most active. (b) - (f): Probability ratio (scenario/control) for the compound hot and dry years (Noextremes (b), Nocompound (c), Hot (d), Dry (e) and Hotdry (f)).

## 2.5 Supporting information

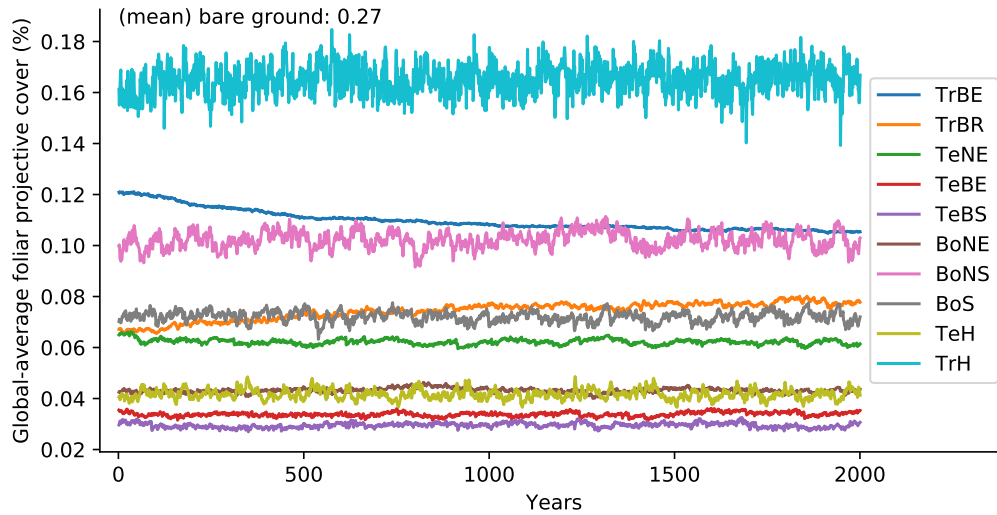


**Figure 2.8:** Annual global-average foliar projective cover by each PFT in LPX-Bern for the 2000-year simulation with the entire climate data set (TrBE: tropical broad evergreen, TrBR: tropical broad raingreen, TeNE: temperate needle evergreen, TeBE: temperate broad evergreen, TeBS: temperate broad summergreen, BoNE: boreal needle evergreen, BoNS: boreal needle summergreen, BoS: boreal broad summergreen, TeH: herbaceous, TrH: herbaceous).

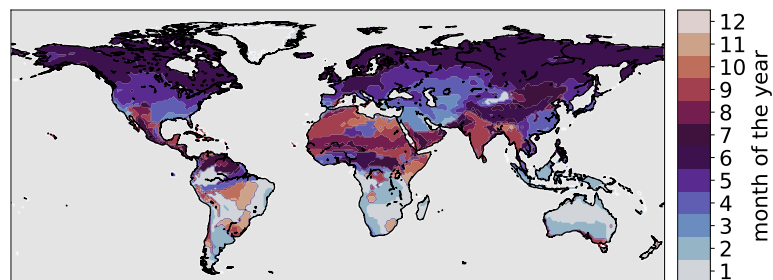


**Figure 2.9:** Map showing the month with highest net primary production (NPP) determined from the seasonal mean over 2000 years.

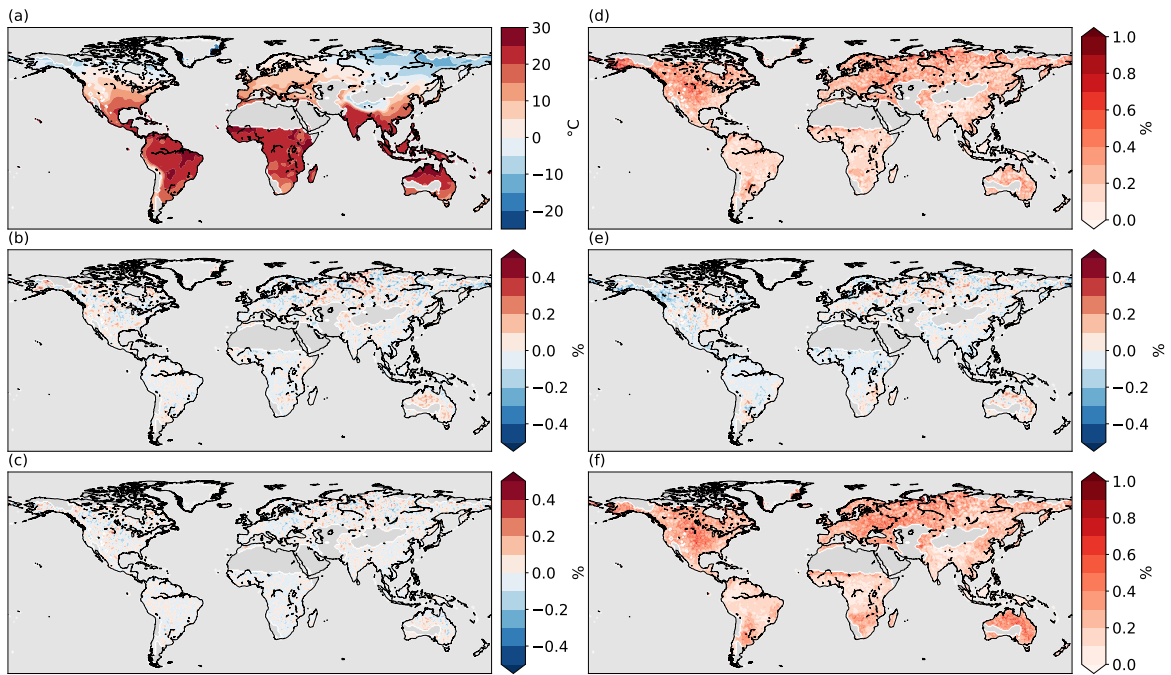


**Figure 2.10:** Regional annual differences in air temperature at two meters. (a) shows the mean temperature for the Control scenario. (b) - (f): relative difference in °C with respect to the Control scenario (Noextremes (b), Nocompound (c), Hot (d), Dry (e) and Hotdry (f)). Global mean temperature over land (excluding Antarctica and most of Greenland) of Control: 13.8 °C. Differences of global means with respect to Control for Noextremes: -0.04 °C; Nocompound: -0.04 °C; Hot: 1.7 °C; Dry: -0.2 °C; Hotdry: 1.7 °C. Desert regions were excluded in these maps and are shown in grey.

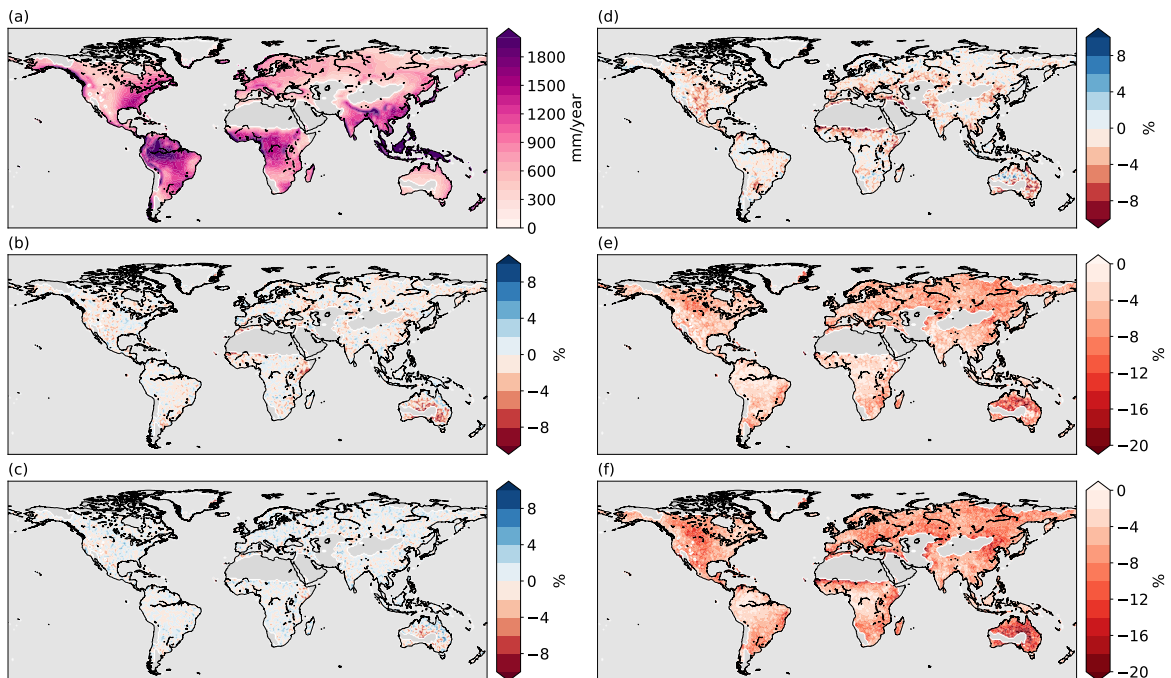


**Figure 2.11:** Regional annual differences in precipitation. (a) shows the mean precipitation for the Control scenario. (b) - (f): relative difference in % with respect to the Control scenario (Noextremes (b), Nocompound (c), Hot (d), Dry (e) and Hotdry (f)). Global precipitation sum over land (excluding Antarctica and most of Greenland) of Control: 810 mm/yr. Relative differences of global sums relative to Control for Noextremes: -0.5 %; Nocompound: 0.01 %; Hot: -0.9 %; Dry: -4.8 %; Hotdry: -6.2 %. Desert regions were excluded in these maps and are shown in grey.

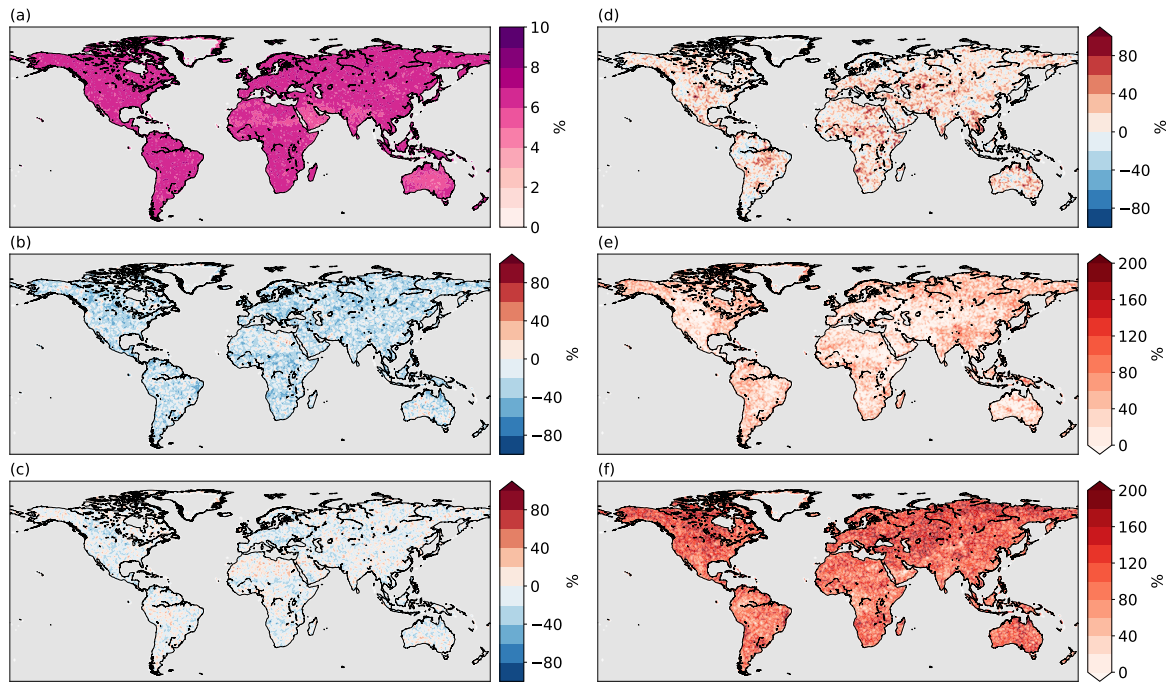


**Figure 2.12:** Standardized Precipitation Evapotranspiration Index (SPEI) for severe droughts ( $SPEI < -1.5$ ). (a) Percentage of severe droughts in the Control scenario. (b) - (f): relative difference in the percentage of severe droughts with respect to the Control scenario in % (Noextremes (b), Nocompound (c), Hot (d), Dry (e) and Hotdry (f)). Global mean of Control: 6.4 %. Global mean of relative change with respect to the Control for Noextremes: -23.6 %; Nocompound: -6.5 %; Hot: 11.1 %; Dry: 37.0 %; Hotdry: 105.8 %.

## Chapter 3

# The effects of varying drought-heat signatures on terrestrial carbon dynamics and vegetation composition

Elisabeth Tschumi, Sebastian Lienert, Karin van der Wiel, Fortunat Joos and Jakob Zscheischler

Published in *Biogeosciences*, 2022;19,1979–1993.

### Abstract

The frequency and severity of droughts and heat waves are projected to increase under global warming. However, the differential impacts of climate extremes on the terrestrial biosphere and anthropogenic CO<sub>2</sub> sink remain poorly understood. In this study, we analyse the effects of six hypothetical climate scenarios with differing drought-heat signatures, sampled from a long stationary climate model simulation, on vegetation distribution and land carbon dynamics, as modelled by a dynamic global vegetation model (LPX-Bern v1.4). The six forcing scenarios consist of a Control scenario representing a natural climate, a Noextremes scenario featuring few droughts and heatwaves, a Nocompound scenario which allows univariate hot or dry extremes but no co-occurring extremes, a Hot scenario with frequent heatwaves, a Dry scenario with frequent droughts, and a Hotdry scenario featuring frequent concurrent hot and dry extremes. We find that a climate with no extreme events increases tree coverage by up to 10 % compared to the Control and also increases ecosystem productivity as well as the terrestrial carbon pools. A climate with many heatwaves leads to an overall increase in tree coverage primarily in higher latitudes, while the ecosystem productivity remains similar to the Control. In the Dry and even more so in the Hotdry scenario, tree cover and ecosystem productivity are reduced by up to -4 % compared to the Control. Regionally, this value can be much larger, for example, up to -80 % in mid-western U.S. or up to -50 % in mid-Eurasia for Hotdry tree ecosystem productivity. Depending on the vegetation type, the effects from the Hotdry scenario are stronger than the effects from the Hot and Dry scenario combined, illustrating the importance of correctly simulating compound extremes for future impact assessment. Overall, our study illustrates how factorial model experiments can be employed to disentangle the effects from single and compound extremes.



This work is distributed under the Creative Commons Attribution 4.0 License. Please visit <https://creativecommons.org/licenses/by/4.0/> to see the licence.

### 3.1 Introduction

The terrestrial biosphere sequesters about 30 % of the anthropogenic CO<sub>2</sub> emissions (Friedlingstein et al., 2020). Different factors such as increasing atmospheric CO<sub>2</sub> concentrations, higher temperatures, or, on a more regional scale, water or nutrient availability, can increase or decrease the terrestrial carbon sink. Different biomes may also react differently. While warmer temperatures are likely to increase productivity in high latitudes and altitudes due to an increase in the growing season length, productivity may be reduced in warmer regions because of higher evaporation and stomatal closure (Friend et al., 2014). Overall, there is evidence that the vulnerability of trees to hotter droughts may increase but this may also be compensated by higher CO<sub>2</sub> concentrations and associated increased water use efficiency (De Kauwe et al., 2013). However, future projections of the terrestrial carbon sink remain highly uncertain (Friedlingstein et al., 2014).

A potentially large contribution to the uncertainty in carbon cycle response to climate change may stem from the impacts of climate extremes. Climate extremes can cause devastating impacts on the natural environment (IPCC, 2012; Reichstein et al., 2013; Frank et al., 2015; von Buttlar et al., 2018; Senf et al., 2020). At the same time, extreme impacts are often not linked to single climate extremes but to a combination of anomalous drivers (Zscheischler et al., 2016; Flach et al., 2017; Pan et al., 2020; Tschumi & Zscheischler, 2020; van der Wiel et al., 2020; Vogel et al., 2021), also called compound events (Zscheischler et al., 2018, 2020).

Arguably, drought and heat are among the most damaging hazards to terrestrial vegetation (Allen et al., 2010; Reichstein et al., 2013; Zscheischler et al., 2014b; Frank et al., 2015; Sippel et al., 2018; von Buttlar et al., 2018; Senf et al., 2020). In many cases, drought and heat predispose or interact with other hazards and disturbances such as forest fires and insect outbreaks (Seidl et al., 2017). In particular, an increasing occurrence of warm droughts has already lead to increased vegetation impacts on northern hemispheric ecosystems over the observational period (1982-2016, Gampe et al., 2021). However, differentiating impacts between drought and heat alone and compound drought and heat remains a challenging task. Disentangling these impacts is important, as co-occurring droughts and heatwaves tend to have larger impacts compared to the sum of impacts from droughts and heatwaves separately (Zscheischler et al., 2014b; Ribeiro et al., 2020), for example, because a drought exacerbates the impacts of a heatwave through reduced evaporative cooling (Yuan et al., 2016). Furthermore, projections of droughts and heatwaves can differ strongly across different climate models (Herrera-Estrada & Sheffield, 2017; Zscheischler & Seneviratne, 2017).

The impacts of climate extremes on vegetation and the terrestrial carbon cycle can be studied using different approaches including (i) lab or field experiments (De Boeck et al., 2011; Beier et al., 2012; Song et al., 2019); (ii) observational data such as long-term forest observations (Anderegg et al., 2013a) and local measurements of carbon exchange (Ciais et al., 2005; von Buttlar et al., 2018; Pastorello et al., 2020); (iii) indirect estimates from satellite observations (Ciais et al., 2005; Zhao & Running, 2010; Zscheischler et al., 2013; Stocker et al., 2019); and (iv) dynamical vegetation models (Ciais et al., 2005; Zscheischler et al., 2014a,b,c,d; Rammig et al., 2015; Xu et al., 2019; Bastos et al., 2020a; Pan et al., 2020). Vegetation models offer the benefit of being able to analyse new hypotheses in a strictly controlled environment at global scale.

Despite considerable uncertainties in climate models, it is widely acknowledged that drought and heat extremes will increase in frequency and severity in many land regions in the future (Seneviratne et al., 2012). Though it is still uncertain exactly how these increases will affect the terrestrial biosphere, there are concerns they might substantially reduce the current terrestrial carbon sink (Reichstein et al., 2013). While coupled models of the land and atmosphere allow for a more complete representation of the feedback processes (Humphrey et al., 2021) than stand-alone land biosphere models, the analysis of results is more complicated for coupled models, since the coupling is different for different models and uncertainties depend not only on the land but also on the atmosphere module.

In this study, we aim to disentangle the differential effects of different frequencies of hot conditions, dry conditions, and compound hot-dry events on vegetation composition, carbon pools, and carbon dynamics. Our main motivation is to test the sensitivity of a commonly used vegetation model to differences in the climatology of the occurrence of hot and dry extremes and how these changes in drought and heat occurrence affect vegetation distribution and carbon dynamics. To this end, we force a dynamic global vegetation model, LPX-Bern v1.4, with six 100-year long climate scenarios featuring varying drought-heat signatures, i.e. different occurrence probabilities of dry events, hot events, and concurrent

dry and hot events. These scenarios were sampled from 2000 years of present-day climate data from the EC-Earth climate model, as described in Sect. 3.2.1. They have a constant  $\text{CO}_2$  concentration and do not contain long-term trends. The controlled environment of a model setup allows us to attribute changes in vegetation composition and carbon dynamics to differences in drought-heat occurrence.

## 3.2 Data and Methods

### 3.2.1 Forcing scenarios

Six forcing scenarios featuring different dry and hot signatures were used to run the vegetation model LPX-Bern. These scenarios, each 100 years long, were constructed from a large ensemble climate modelling experiment (Tschumi et al., 2022a). 2000 years of simulated present-day climate data were created with the fully-coupled global climate model EC-Earth (v2.3, Hazeleger et al., 2012). The large ensemble was built out of 400 short five-year runs, which were unique in initial conditions and/or stochastic physics seed. EC-Earth combines atmospheric, oceanic, land, and sea-ice model components, and simulates the global climate including feedbacks between land and atmosphere. Within the ensemble the influence of forced climate change is small. We, therefore, assume all variability in the data set is due to natural variability in the climate system. While the global mean surface temperature in EC-Earth shows no significant bias, there can be biases at the regional and seasonal scale. In particular, there is a mean temperature difference of  $-0.5^\circ\text{C}$  and a precipitation difference of 7 % over land, with regional biases being relatively large (up to  $-1.8^\circ\text{C}$  in the tropics and  $0.2^\circ\text{C}$  in the extratropics, mostly in the very high latitudes). Many land regions show a wet bias in EC-Earth compared to CRU (43.5 % in the extratropics). A more detailed description of the biases can be found in Tschumi et al. (2022a). The biases in the climate forcing compared to observational datasets implies that simulated vegetation cover based on this forcing may differ from observed vegetation cover.

The selection of the different scenarios from this data set was based on temperature and precipitation values during the time of the year where the vegetation is most active. Arguably, the vegetation is most vulnerable to climate extremes during the growing season. Therefore, for the scenario creation, we focused on the three months around the most productive month in the climatology. We identified the most productive month at each pixel, that is, the month with the highest climatological-mean net primary production (NPP) as simulated by LPX-Bern.

We selected the six different scenarios for each pixel separately based on mean temperature and precipitation over the three months around the month of highest NPP: Control, Noextremes, Nocompound, Hot, Dry and Hotdry. Years contributing to the scenarios were sampled based on quantiles of the three-month temperature and precipitation averages, where the quantiles were computed based on the full 2000-year EC-Earth output. If more than the required number of years fall into the quantiles in question, a random selection was performed. If fewer years than necessary were available, some randomly chosen years were selected multiple times. For each of the Hot, Dry, and Hotdry scenarios, 50 years were sampled from the extreme quantiles and 50 years were randomly sampled from the rest. The reason for this is twofold. Firstly, for many pixels, not many years fall into the extreme quantiles. Sampling only 50 years from there reduces the number of times a year is re-sampled. Secondly, the mean climatology is kept more similar to the other scenarios if only half the years were sampled with extreme conditions and the other half from the rest.

This method of scenario creation, for each pixel separately, destroys any spatial coherence, so that the climate in a pixel is not correlated to the climate in nearby pixels. Furthermore, due to the sampling of individual years, there are always slight discontinuities between 31 December and 1 January in the climate forcing. The same is true for leap years since all leap days (29 February) were removed. We assume that these small discontinuities in the atmospheric forcing do not significantly affect our findings. The scenarios have a daily temporal and a  $1^\circ \times 1^\circ$  spatial resolution. The scenarios were sampled from the percentiles of the EC-Earth data at each location separately as described in Tschumi et al. (2022a) and summarized in Table 3.1.

The scenarios differ little in their mean climatic conditions but strongly in the occurrence of dry events, hot events, and concurrent dry and hot events. More specifically, the difference in global mean temperature and precipitation between the scenarios is about  $0.3^\circ\text{C}$  and 6 %, respectively. The Hot and Hotdry scenarios show an increase in heatwaves (based on cooling degree days, which is the sum of all

**Table 3.1:** Sampling design for the six climate scenarios (see Tschumi et al., 2022a)

Scenario name	Sampling procedure
Control	100 randomly selected years representing present-day climate
Noextremes	only years where temperature and precipitation lie between the 40 <sup>th</sup> and 60 <sup>th</sup> percentile
Nocompound	no years where both temperature and precipitation lie above the 85 <sup>th</sup> percentile or below the 15 <sup>th</sup> percentile
Hot	years where temperature exceeds the 85 <sup>th</sup> percentile and precipitation lies between the 40 <sup>th</sup> and 60 <sup>th</sup> percentiles
Dry	years where precipitation lies below the 15 <sup>th</sup> percentile and temperature lies between the 40 <sup>th</sup> and 60 <sup>th</sup> percentile
Hotdry	years where temperature lies above the 85 <sup>th</sup> percentile and precipitation lies below the 15 <sup>th</sup> percentile

exceedances over the 90<sup>th</sup> percentile of the Control at each pixel) by up to 160 % compared to the Control. Dry event occurrences (based on the standardized precipitation index (SPI), which is used to identify severe meteorological droughts, defined as  $SPI > -1.5$ ) are strongly increased for the Dry and Hotdry scenario, by up to 200 % compared to the Control. In the Noextremes and Nocompound scenarios, there is an overall decrease in dry events of up to -80 % and heatwaves up to -50 %. The pattern of concurrent dry and hot events is even more pronounced. There are no or very few concurrent dry and hot events in the Noextremes and the Nocompound scenario. Compound extremes are possible for the Hot and Dry scenario, but occur overall less often than in the Control. In the Hotdry scenario, however, concurrent dry and hot events occur up to 50 times more often than in the Control. A more in-depth description and analysis of these scenarios including the definition of dry and hot events are given in Tschumi et al. (2022a).

### 3.2.2 LPX-Bern

LPX-Bern v1.4 (Lienert & Joos, 2018) is a Dynamic Global Vegetation Model based on the Lund-Potsdam-Jena (LPJ) model (Sitch et al., 2008). The model features coupled water, nitrogen, and carbon cycles and represents different types of vegetation using Plant Functional Types (PFTs). Here, only natural vegetation is considered, which is internally represented by eight tree PFTs and two herbaceous PFTs competing for resources and adhering to bioclimatic limits, which are listed in Table 3.2 as well as other process parameterizations (e.g. temperature dependence of photosynthesis or water balance). These bioclimatic limits and other parameters as well as process representation can differ from model to model, leading to a different response of the vegetation to extreme climatic events. In LPX-Bern, tree coverage is restricted to 95% of the grid cell. If the total fraction summed over all PFTs exceeds 1, the plants that were the least productive are killed, representing self-thinning. Mortality can also occur if a PFT’s bioclimatic limits are reached due to heat stress, negative NPP, or depressed growth efficiency (Sitch et al., 2003). As an example, the bioclimatic parameter governing the upper limit of temperature is implemented in LPX-Bern by inducing mortality proportional to the number of days in the year where this threshold is exceeded. Other models may not only use different values for the threshold and a different relationship between mortality and exceedance, but an altogether different parameterization. This will in turn influence the response to the heat stress in the model.

In this study, daily temperature, precipitation, and incoming short-wave radiation are provided to the model. Additionally, the model uses information on the soil type (Wieder et al., 2014), CO<sub>2</sub> concentration in the atmosphere at 2011-level (389.78 ppm), and nitrogen deposition, also at 2011-level (Tian et al., 2018). Each scenario simulation was preceded by a 1500 year long spin-up, which was forced with climate data of the same scenario (‘individual spin-up’). To test how fast vegetation composition and net ecosystem exchange reach a new equilibrium under an altered frequency of dry and hot events, we also performed simulations in which the spin-up was based on climate from the Control (‘shared spin-up’). By running the model with two different spin-ups per scenario, we explore the model equilibrium and how fast the model reacts after a step change in the frequency of extreme events.

LPX-Bern represents natural vegetation with ten PFTs, as described above. For the following analysis, we aggregate them into four broader classes, namely Tropical trees (including tropical broad-leafed evergreen and tropical broad-leafed raingreen trees), Temperate trees (including temperate needle-leafed evergreen, temperate broad-leafed evergreen and temperate broad-leafed summergreen trees), Boreal trees (including boreal needle-leafed evergreen, boreal needle-leafed summergreen and boreal broad-leafed summergreen trees), and Grasses (including temperate and tropical herbaceous). The dominant vegetation class in the control simulation for each pixel, including its fractional cover (the fraction of a grid cell covered with a certain vegetation class), is shown in Fig. 3.1. Pixels where the total fractional coverage is smaller than 0.1, corresponding to desert regions, are masked white.

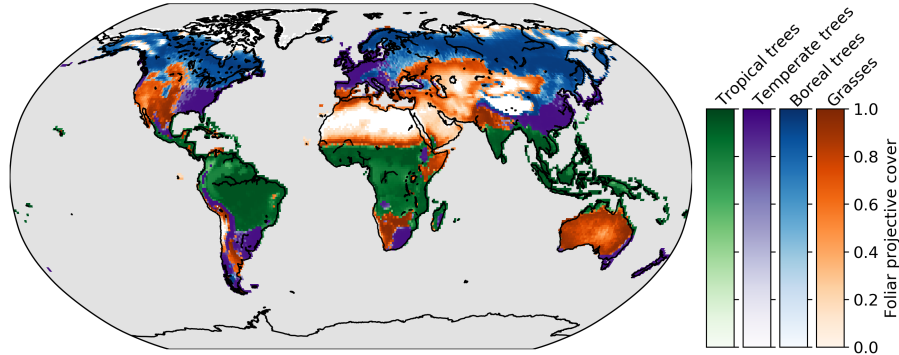


**Figure 3.1:** Dominant vegetation class (mean over time) in the Control simulation. The intensity (color bars) shows the fractional coverage of each dominant class.

### 3.3 Results

We report how different stationary climate conditions (i.e. without long-term trends) with varying intensities of dry events, hot events and compound dry-hot events affect vegetation coverage (Sect. 3.3.1) as well as carbon pools and carbon fluxes (Sect. 3.3.2). These results are based on the simulations using the individual spin-up. In Section 3.3.3 we report how quickly LPX-Bern reaches a new equilibrium by running simulations for each scenario that use the climate of the Control scenario during spin-up (shared spin-up).

#### 3.3.1 Changes in vegetation coverage and associated NPP changes

The different dry and hot scenarios lead to a change in fractional vegetation coverage (Fig. 3.2a). Trees generally benefit from a climate with no dry and hot events. The increase in tree cover is stronger for higher latitudes. While the relative difference in global mean Tropical tree cover is 1.2 %, it is 9.4 % for Boreal trees for the Noextremes scenario (green bars in Fig. 3.2a). Regionally, this increase can be much larger. Total tree cover for the mid-west of the U.S., for example, is increased by up to 400 % and there is a similarly large increase in South Africa (results not shown). These are regions with nearly no trees in the Control scenario (Fig. 3.1). A smaller, but still large increase of up to 100 % is observed in South America, southern Africa and large parts of Eurasia. Grass coverage in turn decreases to make room for the trees. To a lesser extent, the same pattern also holds for a climate with no compound extremes, which however does feature univariate extremes (blue bars in Fig. 3.2a). The increase of tree coverage towards higher latitudes is also evident for the Hot scenario, while for this scenario grass cover does not change compared to the Control (red bars in Fig. 3.2a). The Dry and, even more strongly, the Hotdry scenarios lead to an overall decrease of tree coverage (orange and purple bars in Fig. 3.2a, respectively). The decrease is particularly strong for Temperate tree coverage in the Hotdry scenario (-5.6 %), while there is little change in Boreal tree cover. At the regional scale, the decrease is largest in the mid-west of the U.S. with up to -80 % as well as up to -50 % in mid-Eurasia. For the Hotdry scenario, the overall decrease in tree cover is compensated by an increase in grass cover, mainly in the U.S., Europe, mid-Eurasia and southern South America, in contrast to the Dry scenario, in which grass cover also decreases. While it is generally true that grasses seem to compensate for declining tree coverage, the compensation is not

necessarily complete. As an effect, the total sum of fractional plant cover may change as well. However, at the global scale, there is hardly any change in fractional coverage between the scenarios (not shown). Overall, the differences in vegetation cover between the scenarios are smallest for Tropical trees and tend to be similarly ordered, but larger in magnitude, for the other vegetation classes.

The above-described relative differences in coverage directly translate into changes in annual NPP (Fig. 3.2b). In particular, if tree or grass coverage increases, so does NPP and if coverage decreases, we find an associated decrease in NPP. Overall, at the global scale, the variability in the relative differences in NPP is larger than the variability in the relative differences in vegetation cover (compare lengths of bars in Fig. 3.2a to Fig. 3.2b).

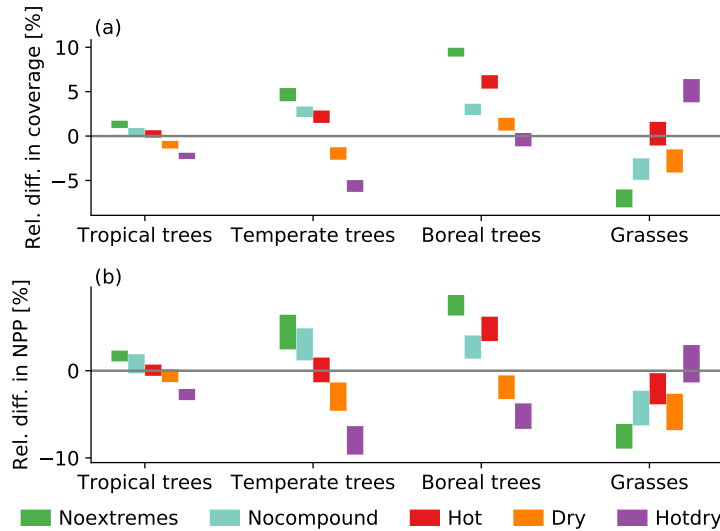


**Figure 3.2:** Relative difference of the scenarios to the Control for (a) coverage and (b) annual NPP. The bars show the minimum to maximum range over the 100-year long simulations.

We compare the spatial patterns of the differences of tree (all tree types aggregated) and grass cover between the two scenarios with the strongest effect and the Control, i.e. Noextremes-Control and Hotdry-Control, in Fig. 3.3. In the Noextremes scenario, tree cover increases on all land pixels compared to the Control, especially in western North America and Mid-Eurasia (Fig. 3.3a). In contrast, grass cover decreases everywhere except in very dry regions such as the Sahara, the Arabian Peninsula, and Australia, where a constant climate without extremes leads to a slight increase in grass cover (Fig. 3.3b). For Hotdry, tree cover decreases in most regions except the very high latitudes, compared to the Control (Fig. 3.3c), while grass coverage increases except for very dry regions (Fig. 3.3d).

### 3.3.2 Changes in carbon dynamics

The effects of the scenarios on vegetation coverage (Sect. 3.3.1) are reflected by the globally aggregated carbon fluxes and pools (Fig. 3.4). The response of NPP to the replacement of trees with grasses and vice versa is varied, as it strongly depends on environmental conditions and vegetation composition. Generally, NPP is greater for trees than for grasses, which implies that global NPP is larger in a world with more trees and smaller if more forest area is replaced by grassland. Consequently, Noextremes, Nocompound, and Hot generally show higher or similar flux magnitudes compared to the Control, whereas fluxes are strongly decreased for Dry and Hotdry, by up to more than -4 % for global gross primary production (GPP) in Hotdry (Fig. 3.4a). Interestingly, although grass cover is increased in the Hot scenario (Fig. 3.2a), NPP in grasslands is reduced (Fig. 3.2b), explaining the lack of change in global NPP for the Hot scenario (Fig. 3.4a). Relative carbon flux reductions can be very large for some regions, for example, up to -80 % in the mid-west of the U.S., mirroring the decrease in tree cover. Similar patterns are evident for changes in global vegetation carbon (Fig. 3.4b). Overall, relative differences are much smaller for global soil carbon.

We further explore the spatial patterns in the differences of NPP separately for trees (all tree types aggregated) and grasses between the two scenarios with the strongest effect, i.e. by looking

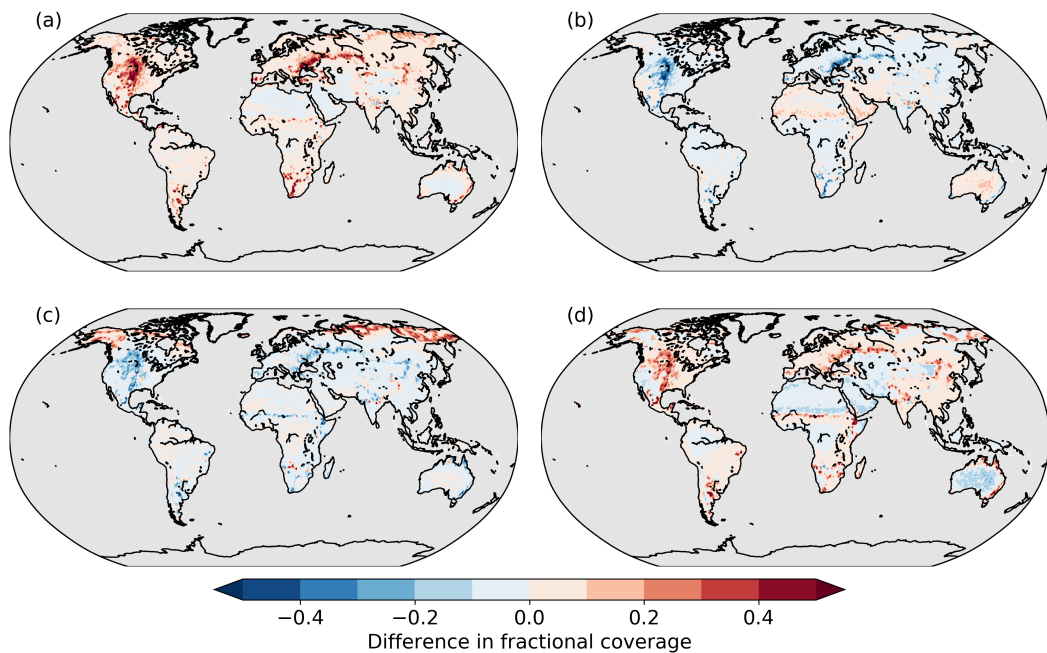


**Figure 3.3:** Difference in fractional coverage of (a) Noextremes trees, (b) Noextremes grasses, (c) Hotdry trees and (d) Hotdry grasses compared to the Control.

at Noextremes-Control and Hotdry-Control (Fig. 3.5). NPP of trees increases nearly everywhere in Noextremes compared to the Control, by up to  $200 \text{ gC m}^2 \text{ yr}^{-1}$  in some regions in the mid-west of the U.S. (Fig. 3.5a). NPP of grasses shows slight increases in the lower latitudes but strong decreases in the higher latitudes, which are of similar magnitude as the increases in tree NPP (Fig. 3.5b). The pattern is more diverse for Hotdry, where NPP of trees generally decreases in the low-to-mid latitudes by up to  $-150 \text{ gC m}^2 \text{ yr}^{-1}$  but increases in the very high latitudes (Fig. 3.5c). NPP of grasses tends to increase in most regions except some very dry regions in the Sahara and Middle East, Australia, Namibia, and the Southwest of the U.S. (Fig. 3.5d).

Finally we investigate whether the interannual variability in NPP for four vegetation classes changes between the Control and the different scenarios. Overall, interannual variability in NPP is smallest in Tropical and Temperate trees and largest in Boreal trees (Fig. 3.6). Most scenarios tend to decrease variability in particular for trees, with Noextremes leading to significant decreases in all vegetation classes. In contrast, Hotdry tends to increase variability, though the difference to the Control is only significant for Boreal trees and Grasses. For Grasses, also the Hot and the Dry scenario lead to a significant increase in NPP variability.

### 3.3.3 Path to model equilibrium

We explore how fast vegetation composition and net ecosystem production adjust towards a new equilibrium after a step-like change in extreme statistics, in this case a change in the frequency of hot and/or dry extremes. To this end, we analyse the 100-yr scenario simulations that started from the shared model spin-up forced by the Control climate. At the start of each scenario simulation, frequencies of dry and hot events suddenly change from those in the Control climate to those in the scenario.

Using the simulations based on the shared spin-up, we explore whether LPX-Bern reaches a new equilibrium (measured in terms of stable vegetation composition and neutral net ecosystem production) within the 100-year simulations after frequencies of dry and hot events suddenly change from Control to the different scenarios. Overall, the Noextremes and the Hotdry scenarios cause the largest disturbance in vegetation cover (Fig. 3.7). For most vegetation classes and most scenarios, the scenario simulations starting from the shared spin-up are within the range of variability of the scenario simulation starting from an individual spin-up at the end of the simulation. Exceptions are Tropical trees in the Noextremes and the Hot scenarios, Temperate trees in the Hot and the Hotdry scenarios and Grasses in the Hotdry scenario.

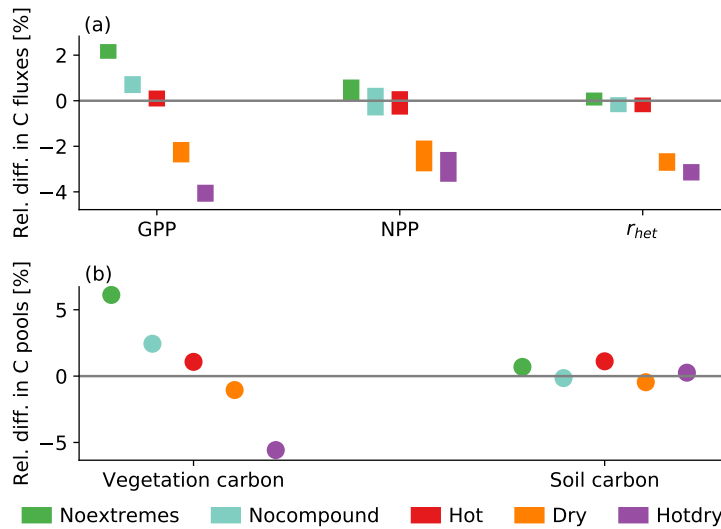


**Figure 3.4:** Relative difference of the scenarios to the Control for (a) the global annual GPP, NPP, and heterotrophic respiration ( $r_{het}$ ) as well as (b) vegetation carbon and soil carbon. The bars in (a) show the minimum to maximum range of the 100 year-long simulations. Because the interannual range for carbon pools in (b) is very small we only show the mean over the 100 years.

The strongest response in vegetation cover occurs in the first 20 years. Grasses show a particularly fast response in the Hotdry scenario, where there is an initial decrease in coverage followed by a rapid increase. The reason for this seems to be that (predominantly temperate) grasses that are adapted to the climate in the control quickly die due to the frequent hot and dry conditions but then a regrowth of (predominantly tropical) grasses that can tolerate such conditions occurs. Overall, the above results suggests that, for the more extreme scenarios, 100 years may not be enough to fully reach equilibrium after a sudden change in dry and hot event occurrences.

The findings based on vegetation cover are confirmed when investigating the temporal evolution of global annual net ecosystem production (NEP) in the simulations with shared spin-up (Fig. 3.8). Again, the disturbance is largest for the Noextremes (about  $1 \text{ PgC yr}^{-1}$  more uptake at the beginning of the simulation) and the Hotdry scenario (about  $3 \text{ PgC yr}^{-1}$  less uptake at the beginning). In all scenarios, global annual NEP converges towards 0 at the end of the 100-year simulations and varies within the range of interannual variability of the individual spin-up simulations. Nevertheless, NEP is slightly larger than 0 in the Noextremes scenario and slightly smaller than 0 in the Hotdry scenario even at the end of the simulation, indicating that not all carbon pools are in full equilibrium after 100 years.

### 3.4 Discussion

Using stationary climate scenarios with varying drought-heat signatures and a dynamic vegetation model we show that different occurrence frequencies of dry, hot, and compound dry-hot events lead to differences in vegetation coverage and related differences in global NPP (Fig. 3.2). The fraction of land area covered with vegetation is similar in all scenarios. However, there are shifts in coverage and NPP between vegetation classes. A key finding is that the climate, as represented by the Noextremes scenario, which features no extreme droughts or heatwaves and relatively little interannual variability, favours tree coverage (Fig. 3.2). This is evident in the tropical biomes to some extent but even more evident at higher latitudes. For trees to grow well, typically more stable environmental conditions are needed as compared to grasses (Sitch et al., 2003). For example, the biomass of grasses, with their fast biomass turnover and short life cycle, recovers much faster after an increase in mortality, e.g., due to a drought-heat event, than tree biomass.

Hence, overall, a more stable climate with few extremes is very beneficial for trees. In models such as LPX-Bern, trees are favoured over grasses. In particular, they get priority for foliar coverage if conditions are suitable for tree growth. This explains why, in a more stable (i.e., less variable) climate, tree cover

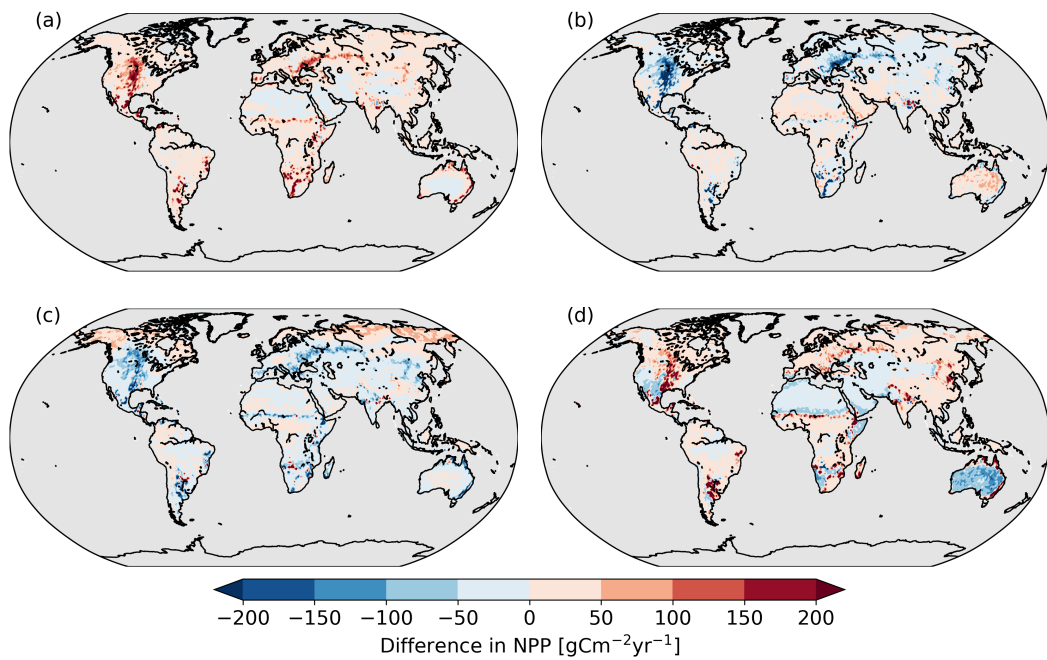


**Figure 3.5:** Difference in NPP for (a) Noextremes trees, (b) Noextremes grasses, (c) Hotdry trees and (d) Hotdry grasses compared to the Control.

increases and grass cover decreases, and vice versa.

While a climate with more heatwaves has little influence on tree coverage in the tropics, it tends to increase coverage in higher latitudes (Fig. 3.2). Trees in higher latitudes are typically temperature limited (Way & Oren, 2010). So a climate with more heatwaves alleviates some of these temperature constraints. While overall more heatwaves increase tree coverage globally, there are strong regional variations, meaning that not everywhere higher temperatures lead to more growth (Ruiz-Pérez & Vico, 2020). In higher latitudes, more frequent heatwaves mean overall warmer temperatures during the growing season without necessarily exceeding the temperature limit of boreal trees, while in other regions such a limit might be reached more quickly, leading to a decrease in tree cover. Grass coverage does not significantly change for the Hot scenario compared to the Control.

If water is restricted, as it is for the Dry scenario, tree coverage is slightly reduced overall. However, unlike in the other scenarios, grasses in a dry climate do not compensate for changes in tree coverage. Rather, grass coverage is decreased as well. This likely happens because grasses tend to grow in already dry regions, where tree coverage is unlikely. If these regions get drier, it might even get too dry for grasses to grow. When comparing the Hot and Dry scenarios, we see that the effects on global NPP as well as the vegetation carbon pool are more negative for the Dry than Hot scenario (Fig. 3.4). A drought event, therefore, does not have to be as extreme as a heat event to have a comparable impact, which is also supported by findings of Ribeiro et al. (2020).

The scenario with frequent compound hot and dry extremes clearly causes the strongest response and leads to a reduction in tree coverage across all climate zones. Hence, here even the warmer conditions in the northern latitudes that generally promote tree growth are superseded by the negative impacts of droughts (Belyazid & Giuliana, 2019; Ruiz-Pérez & Vico, 2020), though the effect is less pronounced for Boreal trees than for Temperate trees. Grass coverage, on the other hand, increases because it can fill the areas that were previously covered by trees. In dry regions, however, grass coverage is reduced for the Hotdry scenario as well, likely because here likely dryness thresholds under which vegetation cannot grow anymore are frequently exceeded. Global NPP as well as vegetation coverage is overall reduced for this scenario compared to the Control (Fig. 3.4).

Generally, trees grow nearly everywhere if the climate is favourable and features few extremes, leading to a reduction in grass cover. Only in dry regions do we observe an increase in grass coverage. There, conditions might still be unfavourable for trees to grow, but grasses benefit from the stable climate. In contrast, in a climate with frequent droughts and heatwaves, tree coverage is generally reduced, leaving

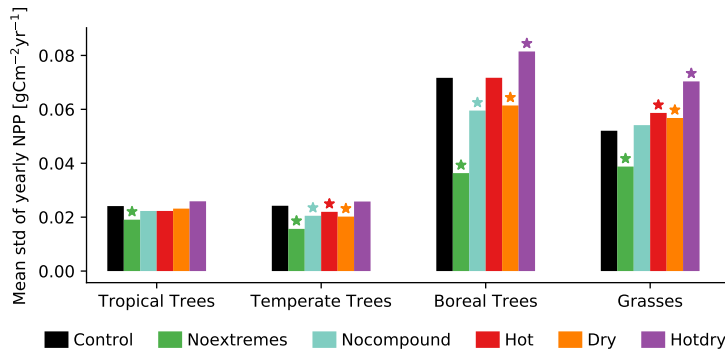


**Figure 3.6:** Variability of NPP (calculated as interannual standard deviation across years for the four vegetation classes with the mean taken over all grid cells). The stars show the scenarios that are significantly different from the Control at a 5 % significance level (based on a t-test).

room for grasses to grow, except in already dry regions, which become too dry even for grasses.

Globally, the effects of extremes are larger in the extratropics than they are in the tropics. The effects on Tropical trees are small for all scenarios compared to the Control, including the Hot and Dry extremes scenarios. One reason for this might be that strong evaporative cooling is maintained in tropical forests, even in a drier climate (Bonan, 2008) since the tropics (in particular tropical forest) are not so much water-limited but rather energy limited. However, case studies on recent droughts in the Amazon forest show how tropical forests can be negatively affected by drought conditions (Doughty et al., 2015; Feldpausch et al., 2016; Machado-Silva et al., 2021). The variability between the scenarios is small for Tropical trees and larger for Temperate and Boreal trees. The latter biomes are more water- and/or temperature-limited than the tropics and therefore react more strongly to variations in these variables. Grasses also show quite a large variability between scenarios owing to the fact that grasses react quicker to climate variations, meaning they die and regrow faster than trees (Ahlström et al., 2015).

While vegetation carbon displays a pattern that correlates with the changes in coverage, the same is not true for soil carbon. Rather, the changes in soil carbon (Fig. 3.9) resemble the changes in grasses (Fig. 3.3).

Choosing an appropriate spin-up when modelling vegetation and the carbon cycle is important to make sure the model is in equilibrium. In our case, 1500 years seems appropriate, since the constant runs are stable over the 100 years. Starting with the same spin-up (based on the Control scenario) and a step change in extreme event occurrence, most but not all scenarios converge to the equilibrium that is reached when doing the spin-up with the scenario forcing within 100 years (Fig. 3.7). Given the trajectories, we do not expect the runs with shared spin-up to reach the same end point as the runs with individual spin-up, even if the simulations were prolonged. Other vegetation models might have other response times to such a step change in extreme event characteristics. For the main analysis, we used the ‘individual spin-up’ runs, since these are the runs where the model had time to reach full equilibrium.

Scenarios, where the occurrence of heatwaves, droughts, and drought-heat events is changed in a step-like manner, reveal the characteristic time scales and magnitudes of the adjustment of a system, here the land biosphere, to the change. Our simulations reveal that plant coverage and NPP adjust on decadal time scales (Fig. 3.7) to altered extreme event statistics, while, in addition, multi-decadal-to-century response time scales are evident for global NEP (Fig. 3.8). The response time scales and magnitudes of change are likely model specific to some extent. It would be illustrative to probe the response to step changes using other models. Though the setup of the step change in the occurrence of droughts and heatwaves is somewhat unrealistic, long-term trends in the dependence between temperature and precipitation have been detected in climate model projections (Zscheischler & Seneviratne, 2017). Such changes in the dependence structure can be quite relevant, for instance they may exacerbate climate change impacts on crops (Lesk et al., 2021).

We run the vegetation model offline, that is, there is no feedback from the land surface to the climate, and keeping the atmospheric CO<sub>2</sub> level constant. Processes in the real world might be more complex. Especially CO<sub>2</sub> fertilization, where higher CO<sub>2</sub> concentrations lead to a more efficient uptake of CO<sub>2</sub> by the plants and thus less chance to lose water through open stomata, may modulate how hot and dry

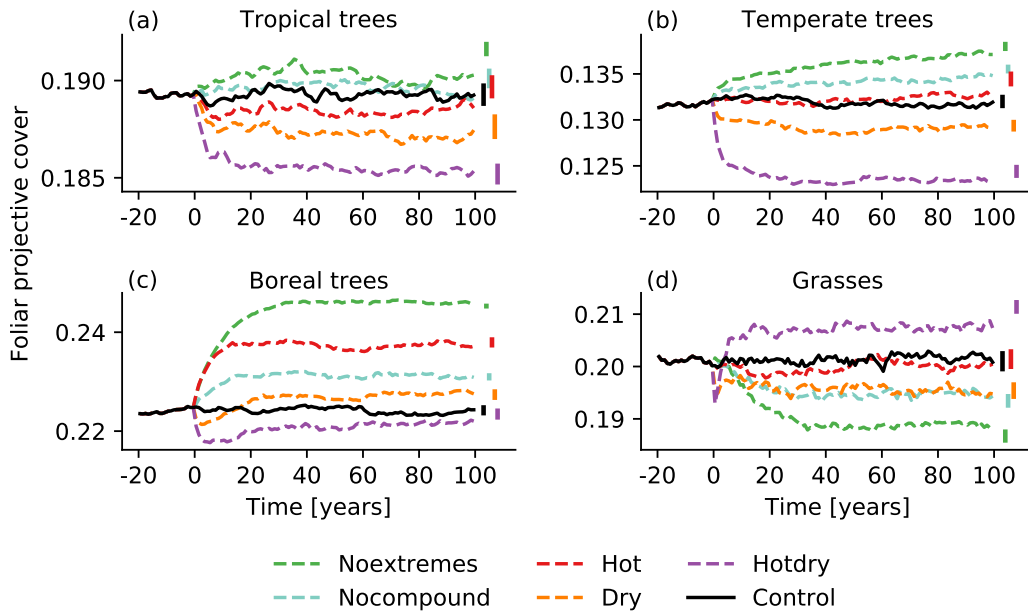


**Figure 3.7:** Time series of the fractional coverage (foliar projective cover) from the simulations that use the shared spin-up (black line). Scenarios are shown in colored dashed lines for (a) Tropical trees, (b) Temperate trees, (c) Boreal trees, and (d) Grasses. The first 20 years (-20 to 0) represent the last 20 years of the shared spin-up. The variability (minimum to maximum) in vegetation cover in the individual spin-up simulation (spin-up uses data from the respective scenarios) is indicated by the bars on the right-hand side. Note the different ranges of the y-axes.

conditions affect vegetation and carbon dynamics in the future (Domec et al., 2017; De Kauwe et al., 2021).

All results, such as the exact changes in vegetation distribution and carbon uptake, are somewhat sensitive to the choice of the dynamic global vegetation model and the employed climate model. Every model has biases and limitations which could be discussed at length, but for argument’s sake we will only discuss some of them briefly. One important component in LPX are the bioclimatic limits, as already mentioned in Sect. 3.2.2. Mortality induced by maximum temperature only affects tropical trees. One could imagine a different extreme response if this parameter also applied for grasses. As it is, C4 grasses are very water-efficient in LPX, which leads to Australia being a bit too green in our simulations compared to observations, as an example. This could also explain why grasses thrive in the Hotdry scenario. A potential increase in atmospheric  $\text{CO}_2$  conditions as it is predicted by socio-economic scenarios would further alleviate drought stress and thus benefit C4 grasses. The parameterization of the water balance is another possible factor that greatly influences the response to dry conditions. LPX has a relatively simple supply and demand driven water limitation and for instance does not consider effects of Xylem damage (Arend et al., 2021). Overall, models may differ strongly depending on model parameterizations and process representations (Paschalis et al., 2020). Furthermore, some uncertainties also arise from the model setup. For example, land-atmosphere feedbacks may play an important role (Humphrey et al., 2021), which are not considered in such an offline model setup as we have conducted in this study. Considering the number of uncertainties that may govern vegetation and carbon cycle response to varying drought-heat signatures, a model intercomparison project using our scenarios as forcings for different vegetation models has already been set up and may reveal insights on how model differences affect the results.

### 3.5 Conclusion

It is widely acknowledged that extreme climate events can have large impacts on ecosystems and society. This study investigates the effects of different drought-heat occurrences in six hypothetical climate scenarios on vegetation distribution and terrestrial carbon dynamics, as simulated by the LPX-Bern

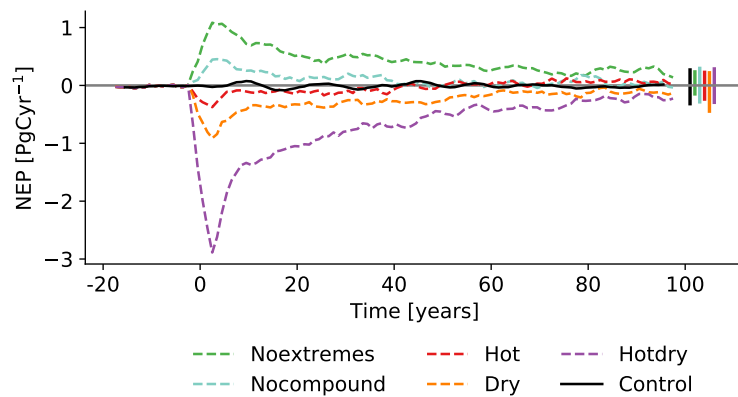


**Figure 3.8:** Time series of global annual NEP from the simulations that use the shared spin-up (black line). Scenarios are shown in colored dashed lines. The first 20 years (-20 to 0) represent the last 20 years of the shared spin-up. The variability (minimum to maximum) in global NEP in the individual spin-up simulation (spin-up uses data from the respective scenarios) is indicated by the bars on the right hand side. A 5-year moving average was applied to smooth the time series.

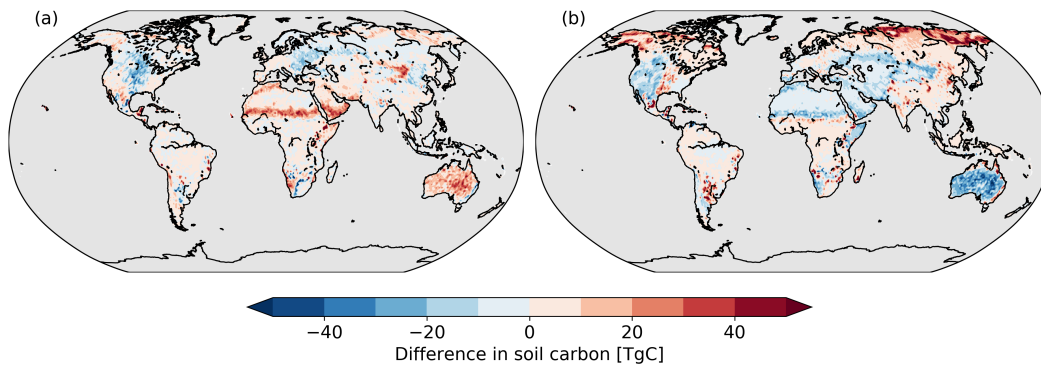


**Figure 3.9:** Difference in soil carbon for (a) Noextremes vegetation (b) and Hotdry vegetation to the Control.

dynamic global vegetation model. Generally, effects of changes in extreme event frequency are more pronounced in the extratropics than in the tropics. We found that global carbon cycle variability is most stable in a climate without any extreme events, which favours more tree cover and a higher global terrestrial carbon stock. The effects on vegetation cover and carbon stocks and fluxes of a climate with many heatwaves are generally smaller than the effects of a climate with many droughts. The largest effect, however, has a climate with frequent concurrent droughts and heatwaves. Here, forest cover and global vegetation carbon is strongly reduced. Grasses, in contrast, are more abundant. These effects surpass the simple linear combination of the effects of single droughts and single heatwaves.

Overall, our results highlight the importance of considering compound events when analysing impacts of climate extremes. Impacts may potentially be underestimated when only looking at single event extremes instead of compounding extremes. Furthermore, the results suggest that uncertainties in projections of vegetation distribution and carbon dynamics in Earth system models may stem from different drought-heat signatures in the atmospheric module (Zscheischler & Seneviratne, 2017), in addition to structural model differences in the vegetation component. It is important to investigate and understand these issues in order to improve models as well as our knowledge about extreme events and their processes, which may lead to significant impacts on society and ecosystems.

### 3.6 Supporting information

**Table 3.2:** Bioclimatic limits of the ten available plant functional types in LPX-Bern.

	Min. coldest monthly mean temperature	Max. coldest monthly mean temperature	Min. growing degree days (at or above 5°C)	Upper limit of temperature
Tropical Broadleaf Evergreen	15.5	no limit	0	no limit
Tropical Broadleaf Raingreen	15.5	no limit	0	no limit
Temperate Needleleaf Evergreen	-2	22	900	no limit
Temperate Broadleaf Evergreen	3	18.8	1200	no limit
Temperate Broadleaf Summergreen	-17	15.5	1200	no limit
Boreal Needleleaf Evergreen	-32	-2	550	30
Boreal Needleleaf Summergreen	no limit	-2	350	30
Boreal Broadleaf Summergreen	no limit	-2	550	30
Temperate Herbaceous	no limit	no limit	0	no limit
Tropical Herbaceous	no limit	no limit	100	no limit



## Chapter 4

# Large variability in simulated response of vegetation composition and carbon dynamics to variations in drought-heat occurrence

Elisabeth Tschumi, Sebastian Lienert, Ana Bastos, Philippe Ciais, Konstantin Gregor, Fortunat Joos, Jürgen Knauer, Philip Papastefanou, Anja Rammig, Karin van der Wiel, Karina Williams, Yidi Xu, Sönke Zaehle, Jakob Zscheischler

In preparation for *JGR Biogeosciences*.

### Abstract

Heatwaves and droughts are expected to become more frequent and severe with climate change. How these changes in extremes and differences in the simulation of droughts and heatwaves affect vegetation distribution and the terrestrial carbon cycle as well as the uncertainties in its projections are not well understood. In previous work, six hypothetical climate scenarios featuring different drought-heat signatures have been developed to investigate how single vs. compound extremes affect vegetation distribution and carbon dynamics. To specifically investigate vegetation and carbon cycle dynamics under extreme conditions, these scenarios are used to force six dynamic global vegetation models. We find that global responses to different drought-heat signatures vary greatly between dynamic global vegetation models, especially for the scenarios with no or only few extremes, for which the models sometimes show opposite responses in vegetation changes. In climate scenarios with frequent droughts or frequent compound drought-heatwave events, models agree on reduced tree cover, which is in most cases replaced by grasses and leads to a decrease in vegetation carbon stocks. We further find that the frequency of concurrent hot and dry conditions is strongly related to the total carbon pools in most land areas, suggesting that this compound extreme occurrence leads to a reduction of the natural land carbon sink.

## 4.1 Introduction

Over the last six decades the terrestrial biosphere has sequestered on average about 28 % of the anthropogenic CO<sub>2</sub> emissions each year (Friedlingstein et al., 2022). While large part of this net carbon sink is likely driven by elevated CO<sub>2</sub> concentrations (Fernández-Martínez et al., 2019), many other factors influence the uptake capacity of the land, including variations in temperature and water availability, which are expected to change with global warming. Many of these effects and their implications for carbon dynamics and vegetation distribution are not well quantified. The effects of higher temperatures and higher CO<sub>2</sub> concentrations, for example, may counteract each other (Peñuelas et al., 2017). Reduced productivity due to higher evaporative demand and stomatal closure (Friend et al., 2014) as a consequence of higher temperatures may be compensated by increased water use efficiency (De Kauwe et al., 2013; Keller et al., 2017; Walker et al., 2021) due to elevated CO<sub>2</sub>. Biomes in higher latitudes may benefit from an increased growing season length but may be limited by nutrient availability (Zaehle et al., 2010; Du et al., 2020). Overall, future projections of the terrestrial carbon sink are highly uncertain and in particular models disagree whether the terrestrial biosphere will continue to act as a carbon sink or become a carbon source under strong climate change (Friedlingstein et al., 2014). While these uncertainties may be largely related to different implementations and parameterizations in vegetation models, they may also be related to differences in climate models regarding their simulation of the occurrence rates of droughts, heatwaves, and their co-occurrence (Herrera-Estrada & Sheffield, 2017; Zscheischler & Seneviratne, 2017; Bevacqua et al., 2022).

Extreme weather and climate events can strongly influence carbon dynamics and may even lead to shifts in vegetation composition (Reichstein et al., 2013; Felton & Smith, 2017). In particular, droughts and heatwaves are among the most damaging hazards for terrestrial vegetation (Allen et al., 2010; Zscheischler et al., 2014b; Frank et al., 2015; Sippel et al., 2018; von Buttlar et al., 2018; Buras et al., 2020; Senf et al., 2020; Arend et al., 2021), and often co-occur as compound events (Bastos et al., 2014; Zscheischler et al., 2018, 2020). Nevertheless, the impacts of droughts and heatwaves can vary substantially, depending on the vegetation type, location, and phenology of the vegetation (Sippel et al., 2016; Bastos et al., 2020b; Flach et al., 2021). Furthermore, in some instances, their individual effects can cancel each other out while in other cases they compound each other, again depending on the location and the underlying vegetation type and state (Li et al., 2022).

In most cases, impacts from compound events are not simply a linear combination of the univariate impacts (Zscheischler et al., 2014b; Ribeiro et al., 2020; Bastos et al., 2021). Furthermore, since droughts and heatwaves often co-occur (Zscheischler & Seneviratne, 2017), it is difficult to disentangle their individual effects from long-term observations. To understand the effects of extreme events on vegetation, we need to know which factors influence the distribution of vegetation. These factors might be climate conditions such as temperature, precipitation, and light availability as well as other environmental conditions such as atmospheric CO<sub>2</sub> concentrations, nutrient availability, or topography (Peng, 2000). Controlling all of these confounding factors in experiments in the real world is expensive and therefore, field experiments typically focus on individual species, often different types of grasslands (Hoover et al., 2014).

Here, we follow a modelling approach that allows generating controlled environments to simulate vegetation responses, where different input variables can be tightly controlled and modified to simulate single and compound extremes and thus estimate and compare their different impacts. To cover different biomes and climate regions, large-scale biogeographical and biogeochemical models are required. Dynamic global vegetation models (DGVMs) incorporate key ecological processes such as tree growth, nutrient cycling, competition, and mortality and simulate the distribution of vegetation types and their response to climate variability. DGVMs are able to predict vegetation structure, carbon pools, and fluxes over time and space. Despite being developed to answer similar questions, DGVMs can differ significantly in their temporal resolution, selection of processes, and parameterizations.

When suitable dynamic vegetation models have been selected, one challenge is how to create suitable forcing data. Adding artificial extremes to an existing time-series may lead to physically inconsistent weather patterns. In contrast, sampling from very long stationary climate simulations offers the opportunity to generate scenarios that are similar in their climatology but differ in the occurrence rate of extremes and compound extremes. For example, Tschumi et al. (2022a) generated six 100-year long scenarios that differ in the occurrence rates of droughts, heatwaves, and compound drought-heatwave events, based on the large ensemble simulation from the climate model EC-Earth.

In previous work Tschumi et al. (2022b) forced the DGVM LPX-Bern with different climate scenarios of Tschumi et al. (2022a) and found that LPX-Bern simulated a much higher forest cover in scenarios with few or no hot and dry extremes and more grasses when frequent compound drought-heatwave events occur (Tschumi et al., 2022b). Here, we extend this analysis to a model intercomparison containing six DGVMs. In particular, we evaluate the agreement in their vegetation and carbon cycle response to scenarios that have varying drought-heat signatures but similar present-day mean climate. We further explore whether the frequency of compound event occurrence affects the magnitude of carbon pools at a regional level.

## 4.2 Data and Setup

### 4.2.1 Climate forcing

We use the forcing scenarios generated by Tschumi et al. (2022a). They consist of a set of six 100-year long climate scenarios with similar climatologies but varying drought-heat signatures, originally derived from long stationary climate model simulations whose global mean temperature is approximately at the level of observed 2011-2015 temperatures. The scenarios differ in the occurrence of droughts and heatwaves during the three months with maximum net primary production (NPP), based on simulations conducted with the DGVM LPX-Bern. In those three months the effects of hot and dry extremes are likely to cause the largest effects.

Besides a control scenario representing natural variability (Control), one scenario has neither heat nor drought extremes (Noextremes), one has univariate extremes (heat or drought) but no compound extremes (Nocompound), one has only heat extremes but few droughts (Hot), one has only droughts but few heatwaves (Dry), and one has many compound heat and drought extremes (Hotdry). See Table 4.1 for an overview of the sampling design.

**Table 4.1:** Sampling design for the six climate scenarios (Tschumi et al., 2022a). Sampling is based on average temperature and precipitation during the three months in which vegetation is most productive in terms of NPP. The table is taken from Tschumi et al. (2022b).

Scenario name	Sampling procedure
Control	100 randomly selected years representing present-day climate
Noextremes	only years where temperature and precipitation lie between the 40 <sup>th</sup> and 60 <sup>th</sup> percentile
Nocompound	no years where both temperature and precipitation lie above the 85 <sup>th</sup> percentile or below the 15 <sup>th</sup> percentile
Hot	years where temperature exceeds the 85 <sup>th</sup> percentile and precipitation lies between the 40 <sup>th</sup> and 60 <sup>th</sup> percentiles
Dry	years where precipitation lies below the 15 <sup>th</sup> percentile and temperature lies between the 40 <sup>th</sup> and 60 <sup>th</sup> percentile
Hotdry	years where temperature lies above the 85 <sup>th</sup> percentile and precipitation lies below the 15 <sup>th</sup> percentile

The scenarios differ only moderately in their annual global mean climate (about 0.3 °C in temperature and 6 % in precipitation across all scenarios) and do not contain any long-term trends. Furthermore, at the local level, climatologies are similar among scenarios, which differ primarily in the occurrence of droughts and heatwaves (Tschumi et al., 2022a). The data are provided on a daily time step over land (except Antarctica and parts of Greenland) on a regular 1° × 1° grid. Due to the sampling design, there is no spatial coherence in the climate fields, that is, the climate in one pixel is independent of the climate in the neighbouring pixel. A complete description of the scenarios, including a quantification in how they differ in terms of droughts and heatwaves as well as access to the forcing data can be found in Tschumi et al. (2022a).

## 4.2.2 Modelling setup

This model intercomparison project (MIP) aims at comparing the response of different vegetation models to varying likelihoods of droughts, heatwaves, and compound drought-heatwave events, while keeping everything else approximately equal, in an idealised world. The goal is to better understand uncertainties in the simulation of vegetation composition and carbon dynamics stemming from those climate extremes and compound events. The following models were used in this analysis: CABLE-POP (Haverd et al., 2018), JULES (Best et al., 2011; Clark et al., 2011), LPJ-GUESS (Smith et al., 2014), LPX-Bern (Lienert & Joos, 2018), OCN (Zaehle & Friend, 2010), and ORCHIDEE-MICT (Guimberteau et al., 2018). A short description of each model is provided in Section 4.2.3.

For all models, six simulations are run with the input variables sampled as described in Section 4.2.1. All models are run with dynamic vegetation, except for CABLE-POP, where vegetation distribution is constant over time but differs between the scenarios as its vegetation distribution is calculated from mean climate conditions at the beginning of the runs. The models only simulate natural vegetation, based on the corresponding plant functional types (PFTs) that are represented by each model. CO<sub>2</sub> is kept constant at 389.78 ppm (level of 2011). An input file for nitrogen deposition is provided (from NMIP, Tian et al. (2018)). The nitrogen deposition is also given for the year 2011 and is kept constant. Each model uses its own approach to distribute nitrogen deposition over the year. No nitrogen fertilization is included. The input data is provided on a  $1^\circ \times 1^\circ$  grid. It is important that all models use the spatial resolution of the forcing data, since there is no spatial coherence in the climate forcing due to the nature of the sampling (Section 4.2.1). The spin-up for the scenarios consists of the 100 years of data for each scenario, recycling it as often as needed to ensure that vegetation and carbon pools are in equilibrium during each of the 100-year simulations.

## 4.2.3 Model descriptions

In the following we provide a short description of each vegetation model that participated in the MIP.

### CABLE-POP

CABLE-POP (Haverd et al., 2018) has been developed around a biogeophysics core module (Wang & Leuning, 1998) and a biogeochemistry module including nitrogen cycling (Wang et al., 2010). The 'POP' module (Haverd et al., 2013) simulates woody demography, which represents forest population dynamics such as establishment and mortality, but not competition among vegetation types. The model distinguishes eight plant functional types which can co-occur in a grid cell. The model disaggregates daily meteorological forcing into 3-hourly time steps using a weather generator.

### JULES

The Joint UK Land Environment Simulator (JULES) model (Best et al., 2011; Clark et al., 2011) is a community model and is used in coupled or stand-alone mode forced by meteorological variables. Since JULES runs on sub-daily timesteps, we made use of the JULES disaggregator (Williams & Clark, 2014), which is based on the IMOGEN method (Huntingford et al., 2010). The model parameters (science settings i.e. excluding driving data,  $1^\circ \times 1^\circ$  grid, simulation dates, ancillary data, prescribed data and spin-up method that were specified for this model intercomparison) are described in Mathison et al. (2022). However, we only represent the natural plant function types in this study. We also do not use the fire module.

### LPJ-GUESS

The Lund-Potsdam-Jena General Ecosystem Simulator (LPJ-GUESS) (Smith et al., 2001; Sitch et al., 2003; Buras et al., 2020) is a DGVM simulating processes such as establishment, growth, mortality, and competition of PFTs of various age cohorts. For this study, a spin-up time of 1000 years was used. Disturbances were modeled as patch-destroying disturbances with an average return time of 300 years (Pugh et al., 2019). In addition, fire was modeled via the GLOBFIRM fire model (Thonicke et al., 2001). To model the vegetation, global PFT parameterizations were used. As forcing, the surface air temperature, precipitation, and downward shortwave radiation from this MIP were used, together with LPJ soil codes,

a world soil file for global climate modelling (Zobler, 1986). The nitrogen cycle (Smith et al., 2014; Buras et al., 2020) was turned on and we used 25 replicate patches to simulate a distribution of vegetation stands of different stages after disturbance.

### **LPX-Bern**

The Land surface Processes and eXchanges (LPX-Bern v1.4) model (Lienert & Joos, 2018) is a Dynamic Global Vegetation Model based on the Lund-Potsdam-Jena (LPJ) model (Sitch et al., 2003). It needs as input daily or monthly data of temperature, precipitation and radiation, as well as information on soil type (Wieder et al., 2014), CO<sub>2</sub>, and nitrogen deposition to model water, carbon, and nitrogen cycling in each grid cell. The model represents ten different natural vegetation types (eight tree PFTs and two grass PFTs) on mineral soils. PFTs grow within their bioclimatic limits and compete for resources. Land-use classes for cropland, pastures, and urban area, and for wetlands and peat lands are not enabled in this study. The fire disturbance module and the nitrogen module were activated during the runs.

### **OCN**

The terrestrial biogeochemical model O-CN (referred to as OCN here) is originally based on the ORCHIDEE model (Krinner et al., 2005) but was extended through the addition of dynamic nitrogen cycle processes coupled to the carbon cycle as described in Zaehle et al. (2010) and Zaehle et al. (2011). Biological nitrogen fixation was dynamically simulated with the OPT scheme described by Meyerholt et al. (2016). The model represents 13 PFTs (eight tree types, natural C3 and C4 grasses, C3 and C4 crops and bare-soil). The version of OCN used in this study simulates dynamic vegetation processes (mortality, competition, establishment) based on the LPJ model (Sitch et al., 2003) and includes fire disturbance dynamics based on Thonicke et al. (2001). Only natural vegetation types were included, i.e. 11 PFTS, excluding the two crop types. A spin-up simulation was performed by recycling the 100-year climate forcing with random sampling until vegetation and soil carbon pools were in equilibrium. Fire disturbances and nitrogen dynamics were activated during the spin-up and runs.

### **ORCHIDEE-MICT**

ORCHIDEE-MICT (Organising Carbon and Hydrology in Dynamic Ecosystems- aMeliorated Interactions between Carbon and Temperature) has been developed from ORCHIDEE, a land surface component of the French Institut Pierre Simon Laplace (IPSL) Earth system model (ESM) that simulates water, energy, and carbon processes (Krinner et al., 2005). The ORCHIDEE-MICT incorporates a new vertical soil parameterization scheme, snow processes, and a fire module, improving the representation of high-latitude processes such as permafrost physics and hydrology (Guimberteau et al., 2018). A spin-up simulation following Guimberteau et al. (2018) was performed to reach the equilibria for soil conditions and carbon pools. The model discretizes the vegetation into 13 PFTs (eight for trees, two for natural C3 and C4 grasses, two for crops, and one for bare-soil type). Daily forcings provided by the MIP were used for the simulations. Only the natural PFTs (trees and natural grasses) were represented and the anthropogenic processes such as grass grazing and crop harvesting were disabled.

## **4.3 Results**

### **4.3.1 Features of the input scenarios stemming from the sampling method**

The scenarios differ in the occurrence of droughts and heatwaves during the three months of highest vegetation productivity in terms of NPP, which were identified at the pixel level based on the control simulations from LPX-Bern (Section 4.2.1) (Tschumi et al., 2022b). The seasonal cycle of vegetation activity differs between models, so that for each individual model, the months of highest vegetation activity do not necessarily correspond to those estimated by LPX-Bern, used to derive the forcing scenarios (Fig. 4.8). This may induce uncertainties when analysing the results. In regions with pronounced seasonal cycle in vegetation activity, particularly the mid-to-high latitudes, the models show strong agreement. In contrast, rather large differences are found in the tropics and subtropics. These regions do not have a strongly pronounced seasonal cycle in vegetation activity and we thus assume that the effect is likely not very important for the overall results. Creating the scenarios is a major effort (Tschumi

et al., 2022a), hence, deriving scenarios that are based on different months for each model is beyond the scope of this work. Another important point which needs to be kept in mind when interpreting the simulations is the regional bias of the EC-Earth model when compared to observation-based data. Globally, temperatures differ by  $-0.5$  °C from CRU and precipitation differs by 7 %. Regionally, however, these biases can be much larger (Fig. 4.9). In tropical and subtropical regions, EC-Earth has a cold bias of up to  $-1.8$  °C while in the extratropics it has a small warm bias of  $+0.2$  °C. The largest precipitation bias can be found in the extratropics where EC-Earth displays a wet bias of about 43.5 % in some regions. In the tropics, some regions show very little bias while others show a dry bias compared to observations.

### 4.3.2 Vegetation cover, carbon pools and fluxes in the Control

Total mean global vegetation coverage, based on the foliar projective cover, which is the percentage of ground area occupied by the vertical projection of foliage, ranges from 43 % to 89 % in the Control scenario, depending on the model. For this scenario, most models simulate larger total tree coverage than total grass coverage (Fig. 4.1). Overall vegetation coverage is the lowest for LPJ-GUESS (43 %), OCN shows mainly tree coverage (70 %, with 78 % of vegetated area), whereas ORCHIDEE-MICT simulates the highest grass cover (46 %, with 89 % of vegetated area), with CABLE-POP, LPX-Bern, and JULES being somewhere in-between. Mirroring the variability in global vegetation cover, the models also differ strongly in their spatial patterns of vegetation distribution (Fig. 4.2). White areas in the maps represent land areas with bare soil. Most models agree on grass coverage in Australia, western USA, and central Asia, with some dominantly grass-covered regions in South Africa and southern South America. Some models (particularly ORCHIDEE-MICT) simulate grass cover in the Sahara desert. Tropical regions as well as most temperate to higher latitudes are mainly covered in trees. OCN simulates that nearly all land regions are dominated by tree cover, which is likely a consequence of the wet bias in the extratropics in the forcing data. Please note that the prescribed control climate has strong biases compared to observational data with strong impacts on simulated baseline vegetation distribution.

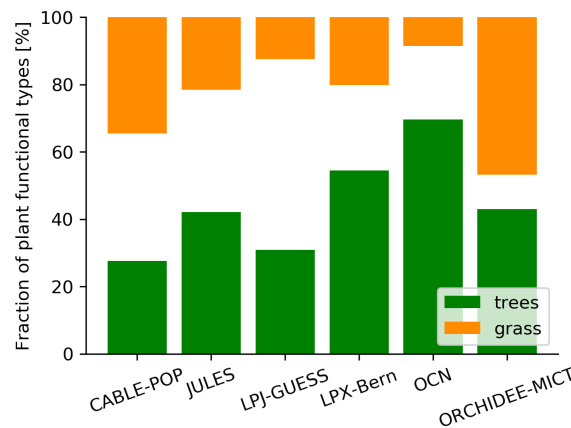


**Figure 4.1:** Tree and grass coverage, represented by foliar projective cover as % of total land grid cells, averaged across all grid cells and over the 100 years of the Control simulation. White spaces represents coverage types other than trees and grasses, mainly bare soil and ice.

Global gross primary production (GPP), net primary production (NPP), and heterotrophic respiration (RH) show some variation across models in the Control simulation, with GPP ranging from 134 to 195 PgC per year, NPP ranging from 68 to 96 PgC per year and RH ranging from 57 to 84 PgC per year (Fig. 4.3a). For most models, soil carbon pools (ranging between 1540 and 2078 PgC, ORCHIDEE-MICT being an exception with 3827 PgC) are generally about twice as large as the vegetation carbon pools (674 to 1876 PgC) (Fig. 4.3b). ORCHIDEE-MICT simulates a soil carbon pool about five times larger than the vegetation carbon pool (3827 PgC in soils compared to 674 PgC in vegetation). The sizes of the vegetation and soil carbon pools correlate with the vegetation distribution, where models with a high tree coverage also simulate a large vegetation carbon pool. The high soil carbon value in ORCHIDEE-MICT is probably related to the fact that it includes permafrost carbon in the soil carbon variable.

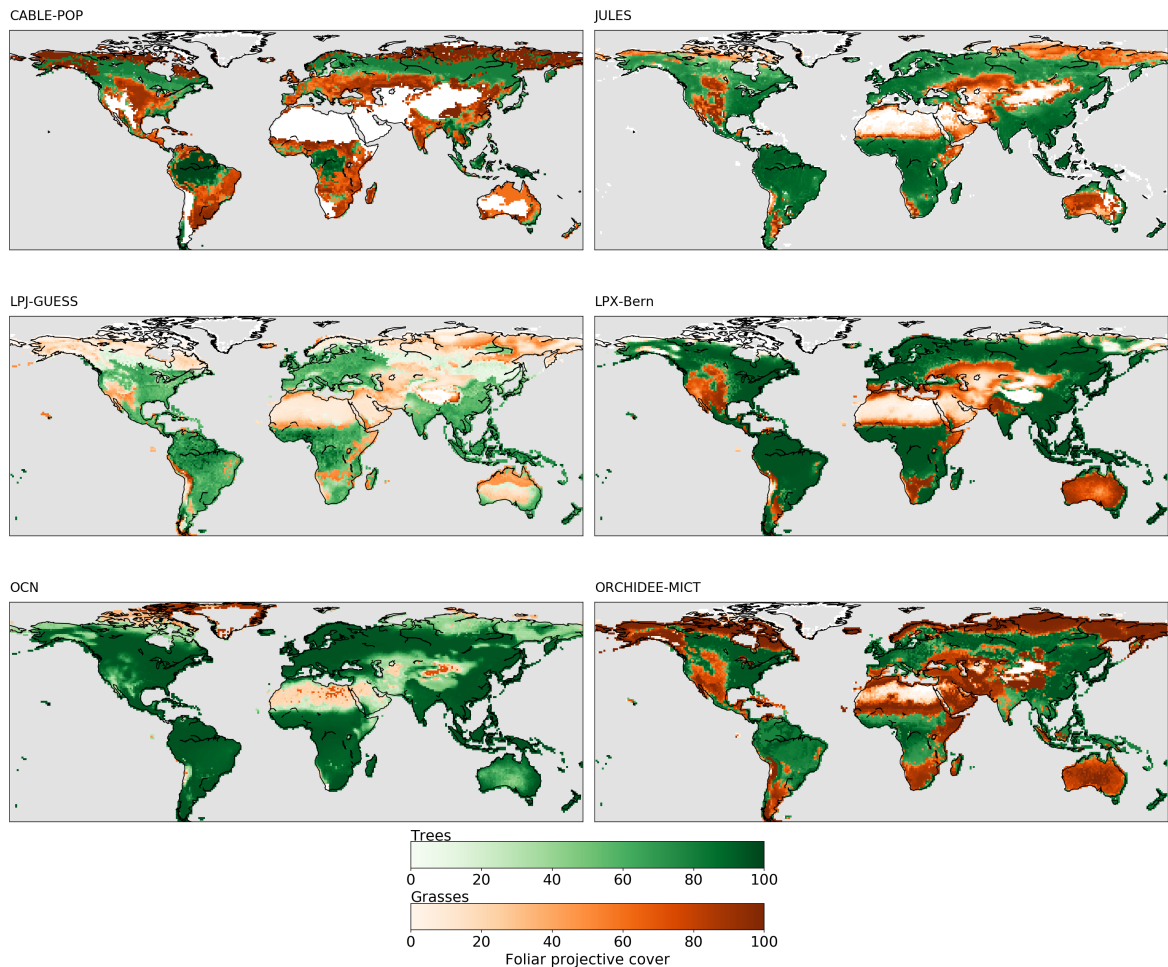


**Figure 4.2:** Fraction of the dominant vegetation class based on foliar projective cover, either trees or grasses, at each pixel. Shown is the mean over the 100 years of the control simulation for each vegetation model. White area represents regions with no tree or grass coverage, which mostly correspond to bare soil and ice.

### 4.3.3 The effect of varying drought-heat signatures

The responses in vegetation coverage to the different scenarios vary strongly between models (Fig. 4.4). The strongest agreement between models is found for the Hotdry scenario, for which all models agree on an increase in grass cover and nearly all models agree on a decrease in tree cover. In the Dry scenario, all models simulate a reduction in tree cover but models disagree as to whether grasses increase or decrease. In contrast, nearly all models simulate an increased tree cover in the Hot scenario. Again, model results vary in the grassland response to this scenario.

Models show relatively weak and inconsistent response to the Nocompound scenario. Finally, the responses to the Noextremes scenario, which represents a climate with both temperature and precipitation always between the 40<sup>th</sup> and 60<sup>th</sup> percentile during the three months of highest growth, are rather large but vary strongly across models: whereas LPX-Bern (red) and ORCHIDEE-MICT (pink) simulate a strong increase in tree coverage, the other models generally show a slight decrease or no change at all (in the case of CABLE-POP, purple). Overall, CABLE-POP generally shows a relatively weak response for most scenarios, possibly related to the fact that it does not simulate vegetation dynamically but uses fixed vegetation determined by the climate in the spin-up (Section 4.2.3).

In absolute terms, the largest relative differences are simulated by the OCN (blue) grass response to the Noextremes (+10.5 %), Dry (+8.9 %) and Hotdry (+7.7 %) scenarios, which is due to the fact that the overall grass fraction is very low in the Control (Fig. 4.1). LPJ-GUESS (green) also simulates an increase in grass cover of +9.5 % for Hotdry whereas LPX-Bern (red) and ORCHIDEE-MICT (pink) both simulate a decrease by about -7 % in grass cover for Noextremes. Regarding changes in tree cover,

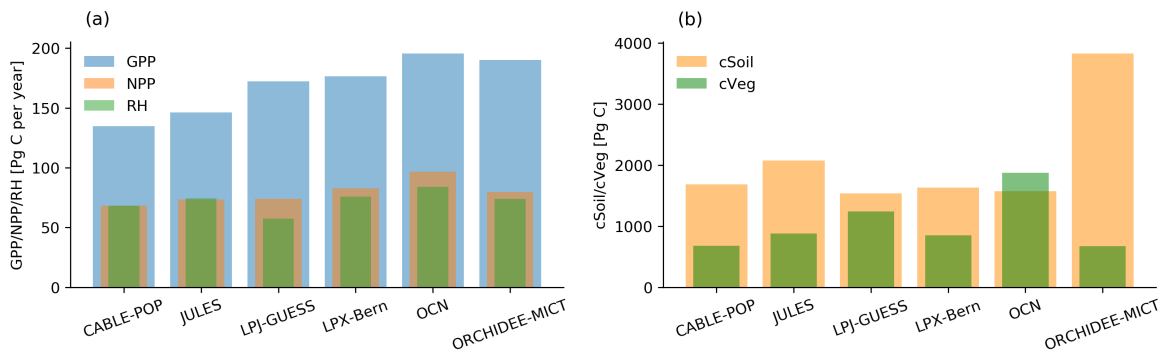


**Figure 4.3:** Global sums of the (a) terrestrial carbon fluxes GPP (blue), NPP (orange) and RH (green) in PgC per year as well as (b) vegetation (cVeg, green) and soil (orange) carbon pools PgC. Shown is the mean over the 100 years of the control simulation.

JULES (orange) simulates the strongest decrease (over -7 %) for Hotdry extremes whereas LPX-Bern and ORCHIDEE-MICT simulate a more than +5 % increase for Noextremes.

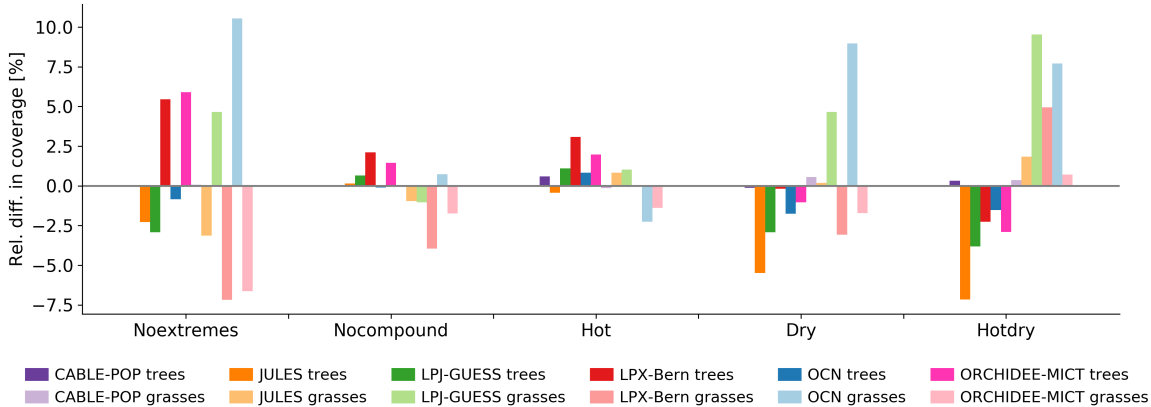


**Figure 4.4:** Relative differences in % of global mean tree (saturated colours) and grass coverage (light colours) based on foliar projective cover for all scenarios compared to the Control. Shown is the mean over the 100 years. The scenarios are indicated on the x-axis while the models are differentiated by colour.

Similar to the response in vegetation cover, the vegetation models show diverse responses in total vegetation and soil carbon pools relative to the Control (Fig. 4.5). For the Noextremes and the Nocompound scenario, most models agree on an increase in both vegetation and soil carbon, with LPX-Bern generally showing the strongest increase followed by ORCHIDEE-MICT. For the Hot scenario the responses across models are more mixed, with LPX-Bern showing an increase in both vegetation and soil carbon pools, JULES showing a slight decrease in both pools, and the remaining models showing both increases and decreases in the carbon pools. The Dry and the Hotdry scenarios overall lead to stronger carbon losses, especially in the vegetation pool, for which nearly all models agree on a loss. For soil carbon in these two scenarios, CABLE-POP, JULES, and ORCHIDEE-MICT show a decrease while the other models show an increase. The amount of decrease or increase is generally largest for the Hotdry scenario, followed by the Dry scenario. An exception is the change in the vegetation carbon pool in LPX-Bern and also to a lesser extent ORCHIDEE-MICT for the Noextremes and Nocompound scenario, which is relatively large and mirrors the increase in forest cover (Fig. 4.4). For most models, the effect of the Hotdry scenario on carbon pools exceeds the combined effect from both the Hot and Dry scenario. The effect from the Hotdry scenario on carbon pools is generally larger than the effect from the Dry scenario, and the effect from the Hot scenario shows an opposite response compared to the effect from the Dry scenario for many models, meaning that it would be difficult to predict the effect of the Hotdry scenario from the individual effects of the Hot and the Dry scenario.

In the previous sections we found an indication that the occurrence of more frequent compound hot and dry conditions may lead to a reduction in the overall carbon pools (vegetation and soil carbon

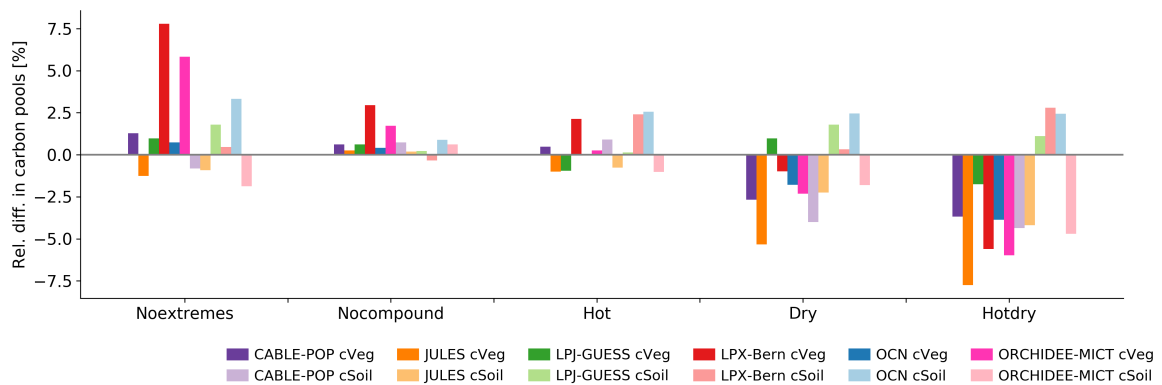


**Figure 4.5:** Relative differences in % of global mean vegetation (saturated colours) and soil carbon (light colours) for all scenarios compared to the Control. Shown is the mean over the 100 years. The scenarios are indicated on the x-axis while the models are differentiated by colour.

combined). The occurrence rate of concurrent hot and dry extremes can be approximated by the seasonal correlation between temperature and precipitation, with a stronger negative correlation indicating more frequent compound hot and dry conditions (Zscheischler & Seneviratne, 2017). We therefore test whether the correlation between temperature and precipitation in the months with highest productivity can serve as an indicator of total carbon accumulation. We find that for many models and most land regions, this is indeed the case (Fig. 4.6). In most regions and most models, we see a rather strong positive relationship. Since temperature and precipitation are generally negatively correlated over land (Fig. 4.10), this means that the stronger negatively correlated temperature and precipitation are, the smaller is the total carbon pool in that region. In other words, in those regions climatologically more frequent concurrent hot and dry conditions reduce the carbon pools at equilibrium in the dynamic vegetation models used in this study.

In some high-latitude regions, mountainous regions such as the Himalayas or the Alps and dry regions such as the Sahara desert, the correlation in Fig. 4.6 is slightly or even strongly negative in most models. In these regions, more frequent compound hot and dry conditions lead to higher carbon pools. Generally, this effect seems to hold for regions that are cold and/or regions that have little vegetation coverage to begin with. The magnitude of the correlation can be interpreted as a sensitivity of the dynamic vegetation and in particular the carbon pools to the occurrence of compound hot and dry events.

So far we have focused on the average and large-scale responses of the models to the different scenarios. However, local analyses might provide additional insights on model differences. Fig. 4.7 shows the variability in tree cover (first row), grass cover (second row), and GPP (third row) across years for all models and all scenarios for a location in the western USA (42.5 °N -110.5 °E). The Control simulation has a bias of +0.2 °C in annual mean temperature and +60 % in annual mean precipitation compared to observations in this location. The plot on the top left shows the cooling degree days (CDD) against the standardized precipitation index (SPI) as indicators for heatwave and drought intensity, respectively, for the different scenarios, as defined in Tschumi et al. (2022a).

Models strongly vary in a number of characteristics: the distribution between tree and grass cover, the interannual variability in vegetation cover and GPP, and their response magnitude to the different scenarios. While JULES, LPJ-GUESS, OCN, and ORCHIDEE-MICT generally simulate a higher tree cover than grass cover, the opposite is true for LPX-Bern and CABLE-POP. However, tree versus grass covers does not seem to affect the difference in GPP much between the models. Some models, in particular LPX-Bern and to some extent also LPJ-GUESS, OCN, and ORCHIDEE-MICT, show a large interannual variability in vegetation coverage (as shown by the length of the boxes), indicating a high sensitivity or fast response to year-to-year variations in weather conditions. This high interannual variability is to some extent also visible in GPP, though much more attenuated. Regarding the response to the different scenarios, LPX-Bern, OCN, and JULES agree on less tree coverage for the scenarios Dry and Hotdry. Also LPJ-GUESS shows a slight reduction in tree coverage for the Dry scenario but similar coverage in the Control and the Hotdry scenario. Consistent with the earlier large-scale analysis, LPX-Bern simulates a much higher tree cover in the Noextremes scenarios. OCN and JULES simulate a much weaker response in the same direction. CABLE-POP simulates no difference between scenarios for this location.

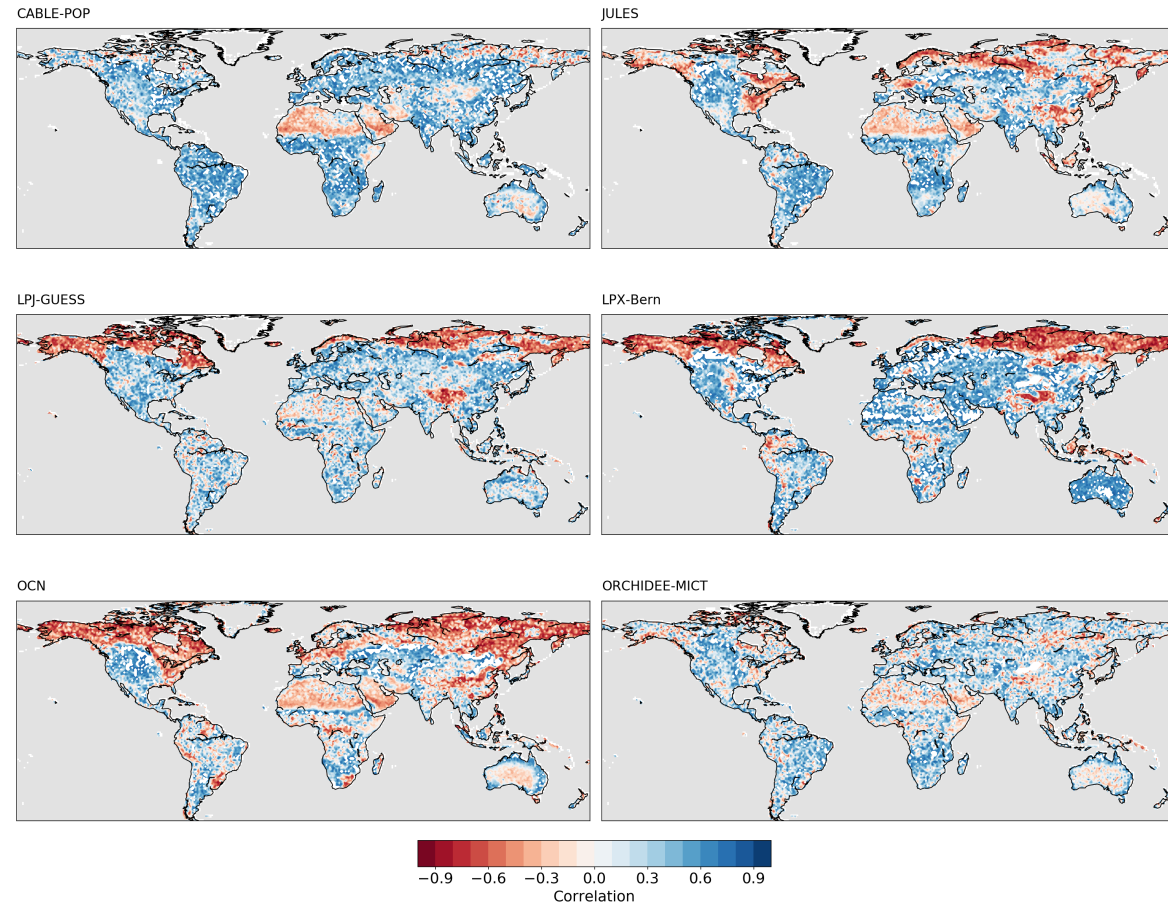


**Figure 4.6:** Correlation between the correlation of temperature and precipitation averaged over the three months with highest vegetation activity and total carbon pools (vegetation carbon + soil carbon). In white are the areas where the correlation is not significant on a 5 % level.

Pixel-based simulations for other locations are shown in Figures 4.11, 4.12, and 4.13 with their corresponding locations indicated in Figure 4.14. The pixel in South Africa has a temperature bias of  $-3.2\text{ }^{\circ}\text{C}$  and a precipitation bias of  $+78.6\%$  in the Control scenario compared to observations. JULES, LPJ-GUESS and OCN simulate a dominant tree cover for all scenarios ( $> 50\%$ ), whereas CABLE-POP, LPX-Bern and ORCHIDEE-MICT simulates mainly grass ( $> 60\%$ ). JULES simulates a pronounced reduction of tree cover for the Hotdry scenario and a corresponding increase in grass cover. Overall, LPX-Bern shows the strongest response to the different scenarios in vegetation cover, though GPP is rather similar in all scenarios. Despite the differences between the models and scenarios in tree or grass coverage, GPP is comparable for all models and most scenarios, with small declines for Hotdry.

The pixel in Siberia has a  $+3.3\text{ }^{\circ}\text{C}$  temperature bias and a  $+28.7\%$  precipitation bias. Here, LPX-Bern simulates mainly trees, with large variations between the scenarios, resulting in moderate tree ( $50\%$ ) cover in the Control and the Nocompound scenario and very high tree cover in the others ( $80\%$ ). OCN also simulates a similar tree cover ( $50\%$ ), with increasing cover in the Hot and Hotdry scenario. CABLE-POP simulates relatively low tree cover in the Control and Nocompound but strong increases in all other scenarios. Grass cover shows the opposite response. JULES, LPJ-GUESS, and ORCHIDEE-MICT simulate a dominance of grasses in this location, with JULES showing a strong increase in tree cover for Hot. Again, interannual variability is largest in LPX-Bern followed by LPJ-GUESS and OCN.

The pixel in Australia has a  $-0.4\text{ }^{\circ}\text{C}$  temperature bias and a  $-2.3\%$  precipitation bias. All models except OCN agree on mainly grass coverage, with LPJ-GUESS and LPX-Bern showing high interannual variations.

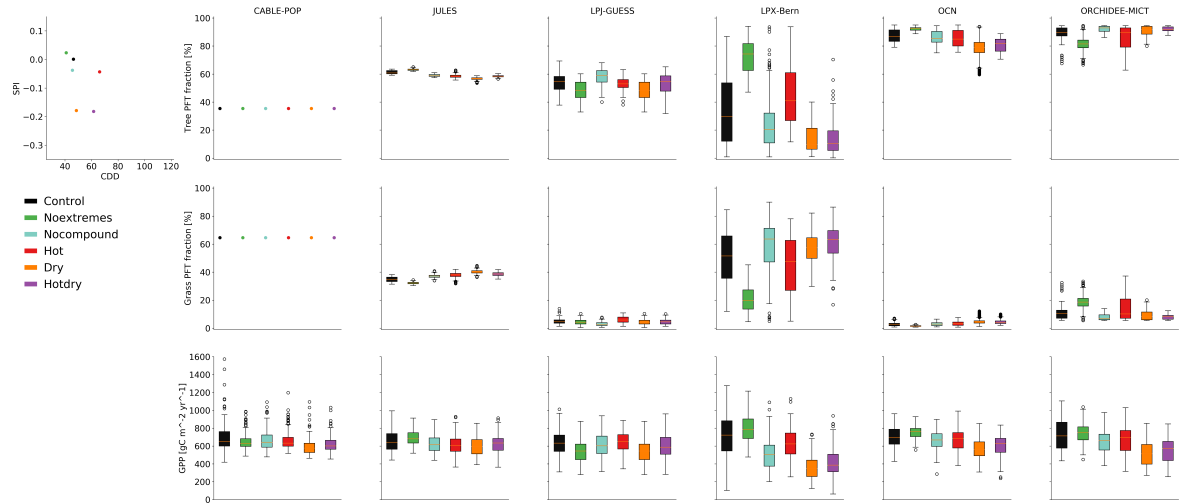


**Figure 4.7:** Pixel analysis for USA ( $42.5^{\circ}\text{N}$  - $110.5^{\circ}\text{E}$ ). The top left panel shows the Standardized Precipitation Index (SPI) as a drought indicator and the Cooling Degree Days (CDD) as a heatwave indicator for all scenarios. The other panels show tree coverage in the top row, grass coverage in the middle row and GPP in the bottom row for all models. The boxplots depict the variation over the years. The temperature bias for the Control scenario is  $+0.2^{\circ}\text{C}$  and the precipitation bias is  $+60\%$  compared to CRU climate data (Harris et al., 2014).

## 4.4 Discussion

Vegetation distribution and terrestrial carbon dynamics are strongly affected by the occurrence rate and intensity of extreme climate events. In this study we investigate how state-of-the-art global vegetation models simulate changes in vegetation distribution and carbon dynamics to differences in the occurrence rate of heatwaves, droughts and compound drought-heatwave events during the three months of largest vegetation activity, keeping annual mean temperature and precipitation approximately equal across scenarios (variation of about  $0.3^{\circ}\text{C}$  in mean global temperature and about  $6\%$  in mean global precipitation). We find that overall, there is large variability across models regarding the response of vegetation distribution and carbon uptake in response to changes in the frequency of extreme events. The differences in responses across models are typically more pronounced than the differences in responses across the six selected scenarios for a given model.

We observe the largest effect in the Dry and Hotdry scenarios (see Table 4.1), where models agree that more frequent droughts/more frequent compound drought-heatwave events lead to a reduction in tree cover and increase in grass cover (Fig. 4.4). Likewise, most models simulate a reduction in the vegetation carbon pool by up to  $-7.5\%$  for those scenarios (Fig. 4.5). This indicates that globally, more frequent droughts lead to the terrestrial biosphere being a smaller carbon sink. The results indicate that in a climate with frequent droughts and compound drought-heatwave events, trees cannot thrive and are outcompeted by grasses, which are less dependent on a stable climate and can adapt easier to strong variations in water availability. Large-scale tree mortality has been linked to extreme droughts in observations (Senf et al., 2020), compound hot-dry conditions (Hammond et al., 2022; Hartmann et al., 2022) and sequences of hot and dry years (Bastos et al., 2021). Although the current set of global vegetation models lacks many processes that are important for vegetation mortality (Meir et al., 2015; Bugmann et al., 2019; McDowell et al., 2018) our results indicate that the models are able to simulate reduced forest cover when droughts and heatwaves are very frequent in the climatology.

The responses to a climate with more frequent heatwaves are much less pronounced at the global scale and are likely an effect of increased forest cover and vegetation productivity in energy-limited regions such as the high latitudes and reduced tree cover in regions that already reach temperature limits in the control climate. For the Nocompound scenario, responses are generally weak. In contrast, for the Noextremes scenario, model responses are strong but in high disagreement. For both scenarios models tend to simulate more vegetation carbon. The variations in the responses to the Noextremes scenario could be an indication to differences in how models deal with the effect of extremes on vegetation and carbon dynamics. Trees in LPX-Bern and ORCHIDEE-MICT seem to thrive under stable conditions with few extremes (Tschumi et al., 2022b) whereas all other models simulate reduced tree cover. This could be due

to the fact that the Noextremes scenario excludes some warm temperature which are actually beneficial for C3 photosynthesis. Excluding these leads to lower foliar projective cover of trees in many models.

In most models, total carbon stocks are strongly correlated with the likelihood of experiencing compound drought-heatwave events (Fig. 4.6). In most tropical and mid-latitude regions and most models, more frequent compound drought-heatwave events lead to lower carbon stocks in vegetation and soils, whereas the opposite is true for the high latitudes in four out of six models. The temperature-precipitation correlation – which determines the likelihood of experiencing compound drought-heatwave events (Zscheischler & Seneviratne, 2017) – can vary substantially across climate models (Bevacqua et al., 2022) due to differences in how atmospheric and land surface processes are simulated (Berg et al., 2015). Climate models can have substantial biases in the temperature-precipitation coupling compared to observations (Vrac et al., 2021). Furthermore, varying long-term trends in the temperature-precipitation coupling have been identified in climate models (Zscheischler & Seneviratne, 2017), which may add to reductions in future crop yields caused by warming temperatures (Lesk et al., 2021). Through the link between total carbon stocks and precipitation-temperature coupling in vegetation models illustrated in our study, we demonstrate how uncertainties in the representation of the temperature-precipitation coupling and changes therein can contribute to uncertainties in the projection of terrestrial carbon stocks (Friedlingstein et al., 2014).

Our model intercomparison shows very high variability in model responses, which is not uncommon in vegetation model intercomparison studies (Paschalis et al., 2020). All models were run with the same forcing, reducing uncertainties related to the choice of forcing data (Wang et al., 2021). Nevertheless, strong differences between models in the Control simulations (Fig. 4.2) could be related to the fact that we used raw model output from a climate model as forcing, which – despite matching the observed global mean temperature of 2011-2015 – is characterized by regional biases in temperature and precipitation. Vegetation models are often calibrated to represent observed vegetation well when forced with observed climate (e.g. when used to estimate the land carbon sink, Friedlingstein et al., 2022) so regional climate biases can lead to very different simulations of vegetation distribution and carbon dynamics for the different models. For instance, Teckentrup et al. (2022) found large differences in the simulation of carbon fluxes and stocks for raw climate model forcing compared to a bias-corrected forcing in water-limited regions of Australia. Not all variables were equally sensitive to the bias, and not all PFTs responded in a similar way, indicating that the bias could have an influence on vegetation composition. To test whether a bias in forcing could affect our conclusions, we restricted the analysis to regions with small biases. The general response patterns look very similar (Fig. 4.15) which leads us to conclude that the bias on the forcing data does not strongly affect our findings.

Uncertainties in the model responses may also be related to the fact that we based the sampling of the scenarios on the three most productive months as simulated by LPX-Bern (Tschumi et al., 2022a). Other models might have strong shifts in the most productive months and thus be sensitive to climate extremes in different seasons. We find that in most of the extratropics the time shift between the most productive months is small. The largest differences occur in the tropics and subtropics, which are regions where the seasonal cycle is not very pronounced and therefore differences in the months does not necessarily mean large differences in productivity.

## 4.5 Conclusion

This model comparison aims at investigating how different vegetation models simulate vegetation distribution and carbon dynamics to climates with few or no droughts and heatwave, only univariate extremes, and frequent compound extremes. Even though all models are run with exactly the same input data, the results tend to vary greatly. Despite large differences, the models generally agree that a climate with more frequent compound hot-dry events would lead to a reduction in forest cover and carbon stocks. Furthermore, in all models, carbon pools are strongly related to the likelihood of experiencing compound hot-dry events. Overall our study highlights how uncertainties in the simulation of compound hot-dry events can propagate to uncertainties in total carbon uptake and pools.

## 4.6 Supporting information

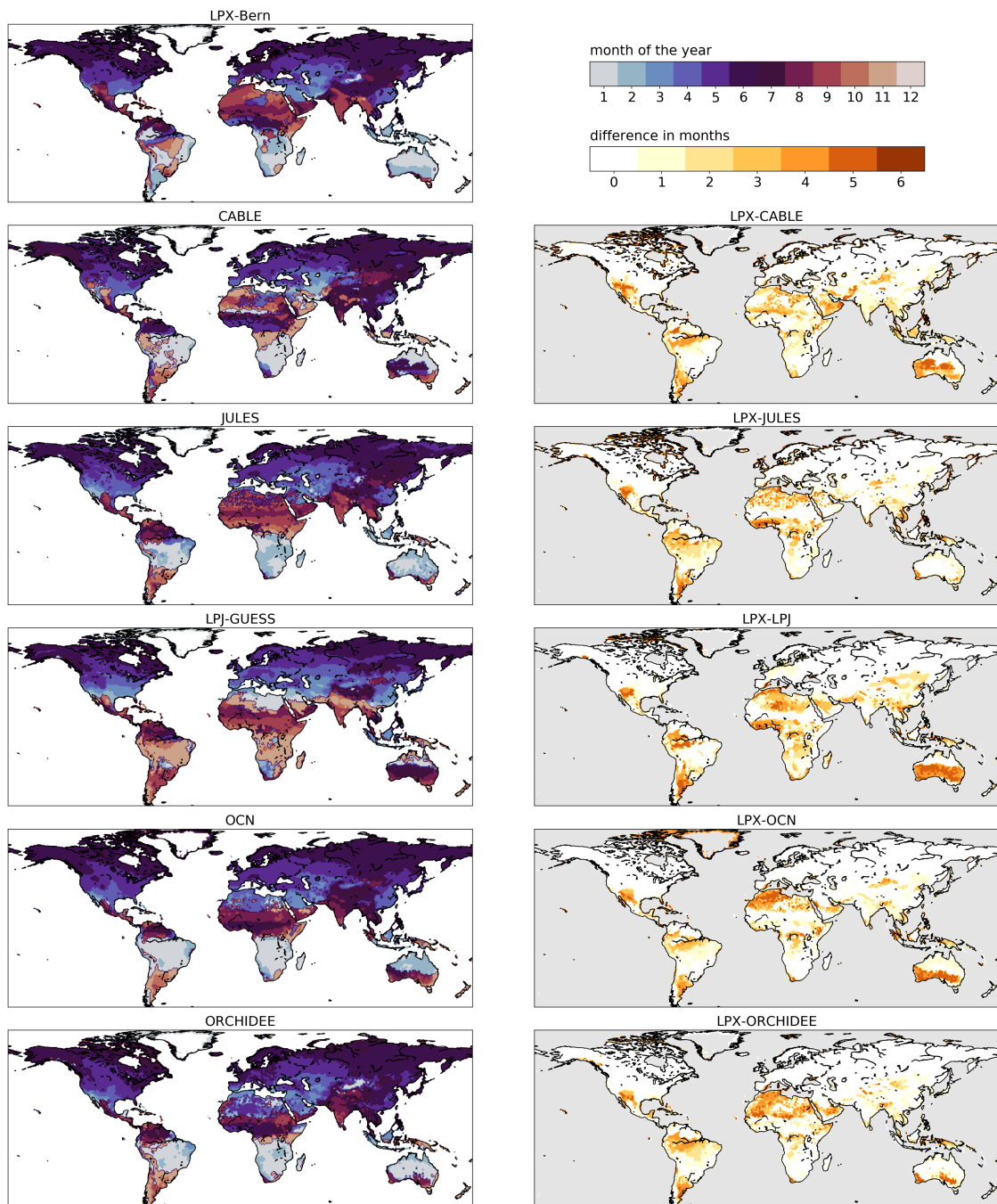


**Figure 4.8:** Most productive months (maximum consecutive 3-month mean of NPP) for all models and compared to LPX-Bern, which was used to sample the input data.

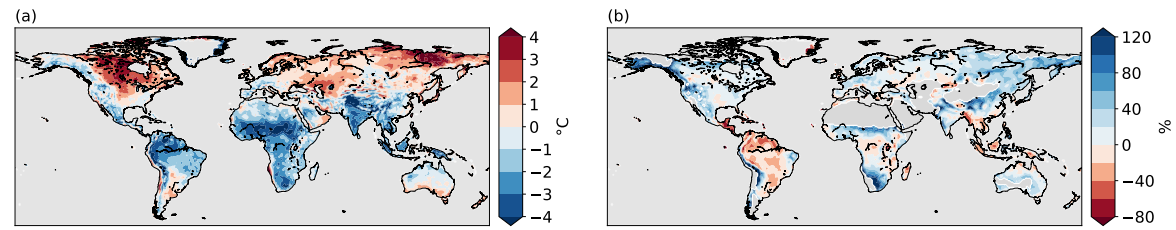


**Figure 4.9:** Biases in EC-Earth simulations with respect to observation-based data from CRU (Harris et al., 2014). (a) Difference in annual mean temperature between EC-Earth and CRU in °C. (b) Relative difference in annual precipitation between EC-Earth and CRU in %. The time period 1988–2017 was used for CRU and randomly sampled 100 years (representing 2011–2015) for EC-Earth. The land regions depicted in grey in (b) are desert regions with a mean annual precipitation of less than 250 mm in the CRU dataset and were excluded in the maps to avoid dividing by very small numbers. Taken from Tschumi et al. (2022a).

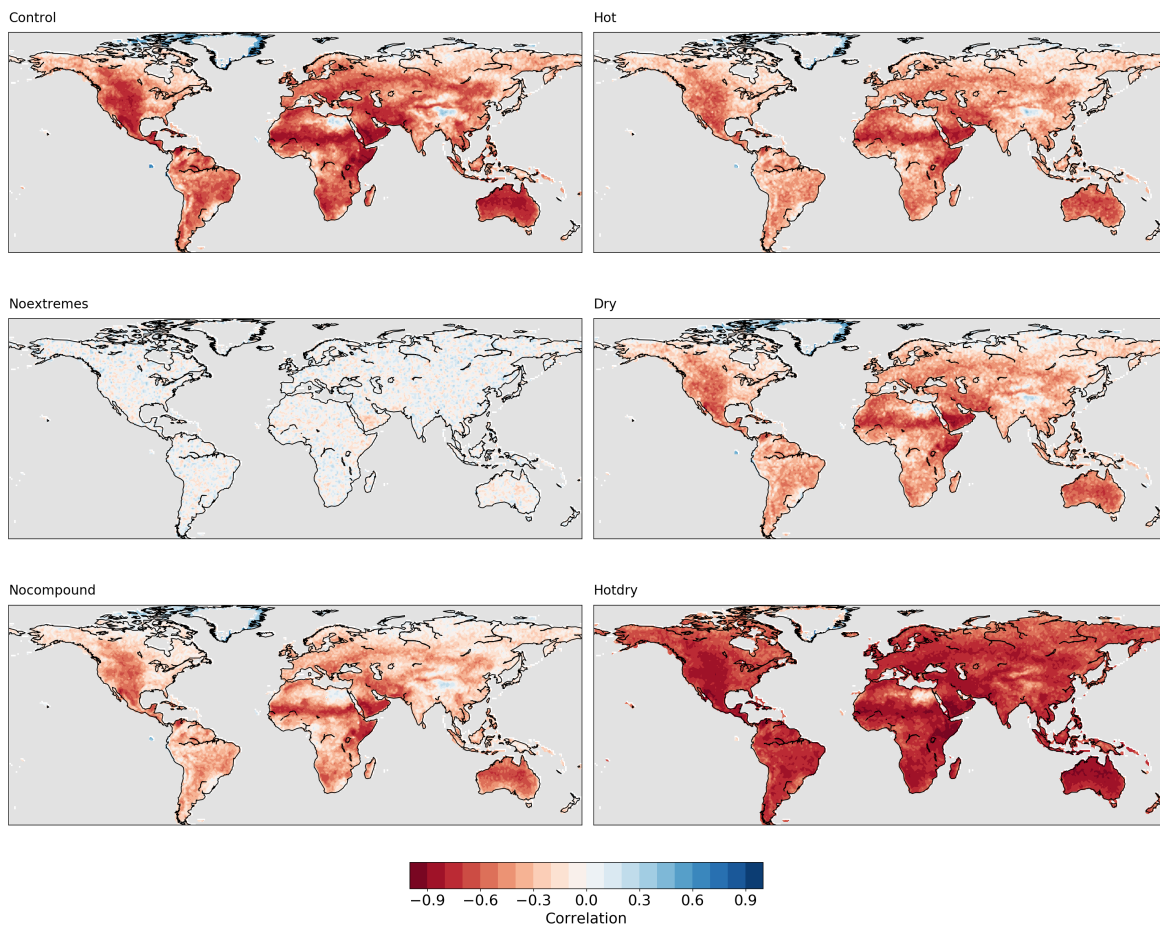


**Figure 4.10:** Correlation maps between temperature and precipitation of the Control scenario input over the three most productive months.

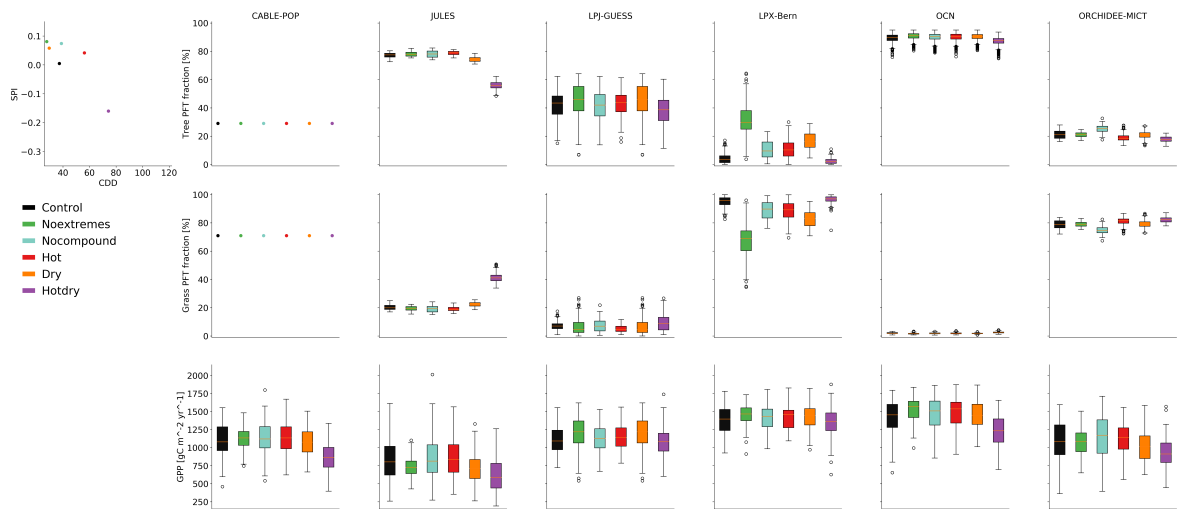


**Figure 4.11:** Pixel analysis for South Africa (-20.5°N 18.5°E). The top left panel shows the Standardized Precipitation Index (SPI) as a drought indicator and the Cooling Degree Days (CDD) as a heat indicator for all scenarios. The other panels show tree coverage in the top row, grass coverage in the middle row and GPP in the bottom row for all models. The boxes depict the variation over the years. The temperature bias for the Control scenario is -3.2°C and the precipitation bias is +78.6% compared to CRU.

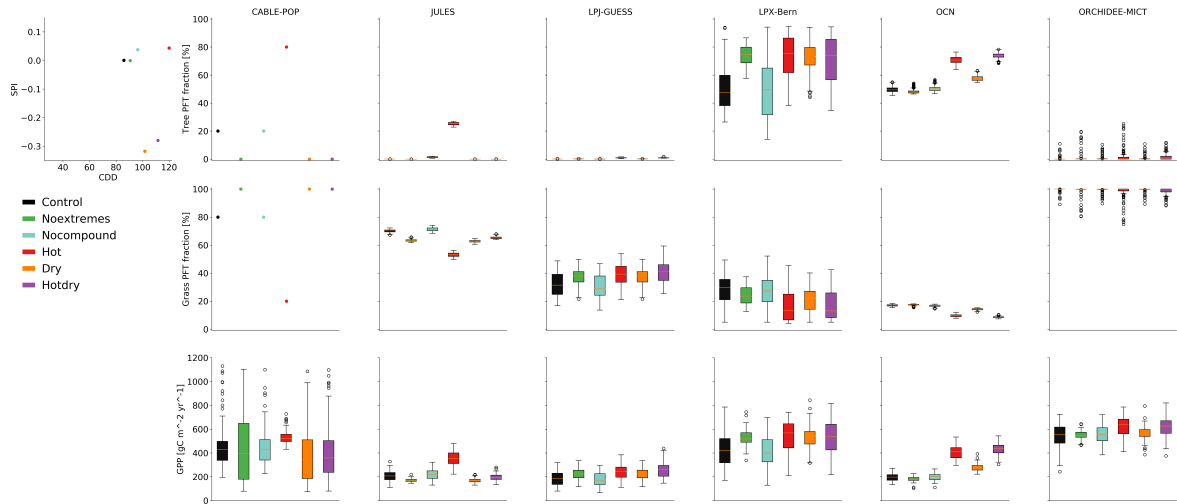


**Figure 4.12:** Pixel analysis for Siberia (70.5°N 120.5°E). The top left panel shows the Standardized Precipitation Index (SPI) as a drought indicator and the Cooling Degree Days (CDD) as a heat indicator for all scenarios. The other panels show tree coverage in the top row, grass coverage in the middle row and GPP in the bottom row for all models. The boxes depict the variation over the years. The temperature bias for the Control scenario is +3.3°C and the precipitation bias is +28.7% compared to CRU.

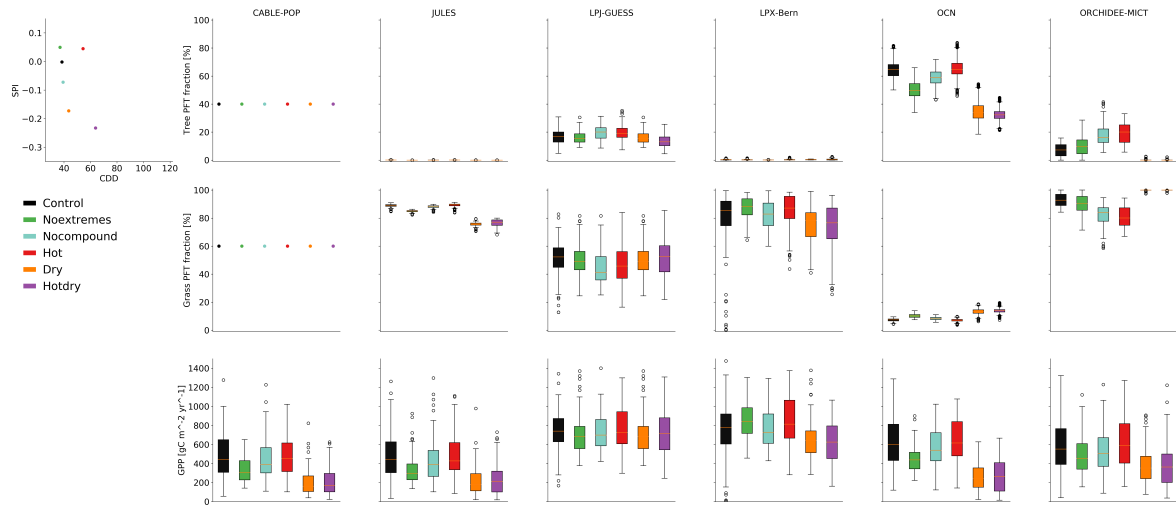


**Figure 4.13:** Pixel analysis for Australia (-20.5°N 130.5°E). The top left panel shows the Standardized Precipitation Index (SPI) as a drought indicator and the Cooling Degree Days (CDD) as a heat indicator for all scenarios. The other panels show tree coverage in the top row, grass coverage in the middle row and GPP in the bottom row for all models. The boxes depict the variation over the years. The temperature bias for the Control scenario is -0.4°C and the precipitation bias is -2.3% compared to CRU.

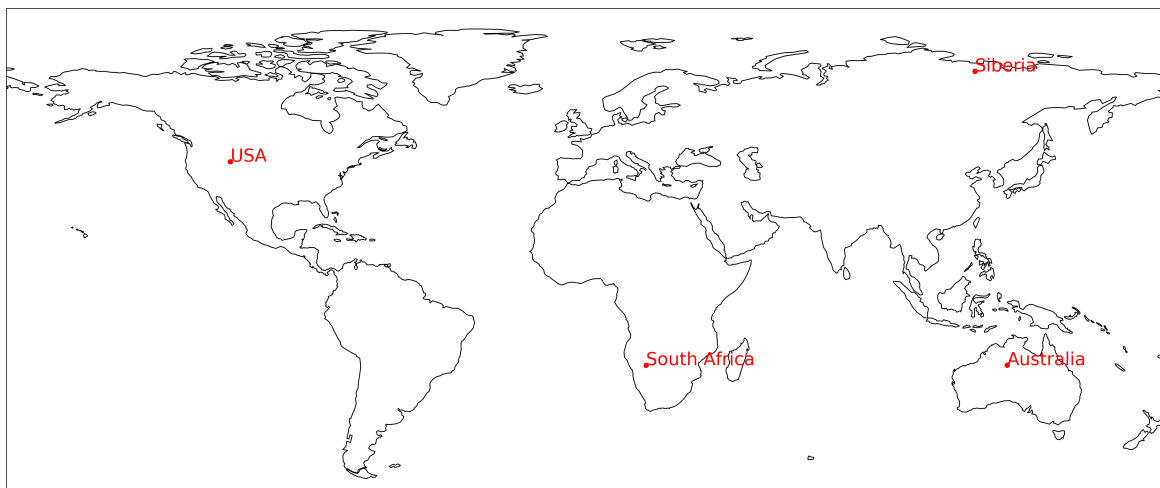


**Figure 4.14:** Map showing the locations of the pixel analyses shown in Figures 4.12, 4.11, 4.7, and 4.13.

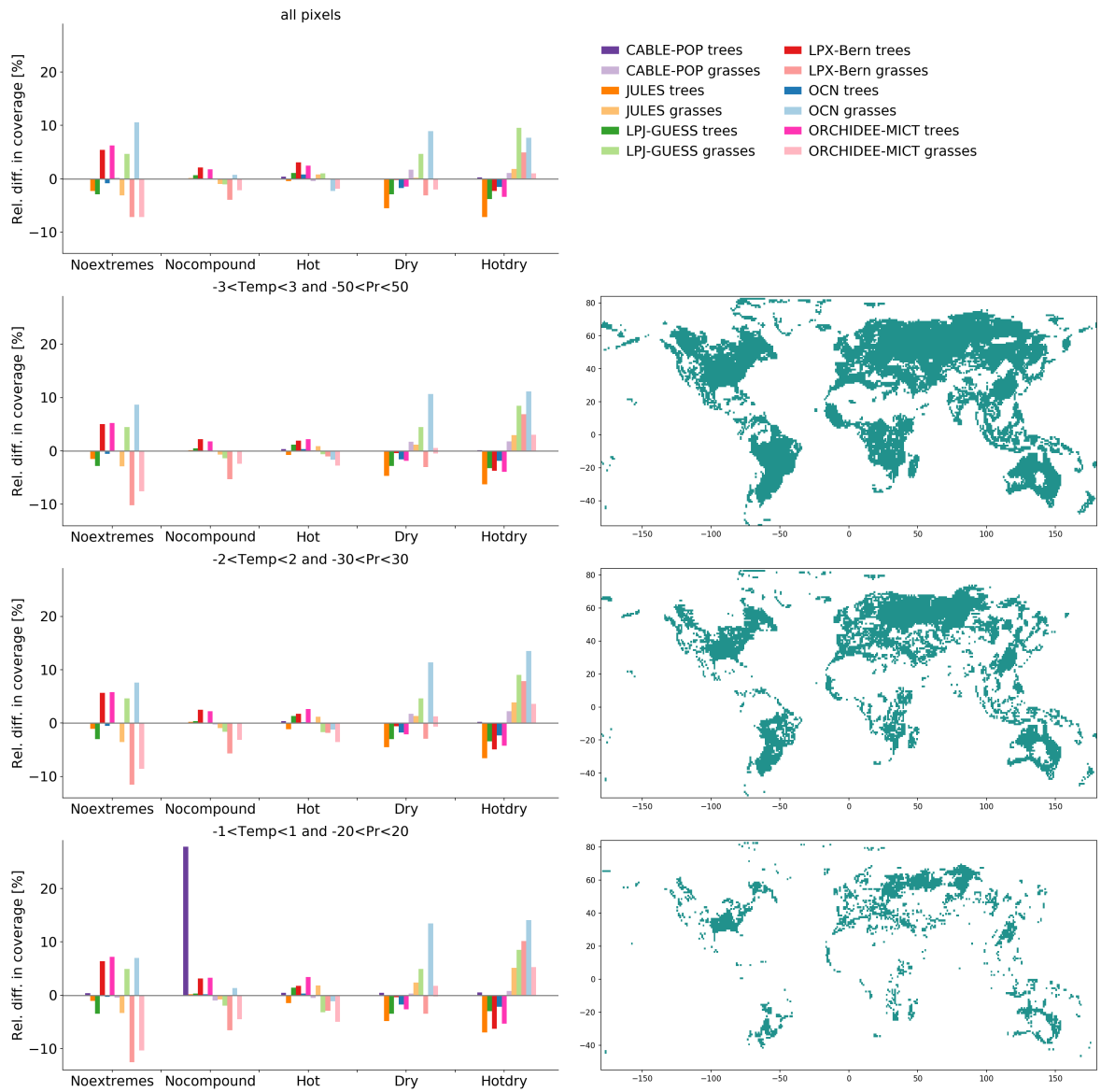


**Figure 4.15:** Relative change in tree and grass coverage as a function of temperature and precipitation bias. The maps show the pixels that were considered for the bar plots. Pixels were excluded based on the magnitude of their temperature and precipitation biases (control compared to CRU).



## Chapter 5

# Conclusions and Outlook

### 5.1 Summary of results

#### 5.1.1 The input data

This thesis investigates the effects of six hypothetical climate scenarios with differing occurrence rates of hot and dry extremes, sampled from a large ensemble simulation, on vegetation distribution and carbon dynamics as modelled by dynamic global vegetation models. Chapter 2 deals with building extreme event input scenarios suitable for vegetation impact modelling. The modelling approach was chosen because process-based impact models in combination with climate models provide the opportunity of a controlled environment to disentangle the effects of single and compound drivers of extreme events. The scenarios are based on a large ensemble simulation generated by the climate model EC-Earth, which offers a long time series without long-term trends covering the whole globe's land area. These are all important advantages which are often missing in observational or reanalysis data. Especially when one is interested in extreme events, a long data series is essential because such events are rare by definition. Thanks to the large ensemble simulation, it was possible to sample 100-year long scenarios. The drought-heat scenarios presented in this thesis differ in their occurrence frequency of droughts and heatwaves but are comparable in their mean climate, representative of the observed 2011-2015 climate. Sampled from EC-Earth, these scenarios are not free of biases in temperature and precipitation at the local to regional scale. A cold-dry bias in the tropics is offset by a warm-wet bias in high latitudes. The biases need to be taken into consideration when using these scenarios for impact modelling, since many models are tuned to a specific climate and biases in the input data can have a large effect (Teckentrup et al., 2019). The sampling of the scenarios is also done in such a way that spatial coherence is destroyed, which means that climate variables have no correlation between neighbouring grid points. This was done intentionally and does not diminish the validity of the results. It is, however, something to keep in mind when using this data for other studies. The sampling of the hot and dry extremes is based on vegetation productivity, i.e. during the time when vegetation is most productive and arguably also most vulnerable to extreme conditions. This makes these scenarios an ideal tool to study drought-heat impacts on vegetation. They can additionally be used to study other impacts, potential other applications being, for example, wildfire occurrence or impacts on agriculture.

#### 5.1.2 The effects of hot and dry extremes

Chapters 3 and 4 discuss the effects of the scenarios described in Chapter 2 on the dynamic global vegetation model (DGVM) LPX-Bern (Chapter 3) specifically and on five additional DGVMs in a model intercomparison study (Chapter 4). Different occurrence frequencies of hot, dry, and compound hot-dry events lead to differences in natural vegetation coverage and related differences in global carbon stocks. We see that vegetation distribution and carbon stocks are strongly affected by the frequency and intensity of extreme climate events. Although variability across the models is overall large, they agree on a clear reduction in tree coverage and an associated reduction in carbon stored in plants of up to -7.5 % as well as an increase in grass coverage for the most extreme scenario featuring compound hot and dry extremes. Tree coverage and vegetation carbon storage are also reduced in a climate with more dry extremes, but to

a lesser extent than for a compound hot and dry climate. Especially in already water-limited regions, the bioclimatic limits of trees and, in very dry regions such as the Sahara desert, also those of grasses are reached quickly under a climate with more dry extremes, leading to a reduction of vegetation and also carbon stored in vegetation. Models mostly agree on this, although it is less pronounced than the more extreme hot and dry scenario. The results indicate that in a climate with frequent droughts and compound drought-heatwave events trees cannot thrive and are outcompeted by grasses, which are less dependent on a stable climate and can adapt easier to strong variations in water availability. Even smaller changes and less agreement between models can be observed for the scenario with only hot extremes. This means that a heatwave event has to be more extreme than a drought event to have a comparable impact. This is most likely due to large regional differences. Higher latitudes are generally energy-limited (Way & Oren, 2010). Tree coverage tends to increase in a warmer climate due to an increased growing season length without necessarily exceeding the temperature limit of boreal trees (Myneni et al., 1997), although these regions might still be limited by nutrient availability (Zaehle et al., 2010; Du et al., 2020). These temperature limits might be reached more quickly in other regions, leading to a reduction in tree coverage due to temperature-induced mortality.

Globally, the extratropics show larger effects of extremes than the tropics. LPX-Bern shows that the effects of hot and dry extremes are smallest on tropical and largest on boreal trees. This is probably due to the fact that evaporative cooling is maintained in tropical forests, even in a drier climate (Bonan, 2008), since tropical forests are generally more energy- instead of water-limited. More frequent hot extremes, in turn, are most beneficial in high latitudes and not so much in the tropics. This is because boreal regions are generally energy-limited and a warmer climate often leads to an increased growing season length and does not necessarily lead to the reaching of the bioclimatic limits for these regions. Semi-arid regions, or, more generally, regions which are transitional between water-limited and energy-limited, show the largest effects on GPP (Zscheischler et al., 2014b).

There are not only regional differences, but also differences between biomes. In our case, we looked at differences between trees and grasses. Tree coverage is generally more reduced under extreme conditions, especially under droughts. While a prolonged growing season length in high latitudes may promote tree growth, the positive effects of a warmer climate are superseded by the negative impacts of droughts (Belyazid & Giuliana, 2019; Ruiz-Pérez & Vico, 2020). While tree roots may reach water reservoirs in deeper soil layers (Bréda et al., 2006) for a longer period of time than grasses under drought conditions, once their limits are reached, they need much longer to recover. Grasses react faster to changes in climate, but they are generally better adapted to already dry regions than trees and they have a much faster recovery time (Teuling et al., 2010; Sippel et al., 2018). In our modelled case, grass coverage often increases when tree coverage is reduced, because it can grow in areas that were previously covered by trees. This also depends on the way vegetation growth is parameterized in a model.

Our results show clearly that a high likelihood of compound hot and dry events, here represented as a strong correlation between temperature and precipitation (also Zscheischler & Seneviratne, 2017), is strongly correlated with a reduction in total carbon stock. This is especially true for most tropical and mid-latitude regions, whereas the opposite is sometimes true for the high latitudes. Since the compound hot and dry scenario shows the strongest response, stronger than even the combination of the hot and the dry scenarios together, the importance of considering multiple drivers together as compound events is evident (Zscheischler et al., 2018, 2020). Impacts may potentially be underestimated when only considering single driver extremes. While it is possible that regions react differently to extremes and some regions might even benefit (like the high latitudes from a prolonged growing season length under a warmer climate), the interactions between drivers might have negative feedbacks on each other, worsening the overall effects of a compound event (Shah & Paulsen, 2003).

## 5.2 Modelling implications

High variability in vegetation model intercomparison studies is common (Paschalis et al., 2020). Our results show how tree mortality is linked to extreme droughts and compound drought-heatwave conditions, which can also be seen in observations (Senf et al., 2020; Hammond et al., 2022; Hartmann et al., 2022). Even though current global vegetation models may lack important processes for vegetation mortality (Meir et al., 2015; Bugmann et al., 2019; McDowell et al., 2018), our results indicate that they are able to simulate reduced forest cover when droughts and heatwaves are very frequent. By running all models with

the same forcing data, we reduce the uncertainties related to the choice of forcing data (Wang et al., 2021). However, the use of raw model output from a climate model which contains some regional biases might partly explain the strong differences between the models. Not all variables are equally sensitive to the bias and not all PFTs respond in a similar way. These variations can lead to very different simulations of vegetation distribution and carbon dynamics because vegetation models are often calibrated to the observed climate.

Especially in a climate without extremes, model agreement on vegetation distribution and carbon stocks is low. Since such a climate is unlikely to challenge the bioclimatic limits, the exact processes with which models simulate these variables is important for the overall results. In LPX-Bern, for example, trees are favoured over grasses. In particular, they receive priority for foliar coverage if conditions are suitable for tree growth. This would explain the increase in tree cover and the decrease in grass cover in a more stable climate.

It is also known that the temperature-precipitation correlation, which determines the occurrence likelihood of compound drought-heatwave events, may vary across climate models due to differences in how atmospheric and land surface processes are simulated (Berg et al., 2015; Zscheischler & Seneviratne, 2017; Bevacqua et al., 2022). This may lead to substantial biases in the temperature-precipitation coupling compared to observations (Vrac et al., 2021) and further to uncertainties in projections of vegetation distribution and carbon dynamics in models. This is due to misrepresented drought-heat signatures in addition to structural model differences in the vegetation component (Zscheischler et al., 2018). By demonstrating the link between total carbon stocks and temperature-precipitation correlation in this thesis, it is clear how the uncertainties of the representation of this coupling in models can contribute to uncertainties in the projection of the terrestrial carbon sink.

While vegetation models are generally a helpful tool to analyse many different hypotheses, they do lack some refined processes, especially when it comes to variable interactions and feedbacks, which are especially important when looking at compound events. Understanding these issues and improving models is crucial for further studies on climate extremes and their effects on vegetation.

## 5.3 Outlook

Our results suggest a reduction in the natural carbon sink under extreme conditions. While human-made changes are, of course, also very important and cannot be ignored when considering the actual total terrestrial carbon sink, it is something that is more directly manageable and therefore easier to control. The change of the natural terrestrial carbon sink is indirectly caused by human activity through the release of fossil fuels, which also alters the occurrence of extremes (Friedlingstein et al., 2022). It is therefore essential to understand how the natural carbon sink will change under future conditions in order to understand the total terrestrial carbon sink. This study addresses one aspect of this process, namely how it evolves under different extreme conditions. Some additional factors would need to be considered for a whole picture, for example, changing CO<sub>2</sub> levels.

Moreover, our modelling setup is designed to study the effects of differing drought-heat signatures in different models. This inevitably means that we cannot allow land-atmosphere feedbacks. Indeed such feedbacks would alter our scenarios over time and they would also likely vary for different models, making it harder to compare them. In a more realistic setup, we would need to use a changing climate, meaning climate input with a time trend, as well as changing CO<sub>2</sub> concentrations, and allow for land-climate feedbacks. A further step to represent reality more accurately is to allow for teleconnections. Our sampling process prevents any teleconnections. In the Hot scenario, for example, we increased the occurrence of hot extremes everywhere. This was done to demonstrate the effect of hot extremes on all different biomes and climate zones. However, in a more realistic setup, not all regions experience the same increase in extremes.

Having said that, the setup as used in this thesis is ideal to understand the effects of single vs. compound drivers and test different hypotheses. Future work along the lines of this thesis could include runs also considering crop and other land uses as well as runs with different concentrations of CO<sub>2</sub>, in order to assess the effect of CO<sub>2</sub> fertilization. Our sampling method can further be used to study other types of compound events and their impacts. One could, for instance, sample temporally compounding or preconditioned events and study their implications on vegetation.





# Bibliography

- Ahlström, A., Raupach, M. R., Schurgers, G., Smith, B., Arneth, A., Jung, M., Reichstein, M., Canadell, J. G., Friedlingstein, P., Jain, A. K., Kato, E., Poulter, B., Sitch, S., Stocker, B. D., Viovy, N., Wang, Y. P., Wiltshire, A., Zaehle, S., & Zeng, N., 2015. The dominant role of semi-arid ecosystems in the trend and variability of the land co<sub>2</sub> sink, *Science*, 348(6237), 895–899.
- Allen, C. D., Macalady, A. K., Chenchouni, H., Bachelet, D., McDowell, N., Vennetier, M., Kitzberger, T., Rigling, A., Breshears, D. D., Hogg, E. T., Gonzalez, P., Fensham, R., Zhang, Z., Castro, J., Demidova, N., Lim, J.-H., Allard, G., Running, S. W., Semerci, A., & Cobb, N., 2010. A global overview of drought and heat-induced tree mortality reveals emerging climate change risks for forests, *Forest Ecology and Management*, 259(4), 660 – 684.
- Allison, C., Francey, R., Law, R., & Rayner, P., 2005. Global carbon fluxes inferred from the csiro global flask network: 1983–2004, in *Seventh Int. Conf. Carbon Dioxide, Broomfield, CO (Abstr.)* by MARINE BIOLOGY LABORATORY/WHOI LIBRARY on, vol. 5, pp. 01–07.
- Anderegg, W. R., Kane, J. M., & Anderegg, L. D., 2013a. Consequences of widespread tree mortality triggered by drought and temperature stress, *Nature climate change*, 3(1), 30–36.
- Anderegg, W. R., Plavcová, L., Anderegg, L. D., Hacke, U. G., Berry, J. A., & Field, C. B., 2013b. Drought's legacy: multiyear hydraulic deterioration underlies widespread aspen forest die-off and portends increased future risk, *Global change biology*, 19(4), 1188–1196.
- Angert, A., Biraud, S., Bonfils, C., Henning, C., Buermann, W., Pinzon, J., Tucker, C., & Fung, I., 2005. Drier summers cancel out the co<sub>2</sub> uptake enhancement induced by warmer springs, *Proceedings of the National Academy of Sciences*, 102(31), 10823–10827.
- Archer, D., Eby, M., Brovkin, V., Ridgwell, A., Cao, L., Mikolajewicz, U., Caldeira, K., Matsumoto, K., Munhoven, G., Montenegro, A., & Tokos, K., 2009. Atmospheric lifetime of fossil fuel carbon dioxide, *Annual review of earth and planetary sciences*, 37.
- Arend, M., Link, R. M., Patthey, R., Hoch, G., Schuldt, B., & Kahmen, A., 2021. Rapid hydraulic collapse as cause of drought-induced mortality in conifers, *Proceedings of the National Academy of Sciences*, 118(16).
- Arneth, A., Sitch, S., Pongratz, J., Stocker, B. D., Ciais, P., Poulter, B., Bayer, A. D., Bondeau, A., Calle, L., Chini, L. P., Gasser, T., Fader, M., Friedlingstein, P., Kato, E., Li, W., Lindeskog, M., Nabel, J. E. M. S., Pugh, T. A. M., Robertson, E., Viovy, N., Yue, C., & Zaehle, S., 2017. Historical carbon dioxide emissions caused by land-use changes are possibly larger than assumed, *Nature Geoscience*, 10(2), 79–84.
- Baccini, A., Walker, W., Carvalho, L., Farina, M., Sulla-Menashe, D., & Houghton, R., 2017. Tropical forests are a net carbon source based on aboveground measurements of gain and loss, *Science*, 358(6360), 230–234.

- Barber, V. A., Juday, G. P., & Finney, B. P., 2000. Reduced growth of alaskan white spruce in the twentieth century from temperature-induced drought stress, *Nature*, 405(6787), 668–673.
- Bastos, A., Gouveia, C., Trigo, R., & Running, S. W., 2014. Analysing the spatio-temporal impacts of the 2003 and 2010 extreme heatwaves on plant productivity in europe, *Biogeosciences*, 11(13), 3421–3435.
- Bastos, A., Ciais, P., Friedlingstein, P., Sitch, S., Pongratz, J., Fan, L., Wigneron, J. P., Weber, U., Reichstein, M., Fu, Z., Anthoni, P., Arneth, A., Haverd, V., Jain, A. K., Joetzjer, E., Knauer, J., Lienert, S., Loughran, T., McGuire, P. C., Tian, H., Viovy, N., & Zaehle, S., 2020a. Direct and seasonal legacy effects of the 2018 heat wave and drought on european ecosystem productivity, *Science Advances*, 6(24), eaba2724.
- Bastos, A., Fu, Z., Ciais, P., Friedlingstein, P., Sitch, S., Pongratz, J., Weber, U., Reichstein, M., Anthoni, P., Arneth, A., Haverd, V., Jain, A., Joetzjer, E., Knauer, J., Lienert, S., Loughran, T., McGuire, P. C., Obermeier, W., Padrón, R. S., Shi, H., Tian, H., Viovy, N., & Zaehle, S., 2020b. Impacts of extreme summers on european ecosystems: a comparative analysis of 2003, 2010 and 2018, *Philosophical Transactions of the Royal Society B*, 375(1810), 20190507.
- Bastos, A., Orth, R., Reichstein, M., Ciais, P., Viovy, N., Zaehle, S., Anthoni, P., Arneth, A., Gentine, P., Joetzjer, E., Lienert, S., Loughran, T., McGuire, P. C., O, S., Pongratz, J., & Sitch, S., 2021. Vulnerability of european ecosystems to two compound dry and hot summers in 2018 and 2019, *Earth System Dynamics*, 12(4), 1015–1035.
- Beier, C., Beierkuhnlein, C., Wohlgemuth, T., Penuelas, J., Emmett, B., Körner, C., de Boeck, H., Christensen, J. H., Leuzinger, S., Janssens, I. A., & Hansen, K., 2012. Precipitation manipulation experiments—challenges and recommendations for the future, *Ecology letters*, 15(8), 899–911.
- Beierkuhnlein, C., Thiel, D., Jentsch, A., Willner, E., & Kreyling, J., 2011. Ecotypes of european grass species respond differently to warming and extreme drought, *Journal of Ecology*, pp. 703–713.
- Belyazid, S. & Giuliana, Z., 2019. Water limitation can negate the effect of higher temperatures on forest carbon sequestration, *European Journal of Forest Research*, 138(2), 287–297.
- Berg, A., Lintner, B. R., Findell, K., Seneviratne, S. I., van den Hurk, B., Ducharne, A., Chérury, F., Hagemann, S., Lawrence, D. M., Malyshev, S., Meier, A., & Gentine, P., 2015. Interannual coupling between summertime surface temperature and precipitation over land: Processes and implications for climate change, *Journal of Climate*, 28(3), 1308–1328.
- Best, M. J., Pryor, M., Clark, D. B., Rooney, G. G., Essery, Ménard, C. B., Edwards, J. M., Hendry, M. A., Porson, A., Gedney, N., Mercado, L. M., Sitch, S., Blyth, E., Boucher, O., Cox, P. M., Grimmond, C. S. B., & Harding, R. J., 2011. The joint UK land environment simulator (JULES), model description – part 1: Energy and water fluxes, *Geoscientific Model Development*, 4(3), 677–699.
- Bevacqua, E., Zappa, G., Lehner, F., & Zscheischler, J., 2022. Precipitation trends determine future occurrences of compound hot–dry events, *Nature Climate Change*, 12(4), 350–355.
- Bloom, A. J., Chapin, F. S., & Mooney, H. A., 1985. Resource limitation in plants—an economic analogy, *Annual review of Ecology and Systematics*, pp. 363–392.
- Bonan, G. B., 2008. Forests and climate change: forcings, feedbacks, and the climate benefits of forests, *science*, 320(5882), 1444–1449.

- Bonekamp, P. N. J., Wanders, N., van der Wiel, K., Lutz, A. F., & Immerzeel, W. W., 2020. Using large ensemble modelling to derive future changes in mountain specific climate indicators in a 2 and 3°C warmer world in High Mountain Asia, *International Journal of Climatology*, n/a(n/a).
- Botkin, D. B., Janak, J. F., & Wallis, J. R., 1972. Some ecological consequences of a computer model of forest growth, *The Journal of ecology*, pp. 849–872.
- Bréda, N., Huc, R., Granier, A., & Dreyer, E., 2006. Temperate forest trees and stands under severe drought: a review of ecophysiological responses, adaptation processes and long-term consequences, *Annals of Forest Science*, 63(6), 625–644.
- Buermann, W., Bikash, P. R., Jung, M., Burn, D. H., & Reichstein, M., 2013. Earlier springs decrease peak summer productivity in north american boreal forests, *Environmental Research Letters*, 8(2), 024027.
- Bugmann, H., Seidl, R., Hartig, F., Bohn, F., Bruna, J., Cailleret, M., François, L., Heinke, J., Henrot, A.-J., Hickler, T., Hülsmann, L., Huth, A., Jacquemin, I., Kollas, C., Lasch-Born, P., Lexer, M. J., Merganič, J., Merganičová, K., Mette, T., Miranda, B. R., Nadal-Sala, D., Rammer, W., Rammig, A., Reineking, B., Roedig, E., Sabaté, S., Steinkamp, J., Suckow, F., Vacchiano, G., Wild, J., Xu, C., & Reyer, C. P. O., 2019. Tree mortality submodels drive simulated long-term forest dynamics: Assessing 15 models from the stand to global scale, *Ecosphere*, 10(2), e02616.
- Buizza, R., Milleer, M., & Palmer, T. N., 1999. Stochastic representation of model uncertainties in the ECMWF ensemble prediction system, *Quarterly Journal of the Royal Meteorological Society*, 125(560), 2887–2908.
- Bunn, A. G. & Goetz, S. J., 2006. Trends in satellite-observed circumpolar photosynthetic activity from 1982 to 2003: the influence of seasonality, cover type, and vegetation density, *Earth Interactions*, 10(12), 1–19.
- Buras, A., Rammig, A., & Zang, C. S., 2020. Quantifying impacts of the 2018 drought on european ecosystems in comparison to 2003, *Biogeosciences*, 17(6), 1655–1672.
- Canadell, J. G., Pataki, D. E., Gifford, R., Houghton, R. A., Luo, Y., Raupach, M. R., Smith, P., & Steffen, W., 2007. Saturation of the terrestrial carbon sink, in *Terrestrial ecosystems in a changing world*, pp. 59–78, Springer.
- Choat, B., Jansen, S., Brodribb, T. J., Cochard, H., Delzon, S., Bhaskar, R., Bucci, S. J., Feild, T. S., Gleason, S. M., Hacke, U. G., Jacobsen, A. L., Lens, F., Maherali, H., Martínez-Vilalta, J., Mayr, S., Mencuccini, M., Mitchell, P. J., Nardini, A., Pittermann, J., Pratt, R. B., Sperry, J. S., Westoby, M., Wright, I. J., & Zanne, A. E., 2012. Global convergence in the vulnerability of forests to drought, *Nature*, 491(7426), 752–755.
- Ciais, P., Reichstein, M., Viovy, N., Granier, A., Ogée, J., Allard, V., Aubinet, M., Buchmann, N., Bernhofer, C., Carrara, a., Chevallier, F., De Noblet, N., Friend, a. D., Friedlingstein, P., Grünwald, T., Heinesch, B., Keronen, P., Knohl, A., Krinner, G., Loustau, D., Manca, G., Matteucci, G., Miglietta, F., Ourcival, J. M., Papale, D., Pilegaard, K., Rambal, S., Seufert, G., Soussana, J. F., Sanz, M. J., Schulze, E. D., Vesala, T., Valentini, R., Grunwald, T., Heinesch, B., Keronen, P., Knohl, A., Krinner, G., Loustau, D., Manca, G., Matteucci, G., Miglietta, F., Ourcival, J. M., Papale, D., Pilegaard, K., Rambal, S., Seufert, G., Soussana, J. F., Sanz, M. J., Schulze, E. D., Vesala, T., & Valentini, R., 2005. Europe-wide reduction in primary productivity caused by the heat and drought in 2003., *Nature*, 437(7058), 529–33.

- Ciais, P., Sabine, C., Bala, G., Bopp, L., Brovkin, V., Canadell, J., Chhabra, A., DeFries, R., Galloway, J., Heimann, M., Jones, C., Le Quéré, C., Myneni, R. B., Piao, S., & Thornton, P., 2013. Carbon and other biogeochemical cycles. climate change 2013: the physical science basis. contribution of working group i to the fifth assessment report of the intergovernmental panel on climate change, *Comput. Geom.*, 18, 95–123.
- Ciais, P., Tan, J., Wang, X., Roedenbeck, C., Chevallier, F., Piao, S.-L., Moriarty, R., Broquet, G., Le Quéré, C., Canadell, J., Peng, S., Poulter, B., Liu, Z., & Tans, P., 2019. Five decades of northern land carbon uptake revealed by the interhemispheric co<sub>2</sub> gradient, *Nature*, 568(7751), 221–225.
- Clark, D. B., Mercado, L. M., Sitch, S., Jones, C. D., Gedney, N., Best, M. J., Pryor, M., Rooney, G. G., Essery, R. L. H., Blyth, E., Boucher, O., Harding, R. J., Huntingford, C., & Cox, P. M., 2011. The joint UK land environment simulator (JULES), model description – part 2: Carbon fluxes and vegetation dynamics, *Geoscientific Model Development*, 4(3), 701–722.
- Coffel, E. D., Keith, B., Lesk, C., Horton, R. M., Bower, E., Lee, J., & Mankin, J. S., 2019. Future hot and dry years worsen Nile basin water scarcity despite projected precipitation increases, *Earth's Future*, 7(8), 967–977.
- Cohen, I., Zandalinas, S. I., Huck, C., Fritschi, F. B., & Mittler, R., 2020. Meta-analysis of drought and heat stress combination impact on crop yield and yield components, *Physiologia Plantarum*.
- Darenova, E., Holub, P., Krupkova, L., & Pavelka, M., 2017. Effect of repeated spring drought and summer heavy rain on managed grassland biomass production and co<sub>2</sub> efflux, *Journal of Plant Ecology*, 10(3), 476–485.
- De Boeck, H. J., Dreesen, F. E., Janssens, I. A., & Nijs, I., 2011. Whole-system responses of experimental plant communities to climate extremes imposed in different seasons, *New Phytologist*, 189(3), 806–817.
- De Boeck, H. J., Hiltbrunner, E., Verlinden, M., Bassin, S., & Zeiter, M., 2018. Legacy effects of climate extremes in alpine grassland, *Frontiers in plant science*, 9, 1586.
- De Kauwe, M. G., Medlyn, B. E., Zaehle, S., Walker, A. P., Dietze, M. C., Hickler, T., Jain, A. K., Luo, Y., Parton, W. J., Prentice, I. C., Smith, B., Thornton, P. E., Wang, S., Wang, Y.-P., Wårlind, D., Weng, E., Crous, K. Y., Ellsworth, D. S., Hanson, P. J., Kim, H.-S., Warren, J. M., Oren, R., & Norby, R. J., 2013. Forest water use and water use efficiency at elevated co<sub>2</sub>: a model-data intercomparison at two contrasting temperate forest face sites, *Global change biology*, 19(6), 1759–1779.
- De Kauwe, M. G., Medlyn, B. E., & Tissue, D. T., 2021. To what extent can rising [co<sub>2</sub>] ameliorate plant drought stress?, *New Phytologist*, 231(6), 2118–2124.
- DeFries, R. S., Houghton, R. A., Hansen, M. C., Field, C. B., Skole, D., & Townshend, J., 2002. Carbon emissions from tropical deforestation and regrowth based on satellite observations for the 1980s and 1990s, *Proceedings of the National Academy of Sciences*, 99(22), 14256–14261.
- Denton, E. M., Dietrich, J. D., Smith, M. D., & Knapp, A. K., 2017. Drought timing differentially affects above- and belowground productivity in a mesic grassland, *Plant Ecology*, 218(3), 317–328.
- Dieleman, W. I., Vicca, S., Dijkstra, F. A., Hagedorn, F., Hovenden, M. J., Larsen, K. S., Morgan, J. A., Volder, A., Beier, C., Dukes, J. S., King, J., Leuzinger, S., Linder, S., Lou, Y., Oren,

- R., De Angelis, P., Tingey, D., Hoosbeek, M. R., & Janssens, I. A., 2012. Simple additive effects are rare: a quantitative review of plant biomass and soil process responses to combined manipulations of co2 and temperature, *Global change biology*, 18(9), 2681–2693.
- Domec, J.-C., Smith, D. D., & McCulloh, K. A., 2017. A synthesis of the effects of atmospheric carbon dioxide enrichment on plant hydraulics: implications for whole-plant water use efficiency and resistance to drought, *Plant, Cell & Environment*, 40(6), 921–937.
- Doughty, C. E., Metcalfe, D. B., Girardin, C. A. J., Farfán Amézquita, F., Galiano Cabrera, D., Huaraca Huasco, W., Silva-Espejo, J. E., Araujo-Murakami, A., da Costa, M. C., Rocha, W., Feldpausch, T. R., Mendoza, A. L. M., da Costa, A. C. L., Meir, P., Phillips, O. L., & Malhi, Y., 2015. Drought impact on forest carbon dynamics and fluxes in amazonia, *Nature*, 519(7541), 78–82.
- Du, E., Terrer, C., Pellegrini, A. F., Ahlström, A., van Lissa, C. J., Zhao, X., Xia, N., Wu, X., & Jackson, R. B., 2020. Global patterns of terrestrial nitrogen and phosphorus limitation, *Nature Geoscience*, 13(3), 221–226.
- Fearnside, P. M., 2000. Global warming and tropical land-use change: greenhouse gas emissions from biomass burning, decomposition and soils in forest conversion, shifting cultivation and secondary vegetation, *Climatic change*, 46(1), 115–158.
- Feldpausch, T. R., Phillips, O. L., Brienen, R. J. W., Gloor, E., Lloyd, J., Lopez-Gonzalez, G., Monteagudo-Mendoza, A., Malhi, Y., Alarcón, A., Álvarez Dávila, E., Alvarez-Loayza, P., Andrade, A., Aragao, L. E. O. C., Arroyo, L., Ayman, C. G. A., Baker, T. R., Baraloto, C., Barroso, J., Bonal, D., Castro, W., Chama, V., Chave, J., Domingues, T. F., Fauset, S., Groot, N., Honorio Coronado, E., Laurance, S., Laurance, W. F., Lewis, S. L., Licona, J. C., Marimon, B. S., Marimon-Junior, B. H., Mendoza Bautista, C., Neill, D. A., Oliveira, E. A., Oliveira dos Santos, C., Pallqui Camacho, N. C., Pardo-Molina, G., Prieto, A., Quesada, C. A., Ramírez, F., Ramírez-Angulo, H., Réjou-Méchain, M., Rudas, A., Saiz, G., Salomão, R. P., Silva-Espejo, J. E., Silveira, M., ter Steege, H., Stropp, J., Terborgh, J., Thomas-Caesar, R., van der Heijden, G. M. F., Vásquez Martínez, R., Vilanova, E., & Vos, V. A., 2016. Amazon forest response to repeated droughts, *Global Biogeochemical Cycles*, 30(7), 964–982.
- Felton, A. J. & Smith, M. D., 2017. Integrating plant ecological responses to climate extremes from individual to ecosystem levels, *Philosophical Transactions of the Royal Society B: Biological Sciences*, 372(1723), 20160142.
- Fernández-Martínez, M., Sardans, J., Chevallier, F., Ciais, P., Obersteiner, M., Vicca, S., Canadell, J., Bastos, A., Friedlingstein, P., Sitch, S., Piao, S. L., Janssens, I. A., & Peñuelas, J., 2019. Global trends in carbon sinks and their relationships with co2 and temperature, *Nature climate change*, 9(1), 73–79.
- Flach, M., Gans, F., Brenning, A., Denzler, J., Reichstein, M., Rodner, E., Bathiany, S., Bodesheim, P., Guaniche, Y., Sippel, S., & Mahecha, M. D., 2017. Multivariate anomaly detection for earth observations: a comparison of algorithms and feature extraction techniques, *Earth System Dynamics*, 8(3), 677–696.
- Flach, M., Brenning, A., Gans, F., Reichstein, M., Sippel, S., & Mahecha, M. D., 2021. Vegetation modulates the impact of climate extremes on gross primary production, *Biogeosciences*, 18(1), 39–53.
- Forkel, M., Andela, N., Harrison, S. P., Lasslop, G., van Marle, M., Chuvieco, E., Dorigo, W., Forrest, M., Hantson, S., Heil, A., Li, F., Melton, J., Sitch, S., Yue, C., & Arnett, A., 2019. Emergent relationships with respect to burned area in global satellite observations and fire-enabled vegetation models, *Biogeosciences*, 16(1), 57–76.

- Frank, D., Reichstein, M., Bahn, M., Thonicke, K., Frank, D., Mahecha, M. D., Smith, P., Van der Velde, M., Vicca, S., Babst, F., Beer, C., Buchmann, N., Canadell, J. G., Ciais, P., Cramer, W., Ibrom, A., Miglietta, F., Poulter, B., Rammig, A., Seneviratne, S. I., Walz, A., Wattenbach, M., Zavala, M. A., & Zscheischler, J., 2015. Effects of climate extremes on the terrestrial carbon cycle: concepts, processes and potential future impacts, *Global change biology*, 21(8), 2861–2880.
- Friedlingstein, P., Meinshausen, M., Arora, V. K., Jones, C. D., Anav, A., Liddicoat, S. K., & Knutti, R., 2014. Uncertainties in cmip5 climate projections due to carbon cycle feedbacks, *Journal of Climate*, 27(2), 511–526.
- Friedlingstein, P., Jones, M., O’Sullivan, M., Andrew, R., Hauck, J., Peters, G., Peters, W., Pongratz, J., Sitch, S., Le Quéré, C., Bakker, D. C. E., Canadell, J. G., Ciais, P., Jackson, R. B., Anthoni, P., Barbero, L., Bastos, A., Bastrikov, V., Becker, M., Bopp, L., Buitenhuis, E., Chandra, N., Chevallier, F., Chini, L. B., Currie, K. I., Feely, R. A., Gehlen, M., Gilfillan, D., Gkritzalis, T., Goll, D. S., Gruber, N., Gutekunst, S., Harris, I., Haverd, V., Houghton, R. A., Hurtt, G., Ilyina, T., Jain, A. K., Joetzjer, E., Kaplan, J. O., Kato, E., Klein Goldewijk, K., Korsbakken, J. I., Landschützer, P., Lauvset, S. K., Lefèvre, N., Lenton, A., Lienert, S., Lombardozzi, D., Marland, G., McGuire, P. C., Melton, J. R., Metzl, N., Munro, D. R., Nabel, J. E. M. S., Nakaoka, S.-I., Neill, C., Omar, A. M., Ono, T., Peregón, A., Pierrot, D., Poulter, B., Rehder, G., Resplandy, L., Robertson, E., Rödenbeck, C., Séférian, R., Schwinger, J., Smith, N., Tans, P. P., Tian, H., Tilbrook, B., Tubiello, F. N., Van der Werf, G. R., Wiltshire, A. J., & Zaehle, S., 2019. Global carbon budget 2019, *Earth System Science Data*, 11(4), 1783–1838.
- Friedlingstein, P., O’Sullivan, M., Jones, M. W., Andrew, R. M., Hauck, J., Olsen, A., Peters, G. P., Peters, W., Pongratz, J., Sitch, S., Le Quéré, C., Canadell, J. G., Ciais, P., Jackson, R. B., Alin, S., Aragão, L. E. O. C., Arneeth, A., Arora, V., Bates, N. R., Becker, M., Benoit-Cattin, A., Bittig, H. C., Bopp, L., Bultan, S., Chandra, N., Chevallier, F., Chini, L. P., Evans, W., Florentie, L., Forster, P. M., Gasser, T., Gehlen, M., Gilfillan, D., Gkritzalis, T., Gregor, L., Gruber, N., Harris, I., Hartung, K., Haverd, V., Houghton, R. A., Ilyina, T., Jain, A. K., Joetzjer, E., Kadono, K., Kato, E., Kitidis, V., Korsbakken, J. I., Landschützer, P., Lefèvre, N., Lenton, A., Lienert, S., Liu, Z., Lombardozzi, D., Marland, G., Metzl, N., Munro, D. R., Nabel, J. E. M. S., Nakaoka, S.-I., Niwa, Y., O’Brien, K., Ono, T., Palmer, P. I., Pierrot, D., Poulter, B., Resplandy, L., Robertson, E., Rödenbeck, C., Schwinger, J., Séférian, R., Skjelvan, I., Smith, A. J. P., Sutton, A. J., Tanhua, T., Tans, P. P., Tian, H., Tilbrook, B., van der Werf, G., Vuichard, N., Walker, A. P., Wanninkhof, R., Watson, A. J., Willis, D., Wiltshire, A. J., Yuan, W., Yue, X., & Zaehle, S., 2020. Global carbon budget 2020, *Earth System Science Data*, 12(4), 3269–3340.
- Friedlingstein, P., Jones, M. W., O’Sullivan, M., Andrew, R. M., Bakker, D. C., Hauck, J., Le Quéré, C., Peters, G. P., Peters, W., Pongratz, J., Sitch, S., Canadell, J. G., Ciais, P., Jackson, R. B., Alin, S. R., Anthoni, P., Bates, N. R., Becker, M., Bellouin, N., Bopp, L., Chau, T. T. T., Chevallier, F., Chini, L. P., Cronin, M., Currie, K. I., Decharme, B., Djéutchouang, L. M., Dou, X., Evans, W., Feely, R. A., Feng, L., Gasser, T., Gilfillan, D., Gkritzalis, T., Grassi, G., Gregor, L., Gruber, N., Gürses, Ö., Harris, I., Houghton, R. A., Hurtt, G. C., Iida, Y., Ilyina, T., Luijkx, I. T., Jain, A., Jones, S. D., Kato, E., Kennedy, D., Goldewijk, K. K., Knauer, J., Korsbakken, J. I., Körtzinger, A., Landschützer, P., Lauvset, S. K., Lefèvre, N., Lienert, S., Liu, J., Marland, G., McGuire, P. C., Melton, J. R., Munro, D. R., Nabel, J. E. M. S., Nakaoka, S.-I., Niwa, Y., Ono, T., Pierrot, D., Poulter, B., Rehder, G., Resplandy, L., Robertson, E., Rödenbeck, C., Rosan, T. M., Schwinger, J., Schwingshackl, C., Séférian, R., Sutton, A. J., Sweeney, C., Tanhua, T., Tans, P. P., Tian, H., Tilbrook, B., Tubiello, F., van der Werf, G. R., Vuichard, N., Wada, C., Wanninkhof, R., Watson, A. J., Willis, D.,

- Wiltshire, A. J., Yuan, W., Yue, C., Yue, X., Zaehle, S., & Zeng, J., 2022. Global carbon budget 2021, *Earth System Science Data*, 14(4), 1917–2005.
- Friend, A. D., Lucht, W., Rademacher, T. T., Keribin, R., Betts, R., Cadule, P., Ciais, P., Clark, D. B., Dankers, R., Falloon, P. D., Ito, A., Kahana, R., Kleidon, A., Lomas, M. R., Nishina, K., Ostberg, S., Pavlick, R., Peylin, P., Schaphoff, S., Vuichard, N., Warszawski, L., Wiltshire, A., & Woodward, F. I., 2014. Carbon residence time dominates uncertainty in terrestrial vegetation responses to future climate and atmospheric  $\text{CO}_2$ , *Proceedings of the National Academy of Sciences*, 111(9), 3280–3285.
- Galvagno, M., Wohlfahrt, G., Cremonese, E., Rossini, M., Colombo, R., Filippa, G., Julitta, T., Manca, G., Siniscalco, C., Di Cella, U. M., & Migliavacca, M., 2013. Phenology and carbon dioxide source/sink strength of a subalpine grassland in response to an exceptionally short snow season, *Environmental Research Letters*, 8(2), 025008.
- Gampe, D., Zscheischler, J., Reichstein, M., O’Sullivan, M., Smith, W. K., Sitch, S., & Buermann, W., 2021. Increasing impact of warm droughts on northern ecosystem productivity over recent decades, *Nature Climate Change*.
- Gaubert, B., Stephens, B. B., Basu, S., Chevallier, F., Deng, F., Kort, E. A., Patra, P. K., Peters, W., Rödenbeck, C., Saeki, T., Schimel, D., Van der Laan-Luijkx, I., Wofsy, S., & Yin, Y., 2019. Global atmospheric  $\text{CO}_2$  inverse models converging on neutral tropical land exchange, but disagreeing on fossil fuel and atmospheric growth rate, *Biogeosciences*, 16(1), 117–134.
- Goetz, S. J., Bunn, A. G., Fiske, G. J., & Houghton, R. A., 2005. Satellite-observed photosynthetic trends across boreal north america associated with climate and fire disturbance, *Proceedings of the National Academy of Sciences*, 102(38), 13521–13525.
- Guimberteau, M., Zhu, D., Maignan, F., Huang, Y., Yue, C., Dantec-Nédélec, S., Ottlé, C., Jornet-Puig, A., Bastos, A., Laurent, P., Goll, D., Bowring, S., Chang, J., Guenet, B., Tifafi, M., Peng, S., Krinner, G., Ducharne, A., Wang, F., Wang, T., Wang, X., Wang, Y., Yin, Z., Lauerwald, R., Joetzjer, E., Qiu, C., Kim, H., & Ciais, P., 2018. Orchidee-mict (v8. 4.1), a land surface model for the high latitudes: model description and validation, *Geoscientific Model Development*, 11(1), 121–163.
- Gurney, K. R., Law, R. M., Denning, A. S., Rayner, P. J., Baker, D., Bousquet, P., Bruhwiler, L., Chen, Y.-H., Ciais, P., Fan, S., Fung, I. Y., Gloor, M., Heimann, M., Higuchi, K., John, J., Maki, T., Maksyutov, S., Masarie, K., Peylin, P., Prather, M., Pak, B. C., Randerson, J., Sarmiento, J., Taguchi, S., Takahashi, T., & Yuen, C.-W., 2002. Towards robust regional estimates of  $\text{CO}_2$  sources and sinks using atmospheric transport models, *Nature*, 415(6872), 626–630.
- Hagedorn, F., Joseph, J., Peter, M., Luster, J., Pritsch, K., Geppert, U., Kerner, R., Molinier, V., Egli, S., Schaub, M., Liu, J.-F., Li, M., Sever, K., Weiler, M., Siegwolf, R. T. W., Gessler, A., & Arend, M., 2016. Recovery of trees from drought depends on belowground sink control, *Nature plants*, 2(8), 1–5.
- Hammond, W. M., Williams, A. P., Abatzoglou, J. T., Adams, H. D., Klein, T., López, R., Sáenz-Romero, C., Hartmann, H., Breshears, D. D., & Allen, C. D., 2022. Global field observations of tree die-off reveal hotter-drought fingerprint for earth’s forests, *Nature communications*, 13(1), 1–11.
- Hao, Z., Singh, V. P., & Hao, F., 2018. Compound extremes in hydroclimatology: a review, *Water*, 10(6), 718.

- Harris, I., Jones, P. D., Osborn, T. J., & Lister, D. H., 2014. Updated high-resolution grids of monthly climatic observations—the cru ts3. 10 dataset, *International journal of climatology*, 34(3), 623–642.
- Hartmann, H., Ziegler, W., Kolle, O., & Trumbore, S., 2013. Thirst beats hunger—declining hydration during drought prevents carbon starvation in norway spruce saplings, *New Phytologist*, 200(2), 340–349.
- Hartmann, H., Bastos, A., Das, A. J., Esquivel-Muelbert, A., Hammond, W. M., Martínez-Vilalta, J., McDowell, N. G., Powers, J. S., Pugh, T. A., Ruthrof, K. X., & Allen, C. D., 2022. Climate change risks to global forest health: emergence of unexpected events of elevated tree mortality worldwide, *Annual Review of Plant Biology*, 73, 673–702.
- Haugen, M. A., Stein, M. L., Moyer, E. J., & Sriver, R. L., 2018. Estimating changes in temperature distributions in a large ensemble of climate simulations using quantile regression, *Journal of CLIMATE*, 31(20), 8573–8588.
- Haverd, V., Smith, B., Cook, G. D., Briggs, P. R., Nieradzic, L., Roxburgh, S. H., Liedloff, A., Meyer, C. P., & Canadell, J. G., 2013. A stand-alone tree demography and landscape structure module for earth system models, *Geophysical Research Letters*, 40(19), 5234–5239.
- Haverd, V., Smith, B., Nieradzic, L., Briggs, P. R., Woodgate, W., Trudinger, C. M., Canadell, J. G., & Cuntz, M., 2018. A new version of the cable land surface model (subversion revision r4601) incorporating land use and land cover change, woody vegetation demography, and a novel optimisation-based approach to plant coordination of photosynthesis, *Geoscientific Model Development*, 11(7), 2995–3026.
- Hazeleger, W., Wang, X., Severijns, C., Ștefănescu, S., Bintanja, R., Sterl, A., Wyser, K., Semmler, T., Yang, S., Van den Hurk, B., van Noije, T., van der Linden, E., & van der Wiel, K., 2012. EC-Earth v2. 2: description and validation of a new seamless earth system prediction model, *Climate dynamics*, 39(11), 2611–2629.
- Hendry, A., Haigh, I. D., Nicholls, R. J., Winter, H., Neal, R., Wahl, T., Joly-Laugel, A., & Darby, S. E., 2019. Assessing the characteristics and drivers of compound flooding events around the uk coast, *Hydrology and Earth System Sciences*, 23(7), 3117–3139.
- Herrera-Estrada, J. E. & Sheffield, J., 2017. Uncertainties in future projections of summer droughts and heat waves over the contiguous united states, *Journal of Climate*, 30(16), 6225 – 6246.
- Hicke, J. A., Asner, G. P., Randerson, J. T., Tucker, C., Los, S., Birdsey, R., Jenkins, J. C., Field, C., & Holland, E., 2002. Satellite-derived increases in net primary productivity across north america, 1982–1998, *Geophysical Research Letters*, 29(10), 69–1.
- Hoover, D., Knapp, A., & Smith, M., 2014. Contrasting sensitivities of two dominant c4 grasses to heat waves and drought, *Plant Ecology*, 215(7), 721–731.
- Houghton, R., 2005. Aboveground forest biomass and the global carbon balance, *Global change biology*, 11(6), 945–958.
- Houghton, R., 2007. Balancing the global carbon budget, *Annual Review of Earth and Planetary Sciences*, 35(1), 313–347.
- Houghton, R. A., 2003. Revised estimates of the annual net flux of carbon to the atmosphere from changes in land use and land management 1850–2000, *Tellus B: Chemical and Physical Meteorology*, 55(2), 378–390.

- Humphrey, V., Berg, A., Ciais, P., Gentine, P., Jung, M., Reichstein, M., Seneviratne, S. I., & Frankenberg, C., 2021. Soil moisture–atmosphere feedback dominates land carbon uptake variability, *Nature*, 592(7852), 65–69.
- Huntingford, C., Booth, B. B. B., Sitch, S., Gedney, N., Lowe, J. A., Liddicoat, S. K., Mercado, L. M., Best, M. J., Weedon, G. P., Fisher, R. A., Lomas, M. R., Good, P., Zelazowski, P., Everitt, A. C., Spessa, A. C., & Jones, C. D., 2010. IMOGEN: an intermediate complexity model to evaluate terrestrial impacts of a changing climate, *Geoscientific Model Development*, 3(2), 679–687.
- Huntzinger, D., Michalak, A., Schwalm, C., Ciais, P., King, A., Fang, Y., Schaefer, K., Wei, Y., Cook, R., Fisher, J., Hayes, D., Huang, M., Ito, A., Jain, A. K., Lei, H., Lu, C., Maignan, F., Mao, J., Parazoo, N., Peng, S., Poulter, B., Ricciuto, D., Shi, X., Tian, H., Wang, W., Zeng, N., & Zhao, F., 2017. Uncertainty in the response of terrestrial carbon sink to environmental drivers undermines carbon-climate feedback predictions, *Scientific reports*, 7(1), 1–8.
- IPCC, 2012. *Managing the Risks of Extreme Events and Disasters to Advance Climate Change Adaptation: Special Report of the Intergovernmental Panel on Climate Change*, Cambridge University Press.
- Jackson, R. B., Banner, J. L., Jobbágy, E. G., Pockman, W. T., & Wall, D. H., 2002. Ecosystem carbon loss with woody plant invasion of grasslands, *Nature*, 418(6898), 623–626.
- Jactel, H., Petit, J., Desprez-Loustau, M.-L., Delzon, S., Piou, D., Battisti, A., & Koricheva, J., 2012. Drought effects on damage by forest insects and pathogens: a meta-analysis, *Global Change Biology*, 18(1), 267–276.
- Jastrow, J. D., Michael Miller, R., Matamala, R., Norby, R. J., Boutton, T. W., Rice, C. W., & Owensby, C. E., 2005. Elevated atmospheric carbon dioxide increases soil carbon, *Global Change Biology*, 11(12), 2057–2064.
- Jentsch, A., Kreyling, J., Elmer, M., Gellesch, E., Glaser, B., Grant, K., Hein, R., Lara, M., Mirzae, H., Nadler, S. E., Nagy, L., Otieno, D., Pritsch, K., Rascher, U., Schädler, M., Schloter, M., Singh, B. K., Stadler, J., Walter, J., Wellstein, C., Wöllecke, J., & Beierkuhnlein, C., 2011. Climate extremes initiate ecosystem-regulating functions while maintaining productivity, *Journal of ecology*, 99(3), 689–702.
- Jones, C., Cox, P., Simmonds, P., & Manning, A., 2005. Atmospheric co<sub>2</sub> growth-rate anomalies in 2002–03, in *Seventh Int. Conf. Carbon Dioxide, Broomfield, CO (Abstr.) Google Scholar Article Location*.
- Joos, F., Meyer, R., Bruno, M., & Leuenberger, M., 1999. The variability in the carbon sinks as reconstructed for the last 1000 years, *Geophysical Research Letters*, 26(10), 1437–1440.
- Kasischke, E. S. & Turetsky, M. R., 2006. Recent changes in the fire regime across the north american boreal region – spatial and temporal patterns of burning across canada and alaska, *Geophysical research letters*, 33(9).
- Keller, K. M., Lienert, S., Bozbiyik, A., Stocker, T. F., Frank, D. C., Klesse, S., Koven, C. D., Leuenberger, M., Riley, W. J., Saurer, M., Siegwolf, R., Weigt, R. B., & Joos, F., 2017. 20th century changes in carbon isotopes and water-use efficiency: tree-ring-based evaluation of the clm4. 5 and lpx-bern models, *Biogeosciences*, 14(10), 2641–2673.
- Krinner, G., Viovy, N., de Noblet-Ducoudré, N., Ogée, J., Polcher, J., Friedlingstein, P., Ciais, P., Sitch, S., & Prentice, I. C., 2005. A dynamic global vegetation model for studies of the coupled atmosphere-biosphere system, *Global Biogeochemical Cycles*, 19(1).

- Larcher, W., 2003. *Physiological plant ecology: ecophysiology and stress physiology of functional groups*, Springer Science & Business Media.
- Laufkötter, C., Zscheischler, J., & Frölicher, T. L., 2020. High-impact marine heatwaves attributable to human-induced global warming, *Science*, 369, 1621–1625.
- Lemordant, L., Gentine, P., Stéfanon, M., Drobinski, P., & Fatichi, S., 2016. Modification of land-atmosphere interactions by co2 effects: Implications for summer dryness and heat wave amplitude, *Geophysical Research Letters*, 43(19), 10–240.
- Leonard, M., Westra, S., Phatak, A., Lambert, M., van den Hurk, B., McInnes, K., Risbey, J., Schuster, S., Jakob, D., & Stafford-Smith, M., 2014. A compound event framework for understanding extreme impacts, *Wiley Interdisciplinary Reviews: Climate Change*, 5(1), 113–128.
- Lesk, C., Coffel, E., Winter, J., Ray, D., Zscheischler, J., Seneviratne, S., & Horton, R., 2021. Stronger temperature-moisture couplings exacerbate the impact of climate warming on global crop yields, *Nature Food*, 2(9), 683–691.
- Li, J., Bevacqua, E., Chen, C., Wang, Z., Chen, X., Myneni, R. B., Wu, X., Xu, C.-Y., Zhang, Z., & Zscheischler, J., 2022. Regional asymmetry in the response of global vegetation growth to springtime compound climate events, *Communications Earth & Environment*, 3(1), 1–9.
- Lienert, S., 2018. *Modelling the Terrestrial Biosphere: Uncertainties and Constraints*, Ph.D. thesis, Philosophisch-naturwissenschaftliche Fakultät der Universität Bern.
- Lienert, S. & Joos, F., 2018. A bayesian ensemble data assimilation to constrain model parameters and land-use carbon emissions, *Biogeosciences*, 15(9), 2909–2930.
- Lindgren, A., Hugelius, G., & Kuhry, P., 2018. Extensive loss of past permafrost carbon but a net accumulation into present-day soils, *Nature*, 560(7717), 219–222.
- Lloyd, A. H. & Fastie, C. L., 2002. Spatial and temporal variability in the growth and climate response of treeline trees in alaska, *Climatic change*, 52(4), 481–509.
- Luo, Y., Hui, D., & Zhang, D., 2006. Elevated co2 stimulates net accumulations of carbon and nitrogen in land ecosystems: A meta-analysis, *Ecology*, 87(1), 53–63.
- Machado-Silva, F., Peres, L. F., Gouveia, C. M., Enrich-Prast, A., Peixoto, R. B., Pereira, J. M., Marotta, H., Fernandes, P. J., & Libonati, R., 2021. Drought resilience debt drives npp decline in the amazon forest, *Global Biogeochemical Cycles*, 35(9), e2021GB007004.
- Madden, R. A. & Williams, J., 1978. The correlation between temperature and precipitation in the united states and europe, *Monthly Weather Review*, 106(1), 142–147.
- Maher, N., Milinski, S., & Ludwig, R., 2021. Large ensemble climate model simulations: introduction, overview, and future prospects for utilising multiple types of large ensemble, *Earth System Dynamics*, 12(2), 401–418.
- Manning, A. & Keeling, R. F., 2006. Global oceanic and land biotic carbon sinks from the scripps atmospheric oxygen flask sampling network, *Tellus B: Chemical and Physical Meteorology*, 58(2), 95–116.
- Mathison, C., Burke, E., Hartley, A., Kelley, D., Robertson, E., Burton, C., Gedney, N., Williams, K., Wiltshire, A., Ellis, R., Sellar, A., & Jones, C., 2022. Description and evaluation of the jules-es setup for isip2b.

- McDowell, N., Allen, C. D., Anderson-Teixeira, K., Brando, P., Brienen, R., Chambers, J., Christoffersen, B., Davies, S., Doughty, C., Duque, A., Espirito-Santo, F., Fisher, R., Fontes, C. G., Galbraith, D., Goodsman, D., Grossiord, C., Hartmann, H., Holm, J., Johnson, D. J., Kassim, A. R., Keller, M., Koven, C., Kueppers, L., Kumagai, T., Malhi, Y., McMahon, S. M., Mencuccini, M., Meir, P., Moorcroft, P., Muller-Landau, H. C., Phillips, O. L., Powell, T., Sierra, C. A., Sperry, J., Warren, J., Xu, C., & Xu, X., 2018. Drivers and mechanisms of tree mortality in moist tropical forests, *New Phytologist*, 219(3), 851–869.
- McDowell, N. G., Beerling, D. J., Breshears, D. D., Fisher, R. A., Raffa, K. F., & Stitt, M., 2011. The interdependence of mechanisms underlying climate-driven vegetation mortality, *Trends in ecology & evolution*, 26(10), 523–532.
- McKee, T. B., Doesken, N. J., & Kleist, J., 1993. The relationship of drought frequency and duration to time scales, in *Proceedings of the 8th Conference on Applied Climatology*, vol. 17, pp. 179–183, Boston.
- Mehrabi, Z. & Ramankutty, N., 2019. Synchronized failure of global crop production, *Nature ecology & evolution*, 3(5), 780–786.
- Meir, P., Mencuccini, M., & Dewar, R. C., 2015. Drought-related tree mortality: addressing the gaps in understanding and prediction, *New Phytologist*, 207(1), 28–33.
- Meyerholt, J., Zaehle, S., & Smith, M. J., 2016. Variability of projected terrestrial biosphere responses to elevated levels of atmospheric CO<sub>2</sub> due to uncertainty in biological nitrogen fixation, *Biogeosciences*, 13(5), 1491–1518.
- Moftakhari, H. R., Salvadori, G., AghaKouchak, A., Sanders, B. F., & Matthew, R. A., 2017. Compounding effects of sea level rise and fluvial flooding, *Proceedings of the National Academy of Sciences*, 114(37), 9785–9790.
- Myneni, R. B., Los, S. O., & Asrar, G., 1995. Potential gross primary productivity of terrestrial vegetation from 1982–1990, *Geophysical Research Letters*, 22(19), 2617–2620.
- Myneni, R. B., Keeling, C., Tucker, C. J., Asrar, G., & Nemani, R. R., 1997. Increased plant growth in the northern high latitudes from 1981 to 1991, *Nature*, 386(6626), 698–702.
- Nanditha, J., van der Wiel, K., Bhatia, U., Stone, D., Selton, F., & Mishra, V., 2020. A seven-fold rise in the probability of exceeding the observed hottest summer in India in a 2°C warmer world, *Environmental Research Letters*, 15(4), 044028.
- Nepstad, D. C., Verssimo, A., Alencar, A., Nobre, C., Lima, E., Lefebvre, P., Schlesinger, P., Potter, C., Moutinho, P., Mendoza, E., Cochrane, M., & Brooks, V., 1999. Large-scale impoverishment of Amazonian forests by logging and fire, *Nature*, 398(6727), 505–508.
- Norby, R. J., DeLucia, E. H., Gielen, B., Calfapietra, C., Giardina, C. P., King, J. S., Ledford, J., McCarthy, H. R., Moore, D. J., Ceulemans, R., De Angelis, P., Finzi, A. C., Karnosky, D. F., Kubiske, M. E., Lukac, M., Pregitzer, K. S., Scarascia-Mugnozza, G. E., Schlesinger, W. H., & Oren, R., 2005. Forest response to elevated CO<sub>2</sub> is conserved across a broad range of productivity, *Proceedings of the National Academy of Sciences*, 102(50), 18052–18056.
- Obermeier, W. A., Lehnert, L. W., Kammann, C., Müller, C., Grünhage, L., Luterbacher, J., Erbs, M., Moser, G., Seibert, R., Yuan, N., & Bendix, J., 2017. Reduced CO<sub>2</sub> fertilization effect in temperate C<sub>3</sub> grasslands under more extreme weather conditions, *Nature Climate Change*, 7(2), 137–141.

- Orth, R., Zscheischler, J., & Seneviratne, S. I., 2016. Record dry summer in 2015 challenges precipitation projections in Central Europe, *Scientific Reports*, 6(1), 1–8.
- O'sullivan, O. S., Heskell, M. A., Reich, P. B., Tjoelker, M. G., Weerasinghe, L. K., Penillard, A., Zhu, L., Egerton, J. J., Bloomfield, K. J., Creek, D., Bahar, N. H. A., Griffin, K. L., Hurry, V., Meir, P., Turnbull, M. H., & Atkin, O. K., 2017. Thermal limits of leaf metabolism across biomes, *Global Change Biology*, 23(1), 209–223.
- Page, S. E., Siegert, F., Rieley, J. O., Boehm, H.-D. V., Jaya, A., & Limin, S., 2002. The amount of carbon released from peat and forest fires in indonesia during 1997, *Nature*, 420(6911), 61–65.
- Pan, S., Yang, J., Tian, H., Shi, H., Chang, J., Ciais, P., Francois, L., Frieler, K., Fu, B., Hickler, T., Ito, A., Nishina, K., Ostberg, S., Reyer, C. P., Schaphoff, S., Steinkamp, J., & Zhao, F., 2020. Climate Extreme Versus Carbon Extreme: Responses of Terrestrial Carbon Fluxes to Temperature and Precipitation, *Journal of Geophysical Research: Biogeosciences*, 125(4), e2019JG005252.
- Papagiannopoulou, C., Miralles, D., Dorigo, W. A., Verhoest, N., Depoorter, M., & Waegeman, W., 2017. Vegetation anomalies caused by antecedent precipitation in most of the world, *Environmental Research Letters*, 12(7), 074016.
- Paschalis, A., Fatichi, S., Zscheischler, J., Ciais, P., Bahn, M., Boysen, L., Chang, J., De Kauwe, M., Estiarte, M., Goll, D., Hanson, P. J., Harper, A. B., Hou, E., Kigel, J., Knapp, A. K., Larse, K. S., Li, W., Lienert, S., Luo, Y., Meir, P., Nabel, J. E. M. S., Ogaya, R., Parolari, A. J., Peng, C., Peñuelas, J., Pongratz, J., Rambal, S., Schmidt, I. K., Shi, H., Sternberg, M., Tian, H., Tschumi, E., Ukkola, A., Vicca, S., Viovy, N., Wang, Y.-P., Wang, Z., Williams, K., Wu, D., & Zhu, Q., 2020. Rainfall manipulation experiments as simulated by terrestrial biosphere models: Where do we stand?, *Global change biology*, 26(6), 3336–3355.
- Pastorello, G., Trotta, C., Canfora, E., Chu, H., Christianson, D., Cheah, Y.-W., Poindexter, C., Chen, J., Elbashandy, A., Humphrey, M., Isaac, P., Polidori, D., Ribeca, A., van Ingen, C., Zhang, L., Amiro, B., Ammann, C., Arain, M. A., Ardö, J., Arkebauer, T., Arndt, S. K., Arriga, N., Aubinet, M., Aurelia, M., Baldocchi, D., Barr, A., Beamesderfer, E., Beletti Marchesini, L., Bergeron, O., Beringer, J., Bernhofer, C., Berveiller, D., Billesbach, D., Andrew Black, T., Blanken, P. D., Bohrer, G., Boike, J., Bolstad, P. V., Bonal, D., Bonnefond, J.-M., Bowling, D. R., Bracho, R., Brodeur, J., Brümmer, C., Buchmann, N., Burban, B., Burns, S. P., Buysse, P., Cale, P., Cavagna, M., Cellier, P., Chen, S., Chini, I., Christensen, T. R., Cleverly, J., Collalti, A., Consalvo, C., Cook, B. D., Cook, D., Coursolle, C., Cremonese, E., Curtis, P. S., D'Andrea, E., da Rocha, H., Dai, X., Davis, K. J., De Cinti, B., de Grandcourt, A., De Ligne, A., De Oliveira, R. C., Delpierre, N., Desai, A. R., Marcelo Di Bella, C., di Tommasi, P., Dolman, H., Domingo, F., Dong, G., Dore, S., Duce, P., Dufrêne, E., Dunn, A., Dušek, J., Eamus, D., Eichelmann, U., Abdalla M ElKhidir, H., Eugster, W., Ewenz, C. M., Ewers, B., Famulari, D., Fares, S., Feigenwinter, I., Feitz, A., Fensholt, R., Filippa, G., Fischer, M., Frank, J., Galvagno, M., Gharun, M., Gianelle, D., Gielen, B., Gioli, B., Gitelson, A., Goded, I., Goeckede, M., Goldstein, A. H., Gough, C. M., Goulden, M. L., Graf, A., Griebel, A., Gruening, C., Grünwald, T., Hammerle, A., Han, S., Han, X., Hansen, B. U., Hanson, C., Hatakka, J., He, Y., Hehn, M., Heinesch, B., Hinko-Najera, N., Hörtnagl, L., Hutley, L., Ibrom, A., Ikawa, H., Jackowicz-Korczynski, M., Janouš, D., Jans, W., Jassal, R., Jiang, S., Kato, T., Khomik, M., Klatt, J., Knohl, A., Knox, S., Kobayashi, H., Koerber, G., Kolle, O., Kosugi, Y., Kotami, A., Kowalski, A., Kruijt, B., Kurbatova, J., Kutsch, W. L., Kwon, H., Launiainen, S., Laurila, T., Law, B., Leuning, Ray and Li, Y., Liddell, M., Limousin, J.-M., Lion, M., Liska, A. J., Lohila, A., López-Ballesteros, A., López-Blanco, E., Loubet, B., Loustau, D., Lucas-Moffat, A., Lüers,

- J., Ma, S., Macfarlane, C., Magliulo, V., Maier, R., Mammarella, I., Manca, G., Marcolla, B., Margolis, H. A., Marras, S., Massman, W., Mastepanov, M., Matamala, R., Hatala Matthes, J., Mazzenga, F., McCaughey, Harry McHugh, I., McMillan, A. M. S., Merbold, L., Meyer, W., Meyers, T., Miller, S. D., Minerbi, S., Moderow, U., Monson, R. K., Montagnani, L., Moore, C. E., Moors, E., Moreaux, V., Moureaux, C., Munger, J. W., Nakai, T., Neiryneck, J., Nesic, Z., Nicolini, G., Noormets, A., Northwood, M., Noretto, M., Nouvellon, Y., Novick, K., Oechel, W., Olesen, J. E., Ourcival, J.-M., Papuga, S. A., Parmentier, F.-J., Paul-Limoges, E., Pavelka, M., Peichl, M., Pendall, E., Phillips, R. P., Pilegaard, K., Pirk, N., Posse, G., Powell, T., Prasse, H., Prober, S. M., Rambal, S., Rannik, Ü., Raz-Yaseef, N., Reed, D., Resco de Dios, V., Restrepo-Coupe, N., Reverter, B. R., Roland, M., Sabbatini, S., Sachs, T., Saleska, S. R., Sánchez-Cañete, E. P., Sanches-Mejia, Z. M., Schmid, H. P., Schmidt, M., Schneider, K., Schrader, F., Schroder, I., Scott, R. L., Sedlák, P., Serrano-Ortiz, P., Shao, C., Shi, P., Shironya, I., Siebicke, L., Šigut, L., Silberstein, R., Sirca, C., Spano, D., Steinbrecher, R., Stevens, R. M., Sturtevant, C., Suyker, A., Tagesson, T., Satoru, T., Tang, Y., Tapper, N., Thom, J., Tiedemann, F., Tomassucci, M., Tuovinen, J.-P., Urbanski, S., Valentini, R., van der Molen, M., van Gorsel, E., van Huissteden, K., Varlagin, A., Verfaillie, J., Vesala, T., Vincke, C., Vitale, D., Vygodskaya, N., Walker, J. P., Walter-Shea, E., Wang, H., Weber, R., Westermann, S., Wille, C., Wofsky, S., Wohlfahrt, G., Wolf, S., Woodgate, W., Li, Y., Zampedri, R., Zhang, J., Zhou, G., Zona, D., Agarwal, D., Biraud, S., Torn, M., & Papale, D., 2020. The fluxnet2015 dataset and the oneflux processing pipeline for eddy covariance data, *Scientific data*, 7(1), 1–27.
- Peltier, D. M., Fell, M., & Ogle, K., 2016. Legacy effects of drought in the southwestern united states: A multi-species synthesis, *Ecological Monographs*, 86(3), 312–326.
- Peng, C., 2000. From static biogeographical model to dynamic global vegetation model: a global perspective on modelling vegetation dynamics, *Ecological modelling*, 135(1), 33–54.
- Peñuelas, J., Ciais, P., Canadell, J. G., Janssens, I. A., Fernández-Martínez, M., Carnicer, J., Obersteiner, M., Piao, S., Vautard, R., & Sardans, J., 2017. Shifting from a fertilization-dominated to a warming-dominated period, *Nature ecology & evolution*, 1(10), 1438–1445.
- Perkins, S. E., 2015. A review on the scientific understanding of heatwaves – their measurement, driving mechanisms, and changes at the global scale, *Atmospheric Research*, 164, 242–267.
- Poschlod, B., Zscheischler, J., Sillmann, J., Wood, R. R., & Ludwig, R., 2020. Climate change effects on hydrometeorological compound events over southern norway, *Weather and Climate Extremes*, 28, 100253.
- Prentice, I. & Leemans, R., 1990. Pattern and process and the dynamics of forest structure: a simulation approach, *The Journal of Ecology*, pp. 340–355.
- Prentice, I. C., Cramer, W., Harrison, S. P., Leemans, R., Monserud, R. A., & Solomon, A. M., 1992. Special paper: a global biome model based on plant physiology and dominance, soil properties and climate, *Journal of biogeography*, pp. 117–134.
- Pugh, T. A., Arneith, A., Kautz, M., Poulter, B., & Smith, B., 2019. Important role of forest disturbances in the global biomass turnover and carbon sinks, *Nature Geoscience*, 12(9), 730–735.
- Quesada, B., Vautard, R., Yiou, P., Hirschi, M., & Seneviratne, S. I., 2012. Asymmetric european summer heat predictability from wet and dry southern winters and springs, *Nature Climate Change*, 2(10), 736–741.

- Rabin, S. S., Melton, J. R., Lasslop, G., Bachelet, D., Forrester, M., Hantson, S., Kaplan, J. O., Li, F., Mangeon, S., Ward, D. S., Yue, C., Arora, V. K., Hickler, T., Kloster, S., Knorr, W., Nieradzik, L., Spessa, A., Folberth, G. A., Sheehan, T., Voulgarakis, A., Kelley, D. I., Prentice, I. C., Sitch, S., Harrison, S., & Arneth, A., 2017. The Fire Modeling Intercomparison Project (FireMIP), phase 1: experimental and analytical protocols with detailed model descriptions, *Geoscientific Model Development*, 10(3), 1175–1197.
- Rammig, A., Wiedermann, M., Donges, J. F., Babst, F., von Bloh, W., Frank, D., Thonicke, K., & Mahecha, M. D., 2015. Coincidences of climate extremes and anomalous vegetation responses: comparing tree ring patterns to simulated productivity, *Biogeosciences*, 12(2), 373–385.
- Reichstein, M., Ciais, P., Papale, D., Valentini, R., Running, S., Viovy, N., Cramer, W., Granier, A., Ogee, J., Allard, V., Aubinet, M., Bernhofer, C., Buchmann, N., Carrara, A., Grünwald, T., Heimann, M., Heinesch, B., Knohl, A., Kutsch, W., Loustau, D., Manca, G., Matteucci, G., Miglietta, F., Ourcival, J. M., Pilegaard, K., Pumpanen, J., Rambal, S., Schaphoff, S., Seufert, G., Soussana, J.-F., Sanz, M.-J., Vesala, T., & Zhao, M., 2007. Reduction of ecosystem productivity and respiration during the european summer 2003 climate anomaly: a joint flux tower, remote sensing and modelling analysis, *Global Change Biology*, 13(3), 634–651.
- Reichstein, M., Bahn, M., Ciais, P., Frank, D., Mahecha, M. D., Seneviratne, S. I., Zscheischler, J., Beer, C., Buchmann, N., Frank, D. C., Papale, D., Rammig, A., Smith, P., Thonicke, K., van der Welde, M., Vicca, S., Walz, A., & Wattenbach, M., 2013. Climate extremes and the carbon cycle, *Nature*, 500(7462), 287–295.
- Ribeiro, A. F. S., Russo, A., Gouveia, C. M., Páscoa, P., & Zscheischler, J., 2020. Risk of crop failure due to compound dry and hot extremes estimated with nested copulas, *Biogeosciences*, 17(19), 4815–4830.
- Rosenzweig, C., Jones, J. W., Hatfield, J. L., Ruane, A. C., Boote, K. J., Thorburn, P., Antle, J. M., Nelson, G. C., Porter, C., Janssen, S., Asseng, S., B, B., Ewert, F., Wallach, D., Baigorría, G., & Winter, J. M., 2013. The agricultural model intercomparison and improvement project (agmip): protocols and pilot studies, *Agricultural and Forest Meteorology*, 170, 166–182.
- Rosenzweig, C., Elliott, J., Deryng, D., Ruane, A. C., Müller, C., Arneth, A., Boote, K. J., Folberth, C., Glotter, M., Khabarov, N., Neumann, K., Piontek, F., Pugh, T. A. M., Schmid, E., Stehfest, E., Yang, H., & Jones, J. W., 2014. Assessing agricultural risks of climate change in the 21st century in a global gridded crop model intercomparison, *Proceedings of the National Academy of Sciences*, 111(9), 3268–3273.
- Roy, J., Picon-Cochard, C., Augusti, A., Benot, M.-L., Thiery, L., Darsonville, O., Landais, D., Piel, C., Defosse, M., Devidal, S., Escape, C., Ravel, O., Fromin, N., Volaire, F., Milcu, A., Bahn, M., & Soussana, J.-F., 2016. Elevated co2 maintains grassland net carbon uptake under a future heat and drought extreme, *Proceedings of the National Academy of Sciences*, 113(22), 6224–6229.
- Ruiz-Pérez, G. & Vico, G., 2020. Effects of temperature and water availability on northern european boreal forests, *Frontiers in Forests and Global Change*, 3, 34.
- Saleska, S. R., Miller, S. D., Matross, D. M., Goulden, M. L., Wofsy, S. C., Da Rocha, H. R., De Camargo, P. B., Crill, P., Daube, B. C., De Freitas, H. C., Huttyra, L., Keller, M., Kirchhoff, V., Menton, M., Munger, J. W., Hammond Pyle, E., Rice, A. H., & Silva, H., 2003. Carbon in amazon forests: unexpected seasonal fluxes and disturbance-induced losses, *Science*, 302(5650), 1554–1557.

- Salvadori, G., Durante, F., De Michele, C., Bernardi, M., & Petrella, L., 2016. A multivariate copula-based framework for dealing with hazard scenarios and failure probabilities, *Water Resources Research*, 52(5), 3701–3721.
- Sarhadi, A., Ausín, M. C., Wiper, M. P., Touma, D., & Diffenbaugh, N. S., 2018. Multidimensional risk in a nonstationary climate: Joint probability of increasingly severe warm and dry conditions, *Science Advances*, 4(11), eaau3487.
- Schlesinger, W. H. & Bernhard, E. S., 2013. *Biogeochemistry*, Elsevier, 3rd edn.
- Schwalm, C. R., Williams, C. A., Schaefer, K., Arneth, A., Bonal, D., Buchmann, N., Chen, J., Law, B. E., Lindroth, A., Luyssaert, S., Reichstein, M., & Richardson, A. D., 2010. Assimilation exceeds respiration sensitivity to drought: A fluxnet synthesis, *Global Change Biology*, 16(2), 657–670.
- Schwalm, C. R., Anderegg, W. R., Michalak, A. M., Fisher, J. B., Biondi, F., Koch, G., Litvak, M., Ogle, K., Shaw, J. D., Wolf, A., Huntzinger, D. N., Schaefer, K., Cook, R., Wei, Y., Fang, Y., Hayes, D., Huang, M., & tian, H., 2017. Global patterns of drought recovery, *Nature*, 548(7666), 202–205.
- Seidl, R., Thom, D., Kautz, M., Martin-Benito, D., Peltoniemi, M., Vacchiano, G., Wild, J., Ascoli, D., Petr, M., Honkaniemi, J., Lexer, M. J., Trotsiuk, V., Mairota, P., Svoboda, M., Ffabrika, M., Nagel, T. A., & Reyer, C. P. O., 2017. Forest disturbances under climate change, *Nature climate change*, 7(6), 395–402.
- Seneviratne, S. I., Corti, T., Davin, E. L., Hirschi, M., Jaeger, E. B., Lehner, I., Orlowsky, B., & Teuling, A. J., 2010. Investigating soil moisture–climate interactions in a changing climate: A review, *Earth-Science Reviews*, 99(3-4), 125–161.
- Seneviratne, S. I., Nicholls, N., Easterling, D., Goodess, C., Kanae, S., Kossin, J., Luo, Y., Marengo, J., McInnes, K., Rahimi, M., Reichstein, M., Sorteberg, A., Vera, C., & Zhang, X., 2012. Changes in Climate Extremes and their Impacts on the Natural Physical Environment, in *Managing the Risks of Extreme Events and Disasters to Advance Climate Change Adaptation*, pp. 109–230, eds Field, C., Barros, V., Stocker, T., Qin, D., Dokken, D., Ebi, K., Mastrandrea, M., Mach, K., Plattner, G.-K., Allen, S., Tignor, M., & Midgley, P., Cambridge University Press, Cambridge, UK, and New York, NY, USA.
- Senf, C., Buras, A., Zang, C. S., Rammig, A., & Seidl, R., 2020. Excess forest mortality is consistently linked to drought across europe, *Nature Communications*, 11(1), 1–8.
- Sevanto, S. & Dickman, L. T., 2015. Where does the carbon go? – plant carbon allocation under climate change, *Tree physiology*, 35(6), 581–584.
- Shah, N. & Paulsen, G., 2003. Interaction of drought and high temperature on photosynthesis and grain-filling of wheat, *Plant and Soil*, 257(1), 219–226.
- Shugart, H. H., 1984. *A theory of forest dynamics. The ecological implications of forest succession models.*, Springer-Verlag.
- Shugart Jr, H. & West, D. C., 1980. Forest succession models, *BioScience*, 30(5), 308–313.
- Singh, D., Seager, R., Cook, B. I., Cane, M., Ting, M., Cook, E., & Davis, M., 2018. Climate and the global famine of 1876–78, *Journal of Climate*, 31(23), 9445–9467.
- Sippel, S., Zscheischler, J., & Reichstein, M., 2016. Ecosystem impacts of climate extremes crucially depend on the timing, *Proceedings of the National Academy of Sciences*, 113(21), 5768–5770.

- Sippel, S., Reichstein, M., Ma, X., Mahecha, M. D., Lange, H., Flach, M., & Frank, D., 2018. Drought, heat, and the carbon cycle: a review, *Current Climate Change Reports*, 4(3), 266–286.
- Sitch, S., Smith, B., Prentice, I. C., Arneth, A., Bondeau, A., Cramer, W., Kaplan, J. O., Levis, S., Lucht, W., Sykes, M. T., Thonicke, K., & Venevsky, S., 2003. Evaluation of ecosystem dynamics, plant geography and terrestrial carbon cycling in the lpj dynamic global vegetation model, *Global change biology*, 9(2), 161–185.
- Sitch, S., Huntingford, C., Gedney, N., Levy, P., Lomas, M., Piao, S., Betts, R., Ciais, P., Cox, P., Friedlingstein, P., Jones, C. D., Prentice, I. C., & Woodward, F. I., 2008. Evaluation of the terrestrial carbon cycle, future plant geography and climate-carbon cycle feedbacks using five dynamic global vegetation models (dgvms), *Global Change Biology*, 14(9), 2015–2039.
- Smith, B., Prentice, I. C., & Sykes, M. T., 2001. Representation of vegetation dynamics in the modelling of terrestrial ecosystems: comparing two contrasting approaches within european climate space, *Global ecology and biogeography*, pp. 621–637.
- Smith, B., Wårlind, D., Arneth, A., Hickler, T., Leadley, P., Siltberg, J., & Zaehle, S., 2014. Implications of incorporating n cycling and n limitations on primary production in an individual-based dynamic vegetation model, *Biogeosciences*, 11(7), 2027–2054.
- Song, J., Wan, S., Piao, S., Knapp, A. K., Classen, A. T., Vicca, S., Ciais, P., Hovenden, M. J., Leuzinger, S., Beier, C., Kardol, P., Xia, J., Liu, Q., Ru, J., Zhou, Z., Luo, Y., Guo, D., Langley, A. J., Zscheischler, J., Dukes, J. S., Tang, J., Chen, J., Hofmockel, K. S., Kueppers, L. M., Rustad, L., Liu, L., Smith, M. D., Templer, P. H., Quinn Thomas, R., Norby, R. J., Phillips, R. P., Niu, S., Fatichi, S., Wang, Y., Shao, P., Han, H., Wang, D., Lei, L., Wang, J., Li, X., Zhang, Q., Li, X., Su, F., Liu, B., Yang, F., Ma, G., Li, G., Liu, Y., Liu, Y., Yang, Z., Zhang, K., Miao, Y., Hu, M., Yan, C., Zhang, A., Zhong, M., Hui, Y., Li, Y., & Zheng, M., 2019. A meta-analysis of 1,119 manipulative experiments on terrestrial carbon-cycling responses to global change, *Nature Ecology & Evolution*, 3(9), 1309–1320.
- Stephenson, N. L., 1990. Climatic control of vegetation distribution: the role of the water balance, *The American Naturalist*, 135(5), 649–670.
- Stephoe, H., Jones, S., & Fox, H., 2018. Correlations between extreme atmospheric hazards and global teleconnections: implications for multihazard resilience, *Reviews of Geophysics*, 56(1), 50–78.
- Stocker, B. D., Zscheischler, J., Keenan, T. F., Prentice, I. C., Seneviratne, S. I., & Peñuelas, J., 2019. Drought impacts on terrestrial primary production underestimated by satellite monitoring, *Nature Geoscience*, 12(4), 264–270.
- Suarez-Gutierrez, L., Li, C., Müller, W. A., & Marotzke, J., 2018. Internal variability in european summer temperatures at 1.5 c and 2 c of global warming, *Environmental Research Letters*, 13(6), 064026.
- Sun, Q., Miao, C., Duan, Q., Ashouri, H., Sorooshian, S., & Hsu, K.-L., 2018. A review of global precipitation data sets: Data sources, estimation, and intercomparisons, *Reviews of Geophysics*, 56(1), 79–107.
- Taylor, K. E., Stouffer, R. J., & Meehl, G. A., 2012. An Overview of CMIP5 and the Experiment Design, *Bulletin of the American Meteorological Society*, 93(4), 485–498.
- Taylor, S. H., Ripley, B. S., Martin, T., De-Wet, L.-A., Woodward, F. I., & Osborne, C. P., 2014. Physiological advantages of c4 grasses in the field: a comparative experiment demonstrating the importance of drought, *Global change biology*, 20(6), 1992–2003.

- Teckentrup, L., Harrison, S. P., Hantson, S., Heil, A., Melton, J. R., Forrest, M., Li, F., Yue, C., Arneth, A., Hickler, T., Sitch, S., & Lasslop, G., 2019. Response of simulated burned area to historical changes in environmental and anthropogenic factors: a comparison of seven fire models, *Biogeosciences*, 16(19), 3883–3910.
- Teckentrup, L., De Kauwe, M. G., Abramowitz, G., Pitman, A. J., Ukkola, A. M., Hobeichi, S., François, B., & Smith, B., 2022. Opening pandora’s box: How to constrain regional projections of the carbon cycle, *EGUsphere*, pp. 1–51.
- Teuling, A. J., Seneviratne, S. I., Stöckli, R., Reichstein, M., Moors, E., Ciais, P., Luysaert, S., Van Den Hurk, B., Ammann, C., Bernhofer, C., Dellwik, E., Gianelle, D., Gielen, B., Grünwald, T., Klumpp, K., Montagnani, L., Moureaux, C., & Sottocornola, Matteo an Wohlfahrt, G., 2010. Contrasting response of european forest and grassland energy exchange to heatwaves, *Nature geoscience*, 3(10), 722–727.
- Thonicke, K., Venevsky, S., Sitch, S., & Cramer, W., 2001. The role of fire disturbance for global vegetation dynamics: coupling fire into a dynamic global vegetation model, *Global Ecology and Biogeography*, 10(6), 661–677.
- Tian, H., Yang, J., Lu, C., Xu, R., Canadell, J. G., Jackson, R. B., Arneth, A., Chang, J., Chen, G., Ciais, P., Gerber, S., Ito, A., Huang, Y., Joos, F., Lienert, S., Messina, P., Olin, S., Pan, S., Peng, C., Saikawa, E., Thompson, R. L., Vuichard, N., Winiwarter, W., Zaehle, S., Zhang, B., Zhang, K., & Zhu, Q., 2018. The global n2o model intercomparison project, *Bulletin of the American Meteorological Society*, 99(6), 1231–1251.
- Tilloy, A., Malamud, B. D., Winter, H., & Joly-Laugel, A., 2019. A review of quantification methodologies for multi-hazard interrelationships, *Earth-Science Reviews*, 196, 102881.
- Toreti, A., Deryng, D., Tubiello, F. N., Müller, C., Kimball, B. A., Moser, G., Boote, K., Asseng, S., Pugh, T. A. M., Vanuytrecht, E., Pleijel, H., Webber, H., Durand, J.-L., Dentener, F., Ceglar, A., Wang, X., Badeck, F., Lecerf, R., Wall, G. W., van den Berg, M., Hoegy, P., Lopez-Lozano, R., Zampieri, M., Galmarini, S., O’Leary, G. J., Manderscheid, R., Mencos Contreras, E., & Rosenzweig, C., 2020. Narrowing uncertainties in the effects of elevated CO2 on crops, *Nature Food*, 1(12), 775–782.
- Trenberth, K. E. & Shea, D. J., 2005. Relationships between precipitation and surface temperature, *Geophysical Research Letters*, 32(14).
- Tschumi, E. & Zscheischler, J., 2020. Countrywide climate features during recorded climate-related disasters, *Climatic Change*, 158(3-4), 593–609.
- Tschumi, E., Lienert, S., van der Wiel, K., Joos, F., & Zscheischler, J., 2020. A climate database with varying drought-heat signatures for climate impact modelling.
- Tschumi, E., Lienert, S., van der Wiel, K., Joos, F., & Zscheischler, J., 2022a. A climate database with varying drought-heat signatures for climate impact modelling, *Geoscience Data Journal*, 9(1), 154–166.
- Tschumi, E., Lienert, S., van der Wiel, K., Joos, F., & Zscheischler, J., 2022b. The effects of varying drought-heat signatures on terrestrial carbon dynamics and vegetation composition, *Biogeosciences*, 19(7), 1979–1993.
- Valentini, R., Matteucci, G., Dolman, A., Schulze, E.-D., Rebmann, C., Moors, E., Granier, A., Gross, P., Jensen, N., Pilegaard, K., Lindroth, A., Grelle, A., Bernhofer, C., Grünwald, T., Aubinet, M., Ceulemans, R., Kowalski, A. S., Vesala, T., Rannik, Ü., Berbigier, P., Loustau,

- D., Guðmundsson, J., Thorgeirsson, H., Ibrom, A., Morgenstern, K., Clement, R., Moncrieff, J., Montagnani, L., Minerbi, S., & Jarvis, P. G., 2000. Respiration as the main determinant of carbon balance in european forests, *Nature*, 404(6780), 861–865.
- Van der Wiel, K., Bloomfield, H. C., Lee, R. W., Stoop, L. P., Blackport, R., Screen, J. A., & Selten, F. M., 2019a. The influence of weather regimes on european renewable energy production and demand, *Environmental Research Letters*, 14(9), 094010.
- Van der Wiel, K., Stoop, L. P., Van Zuijlen, B., Blackport, R., Van den Broek, M., & Selten, F., 2019b. Meteorological conditions leading to extreme low variable renewable energy production and extreme high energy shortfall, *Renewable and Sustainable Energy Reviews*, 111, 261–275.
- Van der Wiel, K., Wanders, N., Selten, F., & Bierkens, M., 2019c. Added value of large ensemble simulations for assessing extreme river discharge in a 2 c warmer world, *Geophysical Research Letters*, 46(4), 2093–2102.
- van der Wiel, K., Selten, F. M., Bintanja, R., Blackport, R., & Screen, J. A., 2020. Ensemble climate-impact modelling: extreme impacts from moderate meteorological conditions, *Environmental Research Letters*, 15(3), 034050.
- Vicente-Serrano, S. M., Beguería, S., & López-Moreno, J. I., 2010. A multiscalar drought index sensitive to global warming: the standardized precipitation evapotranspiration index, *Journal of climate*, 23(7), 1696–1718.
- Vogel, J., Rivoire, P., Deidda, C., Rahimi, L., Sauter, C. A., Tschumi, E., van der Wiel, K., Zhang, T., & Zscheischler, J., 2020. Identifying meteorological drivers of extreme impacts: an application to simulated crop yields, *Earth System Dynamics Discussions*, pp. 1–27.
- Vogel, J., Rivoire, P., Deidda, C., Rahimi, L., Sauter, C. A., Tschumi, E., van der Wiel, K., Zhang, T., & Zscheischler, J., 2021. Identifying meteorological drivers of extreme impacts: an application to simulated crop yields, *Earth System Dynamics*, 12(1), 151–172.
- von Buttlar, J., Zscheischler, J., Rammig, A., Sippel, S., Reichstein, M., Knohl, A., Jung, M., Menzer, O., Arain, M. A., Buchmann, N., Cescatti, A., Gianelle, D., Kiely, G., Law, B. E., Magliulo, V., Margolis, H., McCaughey, H., Merbold, L., Migliavacca, M., Montagnano, L., Oechel, W., Pavelka, M., Peichl, M., Rambal, S., Raschi, A., Scott, R. L., Vaccari, F. P., van Gorsel, E., Varlagin, A., Wohlfahrt, G., & Mahecha, M. D., 2018. Impacts of droughts and extreme-temperature events on gross primary production and ecosystem respiration: a systematic assessment across ecosystems and climate zones, *Biogeosciences*, 15(5), 1293–1318.
- Vrac, M., Thao, S., & Yiou, P., 2021. Changes in temperature-precipitation correlations over europe: Are climate models reliable?
- Walker, A. P., De Kauwe, M. G., Bastos, A., Belmecheri, S., Georgiou, K., Keeling, R. F., McMahon, S. M., Medlyn, B. E., Moore, D. J., Norby, R. J., Zaehle, S., Anderson-Teixeira, K. J., Battipaglia, G., Brienens, R. J. W., Cabugao, K. G., Cailleret, M., Campbell, E., Canadell, J. G., Ciais, P., Craig, M. E., Ellsworth, D. S., Farquhar, G. D., Fatichi, S., Fisher, J. B., Frank, D. C., Graven, H., Gu, L., Haverd, V., Heilman, K., Heimann, M., Hungate, B. A., Iversen, C. M., Joos, F., Jiang, M., Keenan, T. F., Knauer, J., Körner, C., Leshyk, V. O., Leuzinger, S., Liu, Y., MacBean, N., Malhi, Y., McVicar, T. R., Penuelas, J., Pongratz, J., Powell, A. S., Riutta, T., Sabot, M. E. B., Schleucher, J., Sitch, S., Smith, W. K., Sulman, B., Taylor, B., Terrer, C., Torn, M. S., Treseder, K. K., Trugman, A. T., Trumbore, S. E., van Mantgem, P. J., Voelker, S. L., Whelan, M. E., & Zuidema, P. A., 2021. Integrating the evidence for a terrestrial carbon sink caused by increasing atmospheric co<sub>2</sub>, *New phytologist*, 229(5), 2413–2445.

- Wang, B. & Ding, Q., 2008. Global monsoon: Dominant mode of annual variation in the tropics, *Dynamics of Atmospheres and Oceans*, 44(3-4), 165–183.
- Wang, M., Wang, J., Cai, Q., Zeng, N., Lu, X., Yang, R., Jiang, F., Wang, H., & Ju, W., 2021. Considerable uncertainties in simulating land carbon sinks induced by different precipitation products, *Journal of Geophysical Research: Biogeosciences*, 126(10), e2021JG006524.
- Wang, Y., Law, R., & Pak, B., 2010. A global model of carbon, nitrogen and phosphorus cycles for the terrestrial biosphere, *Biogeosciences*, 7(7), 2261–2282.
- Wang, Y.-P. & Leuning, R., 1998. A two-leaf model for canopy conductance, photosynthesis and partitioning of available energy i: Model description and comparison with a multi-layered model, *Agricultural and Forest Meteorology*, 91(1-2), 89–111.
- Warszawski, L., Frieler, K., Huber, V., Piontek, F., Serdeczny, O., & Schewe, J., 2014. The inter-sectoral impact model intercomparison project (isi-mip): project framework, *Proceedings of the National Academy of Sciences*, 111(9), 3228–3232.
- Way, D. A. & Oren, R., 2010. Differential responses to changes in growth temperature between trees from different functional groups and biomes: a review and synthesis of data, *Tree physiology*, 30(6), 669–688.
- Wieder, W., Boehnert, J., Bonan, G., & Langseth, M., 2014. RegridDED harmonized world soil database v1. 2, *ORNL DAAC*.
- Williams, A. P. & Abatzoglou, J. T., 2016. Recent advances and remaining uncertainties in resolving past and future climate effects on global fire activity, *Current Climate Change Reports*, 2(1), 1–14.
- Williams, K. & Clark, D., 2014. Disaggregation of daily data in jules, Hadley Centre Technical Note 96.
- Woodward, F. I. & Woodward, F., 1987. *Climate and plant distribution*, Cambridge University Press.
- Wu, J., Albert, L. P., Lopes, A. P., Restrepo-Coupe, N., Hayek, M., Wiedemann, K. T., Guan, K., Stark, S. C., Christoffersen, B., Prohaska, N., Tavares, J. V., Marostica, S., Kobayashi, H., Ferreira, M. L., Campos, K. S., Da Silva, R., Brando, P. M., Dye, D. G., Huxman, T. E., Huete, A. R., Nelson, B. W., & Saleska, S. R., 2016. Leaf development and demography explain photosynthetic seasonality in amazon evergreen forests, *Science*, 351(6276), 972–976.
- Wu, X., Liu, H., Li, X., Ciais, P., Babst, F., Guo, W., Zhang, C., Magliulo, V., Pavelka, M., Liu, S., Juang, Y., Wang, P., Shi, C., & Ma, Y., 2018. Differentiating drought legacy effects on vegetation growth over the temperate northern hemisphere, *Global change biology*, 24(1), 504–516.
- Xu, C., McDowell, N. G., Fisher, R. A., Wei, L., Sevanto, S., Christoffersen, B. O., Weng, E., & Middleton, R. S., 2019. Increasing impacts of extreme droughts on vegetation productivity under climate change, *Nature Climate Change*, 9(12), 948–953.
- Yu, X., Orth, R., Reichstein, M., Bahn, M., Klosterhalfen, A., Knohl, A., Koebsch, F., Migliavacca, M., Mund, M., Nelson, J. A., Stocker, B. D., Walther, S., & Bastos, A., 2022. Contrasting drought legacy effects on gross primary productivity in a mixed versus pure beech forest, *Biogeosciences Discussions*, pp. 1–27.
- Yu, Z., 2012. Northern peatland carbon stocks and dynamics: a review, *Biogeosciences*, 9(10), 4071–4085.

- Yuan, W., Cai, W., Chen, Y., Liu, S., Dong, W., Zhang, H., Yu, G., Chen, Z., He, H., Guo, W., Liu, D., Liu, S., Xiang, W., Xie, Z., Zhao, Z., & Zhou, G., 2016. Severe summer heatwave and drought strongly reduced carbon uptake in southern china, *Scientific Reports*, 6(1), 1–12.
- Zaehle, S. & Friend, A., 2010. Carbon and nitrogen cycle dynamics in the o-cn land surface model: 1. model description, site-scale evaluation, and sensitivity to parameter estimates, *Global Biogeochemical Cycles*, 24(1).
- Zaehle, S., Friedlingstein, P., & Friend, A. D., 2010. Terrestrial nitrogen feedbacks may accelerate future climate change, *Geophysical Research Letters*, 37(1).
- Zaehle, S., Ciais, P., Friend, A. D., & Prieur, V., 2011. Carbon benefits of anthropogenic reactive nitrogen offset by nitrous oxide emissions, *Nature Geoscience*, 4(9), 601–605.
- Zeng, N., Mariotti, A., & Wetzel, P., 2005. Terrestrial mechanisms of interannual co2 variability, *Global biogeochemical cycles*, 19(1).
- Zhang, Y., Xiao, X., Zhou, S., Ciais, P., McCarthy, H., & Luo, Y., 2016. Canopy and physiological controls of gpp during drought and heat wave, *Geophysical Research Letters*, 43(7), 3325–3333.
- Zhao, M. & Running, S. W., 2010. Drought-induced reduction in global terrestrial net primary production from 2000 through 2009., *Science*, 329(5994), 940–943.
- Zhu, Z., Piao, S., Myneni, R. B., Huang, M., Zeng, Z., Canadell, J. G., Ciais, P., Sitch, S., Friedlingstein, P., Arneth, A., Cao, C., Cheng, L., Kato, E., Koven, C., Li, Y., Lian, X., Liu, Y., Liu, R., Mao, J., Pan, Y., Peng, S., Peñuelas, J., Poulter, B., Pugh, T. A. M., Stocker, B. D., Viovy, N., Wang, X., Wang, Y., Xiao, Z., Yang, H., Zaehle, S., & Zeng, N., 2016. Greening of the earth and its drivers, *Nature climate change*, 6(8), 791–795.
- Zobler, L., 1986. A world soil file global climate modeling, *NASA Tech. memo*, 32.
- Zscheischler, J. & Seneviratne, S. I., 2017. Dependence of drivers affects risks associated with compound events, *Science advances*, 3(6), e1700263.
- Zscheischler, J., Mahecha, M. D., Harmeling, S., & Reichstein, M., 2013. Detection and attribution of large spatiotemporal extreme events in Earth observation data, *Ecological Informatics*, 15, 66–73.
- Zscheischler, J., Mahecha, M. D., Von Buttlar, J., Harmeling, S., Jung, M., Rammig, A., Randerson, J. T., Schölkopf, B., Seneviratne, S. I., Tomelleri, E., Zaehle, S., & Reichstein, M., 2014a. A few extreme events dominate global interannual variability in gross primary production, *Environmental Research Letters*, 9(3), 035001.
- Zscheischler, J., Michalak, A. M., Schwalm, C., Mahecha, M. D., Huntzinger, D. N., Reichstein, M., Berthier, G., Ciais, P., Cook, R. B., El-Masri, B., Huang, M., Ito, A., Jain, A., King, A., Lei, H., Lu, C., Mao, J., Peng, S., Poulter, B., Ricciuto, D., Shi, X., Tao, B., Tian, H., Viovy, N., Wang, W., Wei, Y., Yang, J., & Zeng, N., 2014b. Impact of large-scale climate extremes on biospheric carbon fluxes: An intercomparison based on MsTMIP data, *Global Biogeochemical Cycles*, 28(6), 585–600.
- Zscheischler, J., Reichstein, M., Harmeling, S., Rammig, A., Tomelleri, E., & Mahecha, M. D., 2014c. Extreme events in gross primary production: a characterization across continents, *Biogeosciences*, 11(11), 2909–2924.
- Zscheischler, J., Reichstein, M., Von Buttlar, J., Mu, M., Randerson, J. T., & Mahecha, M. D., 2014d. Carbon cycle extremes during the 21st century in cmip5 models: Future evolution and attribution to climatic drivers, *Geophysical Research Letters*, 41(24), 8853–8861.

- Zscheischler, J., Fatichi, S., Wolf, S., Blanken, P. D., Bohrer, G., Clark, K., Desai, A. R., Hollinger, D., Keenan, T., Novick, K. A., & Seneviratne, S. I., 2016. Short-term favorable weather conditions are an important control of interannual variability in carbon and water fluxes, *Journal of Geophysical Research: Biogeosciences*, 121(8), 2186–2198.
- Zscheischler, J., Orth, R., & Seneviratne, S. I., 2017. Bivariate return periods of temperature and precipitation explain a large fraction of european crop yields, *Biogeosciences*, 14(13), 3309–3320.
- Zscheischler, J., Westra, S., Van Den Hurk, B. J., Seneviratne, S. I., Ward, P. J., Pitman, A., AghaKouchak, A., Bresch, D. N., Leonard, M., Wahl, T., & Zhang, X., 2018. Future climate risk from compound events, *Nature Climate Change*, 8(6), 469–477.
- Zscheischler, J., Martius, O., Westra, S., Bevacqua, E., R., C., Horton, R. M., van den Hurk, B., AghaKouchak, A., Jézéquel, A., Mahecha, M. D., Maraun, D., Ramos, A. M., Ridder, N., Thiery, W., & Vignotto, E., 2020. A typology of compound weather and climate events, *Nature Reviews Earth and Environment*, 1, 333–347.

# Acknowledgements

I would like to give a big thank you to everyone at KUP for making this PhD a memorable experience and creating a welcoming, open, and fun environment, even through the Covid-19 pandemic. I would also like to thank a few people specifically, but the list is far from complete:

- My biggest thank goes to my supervisor, Dr. Jakob Zscheischler. First, for offering me a position and second, for your excellent supervision, for letting me figure things out myself but always helping when I got stuck. You also introduced me to the DAMOCLES community within the first few weeks of my PhD, which resulted in many stimulating discussions and, even more importantly, many friendships. Thank you for that. Working with you was a privilege which I hope many other students will have the opportunity to also enjoy.
- I also thank Prof. Dr. Fortunat Joos for making me feel welcome in Bern and for offering assistance whenever needed.
- I want to thank my office mates in B69, Victor Onink and Natacha Legrix, for the many enjoyable moments in the office, for giving advice or sometimes just listening. Our time in the office was unfortunately cut short by the pandemic, but the friendship remains.
- Thanks to Doris Rätz, Claudia Maschke and the whole team in the secretariat for always having a helping hand.

Further I would like to thank:

- Prof. Dr. Anja Rammig for agreeing to be my external referee, despite a very busy schedule
- Manuel Bressan, Pauline Rivoire, and Stephan Tschumi who proofread my thesis and gave me helpful advice
- And last but not least, Manuel Bressan, my family and my friends for their invaluable support throughout these four years at KUP and especially towards the end. Without you all, I would not be where I am today.



# Erklärung

gemäss Art. 18 PromR Phil.-nat. 2019

Name, Vorname: Tschumi, Elisabeth Andrea

Matrikelnummer: 13-919-048

Studiengang: Climate Sciences

Bachelor       Master       Dissertation

Titel der Arbeit: The effects of differing drought-heat signatures on terrestrial carbon dynamics and vegetation composition using dynamic vegetation modelling

Leiter der Arbeit: Dr. Jakob Zscheischler

Ich erkläre hiermit, dass ich diese Arbeit selbständig verfasst und keine anderen als die angegebenen Quellen benutzt habe. Alle Stellen, die wörtlich oder sinngemäss aus Quellen entnommen wurden, habe ich als solche gekennzeichnet. Mir ist bekannt, dass andernfalls der Senat gemäss Artikel 36 Absatz 1 Buchstabe r des Gesetzes über die Universität vom 5. September 1996 und Artikel 69 des Universitätsstatuts vom 7. Juni 2011 zum Entzug des Dokortitels berechtigt ist. Für die Zwecke der Begutachtung und der Überprüfung der Einhaltung der Selbständigkeitserklärung bzw. der Reglemente betreffend Plagiate erteile ich der Universität Bern das Recht, die dazu erforderlichen Personendaten zu bearbeiten und Nutzungshandlungen vorzunehmen, insbesondere die Doktorarbeit zu vervielfältigen und dauerhaft in einer Datenbank zu speichern sowie diese zur Überprüfung von Arbeiten Dritter zu verwenden oder hierzu zur Verfügung zu stellen.

Bern, 27. Oktober 2022

Unterschrift